UNIVERSIDAD NACIONAL AUTÓNOMA DE MÉXICO

POSGRADO EN CIENCIAS FÍSICAS

BLOCKADE AND ANTIBLOCKADE OF RYDBERG ATOMS

TESIS

QUE PARA OPTAR POR EL GRADO DE:

MAESTRA EN CIENCIAS (FÍSICA)

PRESENTA:

SILVIA FERNANDA CÁRDENAS LÓPEZ

TUTORES PRINCIPALES
DRA. ROCÍO JÁUREGUI RENAUD (IF-UNAM)
DR. ASAF PARIS MANDOKI (IF-UNAM)

MIEMBROS DEL COMITÉ TUTOR
DR. PABLO BARBERIS BLOSTEIN (IIMAS-UNAM)

MÉXICO, CIUDAD DE MÉXICO, JUNIO 2020

Agradecimientos

Agradezco todo el apoyo de mi comité tutor. Gracias a Rocío Jáuregui por consejos útiles de física y no física, y pláticas interesantes. Gracias a Asaf Paris por ser la voz escéptica en las reuniones, que a menudo me llevaba a entender las cosas con mayor profundidad. Gracias a Pablo Barberis por el humor, entusiasmo y los comentarios esclarecedores.

Gracias a los miembros del jurado, Fernando Ramírez, Laura Rosales, Santiago Caballero y Carlos Pineda, por las observaciones que ayudaron a mejorar mi tesis.

Agradezco a mi mamá. Gracias por darme la convicción de que con trabajo duro y determinación nada es imposible. A mi papá, gracias por el apoyo incondicional y la paciencia. A Lupita por siempre escucharme y hacerme reír. A Juan, por su curiosidad que hace mi vida infinitamente más interesante y que me impulsa a aprender tantas cosas nuevas. Gracias a Carmen, Lorena y Mónica. Por crecer conmigo y estar siempre ahí para mí. A Carvente por todas las pláticas interminables.

Finalmente, agradezco el apoyo recibido por parte del Proyecto PAPIIT-DGAPA IN103020 "Correlaciones cuánticas en sistemas atómicos interactuando con campos electromagnéticos".

Resumen

Se describe un sistema formado por dos átomos que interactúan entre sí ante la presencia de dos láseres que acoplan a sus estados estacionarios. El nivel superior de cada uno de los átomos es un estado de Rydberg. La interacción interatómica se incorpora a través de un potencial obtenido numéricamente y que asintóticamente reproduce el modelo efectivo de Marinescu [1] para átomos alcalinos. Se usaron parámetros realistas para las intensidades de los láseres y los decaimientos de los niveles excitados en el caso de átomos de rubidio. La correlaciones atómicas resultantes permiten identificar las condiciones en que se presentan los fenómenos de bloqueo y antibloqueo.

La Tesis se divide en cuatro capítulos. En el primero se introducen los conceptos básicos que requiere su desarrollo: matriz de densidad, interacción dipolar eléctrica entre luz y materia, la ecuación maestra para la evolución del sistema y algunas expectativas resultantes de aplicar esta última a átomos de tres niveles. En el segundo capítulo se describen las propiedades de los átomos de Rydberg y se da un breve recuento del papel de estos en espectroscopía, óptica cuántica y física básica. En el tercer capítulo se describe la implementación y las ideas físicas que sustentan al cálculo numérico para obtener los potenciales de interacción entre dos átomos de Rydberg. En el cuarto capítulo se resuelve numéricamente la ecuación maestra que describe a los dos átomos en presencia de los láseres, y se analizan las correlaciones conectadas a diferentes distancias interatómicas. Con ellas se analizan las probabilidades de transiciones conjuntas de cuatro fotones y se identifica la presencia de bloqueo y antibloqueo para los átomos de Rydberg.

Abstract

In this thesis, we describe a system formed by two interacting atoms in the presence of two lasers that couple its stationary states. The upper level of each atom is a Rydberg state. The interatomic interaction is incorporated through a numerical potential that asymptotically reproduces the effective model of Marinescu [1] for alkaline atoms. We used realistic parameters for the laser intensities and the decay rates of excited levels in the case of Rubidium atoms. The resultant atomic correlations allow identifying parameter regions for blockade and antiblockade.

The thesis is organized as follows. In the first chapter, we introduce the basic concepts required for later chapters: density matrix, electric dipole interaction between light and matter, the master equation, and the three-level atom. In the second chapter, we describe the properties of Rydberg atoms and give a brief review of the role played by them in spectroscopy, quantum optics, and basic physics. In the third chapter, we describe the implementation and physical concepts that support the numerical calculation to obtain the interaction potentials between two Rydberg atoms. In the fourth chapter, we numerically solve the master equation describing the two atoms in the presence of lasers, and we analyze the connected correlation obtained for different distances between the atoms. With these correlations, we analyze the probabilities of four-photon transitions, and we identify the presence of blockade and antiblockade for Rydberg atoms.

Contents

Chapter 1

Atom-light interactions

In this chapter we will study atoms interacting with classical fields. The models in consideration are called semiclassical since we consider the fields to be classical and we model the atoms using quantum mechanics. We will explore the dipole approximation to describe the interaction between radiation and atoms. Then, we give a derivation of the master equation describing dissipation in the Born-Markov approximation. In the end, we will review the paradigmatic model of a two-level atom interacting with a quasi-resonant field, Rabi oscillations and the three-level atom. The models and approximations described here will be used in the rest of the thesis.

1.1 Dipole approximation

As we will see in the following chapters, under certain conditions, an atom can be modeled as an electron bound to a positive core (formed by the nucleus and other electrons). In this section, we will study the interaction between such an electron and an external monochromatic electromagnetic field. Wavelengths of optical fields are larger than the typical size of atoms[1]. This will allow us to use the dipole approximation to simplify the Hamiltonian describing the light-atom interaction [2].

Let us denote the center of mass of the atom by $\mathbf{r}_0$, and the relative position of the electron from the center of mass by $\mathbf{r}$. In the absence of an external electromagnetic field, the Schrödinger equation satisfied by the wavefunction of the electron, $\psi(\mathbf{r},t)$, is:

$$\left[-\frac{\hbar^2}{2m}\nabla^2 + V(\mathbf{r})\right]\psi(\mathbf{r},t) = i\hbar\frac{\partial\psi(\mathbf{r},t)}{\partial t}, \tag{1.1}$$

where $V(\mathbf{r})$ is the potential induced by the positive core. $|\psi(\mathbf{r},t)|^2$ represents the probability density of finding the electron at $\mathbf{r}$ at time t. Note that the description is

[1] Wavelengths of optical fields go from 400 to 700 nm, while the size of a hydrogen atom is of the order of $a_0 = 0.05$nm.

invariant under the transformation $\psi(\mathbf{r},t) \to \psi(\mathbf{r},t)e^{i\varphi}$, where φ is a constant phase.

We will describe this field with the aid of the vector and scalar potentials, $\mathbf{A}(\mathbf{x},t)$ and $U(\mathbf{x},t)$, through

$$\begin{aligned} \mathbf{E} &= -\nabla U - \frac{\partial \mathbf{A}}{\partial t}, \\ \mathbf{B} &= \nabla \times \mathbf{A}. \end{aligned} \tag{1.2}$$

Given the form of expressions (1.2), and the fact that all measurable quantities of the electromagnetic field are related to $\mathbf{E}$ or $\mathbf{B}$, and not to $\mathbf{A}$ and U, our description must be invariant under the transformations

$$\begin{aligned} \mathbf{A} &\to \mathbf{A} + \frac{\hbar}{e}\nabla\chi(\mathbf{r},t), \\ U &\to U - \frac{\hbar}{e}\frac{\partial\chi(\mathbf{r},t)}{\partial t}, \end{aligned} \tag{1.3}$$

where $\chi(\mathbf{r},t)$ is any given function. Transformations (1.3) are called gauge transformations.

Now we bring the two ingredients of our system together. Using the minimal coupling Hamiltonian, we can couple the free electron to the external electromagnetic field, preserving the invariance under gauge transformations (1.3). The equation satisfied by the wavefunction of the electron will be now

$$\left[\frac{1}{2m}\left(-i\hbar\nabla - e\mathbf{A}(\mathbf{r}+\mathbf{r}_0,t)\right)^2 + eU(\mathbf{r}+\mathbf{r}_0,t) + V(\mathbf{r})\right]\psi(\mathbf{r},t) = i\hbar\frac{\partial\psi(\mathbf{r},t)}{\partial t}. \tag{1.4}$$

The form of equation (1.4) is invariant under the extended gauge transformations

$$\begin{aligned} \mathbf{A} &\to \mathbf{A} + \frac{\hbar}{e}\nabla\chi(\mathbf{r},t), \\ U &\to U - \frac{\hbar}{e}\frac{\partial\chi(\mathbf{r},t)}{\partial t}, \\ \psi(\mathbf{r},t) &\to \psi(\mathbf{r},t)e^{-i\chi(\mathbf{r},t)}. \end{aligned} \tag{1.5}$$

Notably, the part of the gauge transformation referring to ψ is a local version of the invariance presented in the case of the free electron.

We work in the Coulomb gauge and take $U = 0$ in equation (1.4)[2]. Furthermore, we

[2]In the Coulomb gauge, the equation satisfied by the scalar potential is $\nabla^2 U = -4\pi\rho$, where ρ is the charge density that serves as a source to the external electromagnetic field. If this charge is localized far away from the atom, we can safely take $\rho = 0$ and hence $U =$ cte. We set that constant to zero.

think that the external field is a plane wave with frequency ω and wavevector $\mathbf{k}$,

$$\mathbf{A}(\mathbf{x},t) = \mathbf{A}_0 e^{i(\mathbf{k}\cdot\mathbf{x}-\omega t)}.$$

If $|\mathbf{r}| \ll \lambda$ (that is, if the characteristic size of the atom is much smaller than the wavelength of the field), we can approximate the vector potential at the position of the electron with its value at the nucleus position, $\mathbf{A}(\mathbf{r}+\mathbf{r}_0,t) \simeq \mathbf{A}(\mathbf{r}_0,t)$. This is known as the dipole approximation.

The equation (1.4) becomes

$$\left[\frac{1}{2m}\left(-i\hbar\nabla - e\mathbf{A}(\mathbf{r}_0,t)\right)^2 + V(\mathbf{r})\right]\psi(\mathbf{r},t) = i\hbar\frac{\partial\psi(\mathbf{r},t)}{\partial t}. \tag{1.6}$$

We now perform a gauge transformation (1.5) with $\chi = -\frac{e\mathbf{A}(\mathbf{r}_0,t)\cdot\mathbf{r}}{\hbar}$. We denote the wavefunction in the new gauge as $\phi(\mathbf{r},t) = \psi(\mathbf{r},t)e^{\frac{ie\mathbf{A}(\mathbf{r}_0,t)\cdot\mathbf{r}}{\hbar}}$. The equation satisfied by the wavefunction in the new gauge is

$$\left[-\frac{\nabla^2}{2m} + V(\mathbf{r}) - e\mathbf{E}\cdot\mathbf{r}\right]\phi(\mathbf{r},t) = i\hbar\frac{\partial\phi(\mathbf{r},t)}{\partial t}. \tag{1.7}$$

According to the last equation, the evolution of the electron can be described by the Hamiltonian

$$H = \frac{p^2}{2m} + V(\mathbf{r}) - e\mathbf{E}\cdot\mathbf{r}. \tag{1.8}$$

This is the Hamiltonian we will use to describe atoms interacting with light.

1.2 Density operator

In quantum mechanics of closed systems, the state of a system is represented by $|\psi\rangle$. Through this object we can calculate the expected value of any quantity (via $\langle\psi|\hat{A}|\psi\rangle$ where $\hat{A}$ is the operator associated with the quantity). In this sense, $|\psi\rangle$ contains all the known information about the system.

If the state of the system is $|\psi\rangle$, we define the corresponding density matrix operator as

$$\rho = |\psi\rangle\langle\psi|. \tag{1.9}$$

Sometimes, we cannot be certain that the state of a system is a particular $|\psi\rangle$. For instance, methods that we used to prepare the system could give the state $|\psi_1\rangle$ with probability p_1, $|\psi_2\rangle$ with probability p_2, and so on. If this is the case, we define the density operator of the system to be [3]

$$\rho = \sum_{\alpha} p_{\alpha} \left|\psi_{\alpha}\right\rangle \left\langle\psi_{\alpha}\right| . \tag{1.10}$$

A state of the form (1.9) is said to be pure, while a state of the form (1.10) is said to be mixed.

1.2.1 Properties

Some properties of the density matrix operator are [3]:

- If the Hamiltonian describing the unitary evolution of the system is $\hat{H}$, then ρ evolves according to
$$\partial_t \rho = -\frac{i}{\hbar}\left[\hat{H}, \rho\right]. \tag{1.11}$$
- The expectation value of an operator $\hat{A}$ is given by
$$\left\langle \hat{A} \right\rangle = \mathrm{Tr}[\rho \hat{A}]. \tag{1.12}$$
-
$$\mathrm{Tr}[\rho] = 1. \tag{1.13}$$

1.3 Master equation

Let us assume that we are interested in studying a system described by a Hamiltonian $\hat{H}$. According to what we saw in the last section, the description of the system at time t is given by its density matrix $\rho(t)$. The evolution of $\rho(t)$ is given by the von Neumann equation (1.11). All this is true only if our system is completely isolated from the environment surrounding it. Whereas sometimes this is a reasonable approximation, there are situations where assuming the system to be completely isolated is not valid. To correctly describe situations where the system-environment coupling is not negligible, we will use the master equation. Here we derive it for a general system following the first chapter of [4].

Let us suppose that we have a system S interacting with a large reservoir system R. The Hamiltonian describing the composite system is

$$\hat{H} = \hat{H}_S + \hat{H}_R + \hat{H}_{SR}, \tag{1.14}$$

where $\hat{H}_S$ and $\hat{H}_R$ describe respectively S and R. $\hat{H}_{SR}$ describes the interaction between the subsystems. If we denote the density matrix of the whole system at time t as $\chi(t)$, then the reduced density matrix $\rho(t)$ for the system S is

$$\rho(t) = \mathrm{Tr}_R(\chi(t)), \tag{1.15}$$

where $\mathrm{Tr}_R(\bullet)$ indicates a partial trace over reservoir R. Our objective is to obtain an equation describing the evolution of $\rho(t)$ solely in terms of degrees of freedom of the system S.

The von Neumann equation for the complete density matrix is

$$\dot{\chi} = \frac{1}{i\hbar}\left[\hat{H}, \chi\right]. \tag{1.16}$$

We transform the last equation to the interaction picture

$$\dot{\widetilde{\chi}} = \frac{1}{i\hbar}\left[\widetilde{H}_{SR}, \widetilde{\chi}\right], \tag{1.17}$$

where we have adopted the notation

$$\widetilde{\mathscr{O}}(t) = e^{\frac{i}{\hbar}(\hat{H}_R+\hat{H}_S)}\hat{\mathscr{O}}(t)e^{-\frac{i}{\hbar}(\hat{H}_R+\hat{H}_S)}.$$

The formal solution of (1.17) is

$$\widetilde{\chi}(t) = \chi(0) + \frac{1}{i\hbar}\int_0^t dt' \left[\widetilde{H}_{SR}(t'), \widetilde{\chi}(t')\right]. \tag{1.18}$$

We substitute $\widetilde{\chi}(t)$ in the commutator in (1.17) to obtain

$$\dot{\widetilde{\chi}} = \frac{1}{i\hbar}\left[\widetilde{H}_{SR}(t), \widetilde{\chi}(0)\right] - \frac{1}{\hbar^2}\int_0^t dt' \left[\widetilde{H}_{SR}(t), \left[\widetilde{H}_{SR}(t'), \widetilde{\chi}(t')\right]\right]. \tag{1.19}$$

Note that until now we have made no approximations, and hence (1.19) is exact.

Next, we assume that no correlations exist between S and R at $t = 0$. This means that at the beginning of the evolution we have

$$\chi(0) = \rho(0)R_0, \tag{1.20}$$

where $\rho(0)$ and R_0 are respectively the initial density operators of systems S and R. Since $\widetilde{\rho} = \mathrm{Tr}_R(\widetilde{\chi})$, if we trace out the system R in equation (1.19) we get

$$\dot{\widetilde{\rho}}(t) \approx -\frac{1}{\hbar^2}\int_0^t dt' Tr_R \left[\widetilde{H}_{SR}(t), \left[\widetilde{H}_{SR}(t'), \widetilde{\chi}(t')\right]\right]. \tag{1.21}$$

In the last equation we have assumed $Tr_R(\widetilde{H}_{SR}R_0) = 0$. This condition means that the average energy flux from the reservoir to the system S is zero.

Born approximation

We have assumed that at the beginning, the two subsystems are uncorrelated. At later times, correlations will begin to appear. If we consider that the interaction between the two subsystems is weak enough, and that the reservoir is so large that the interaction with the system S leaves it unaffected, then we can write

$$\widetilde{\chi}(t) = \widetilde{\rho}(t)R_0 + O(\hat{H}_{SR}).$$

We neglect terms higher than second order in H_{SR} and approximate the equation as

$$\dot{\widetilde{\rho}}(t) = -\frac{1}{\hbar^2}\int_0^t dt' Tr_R\left[\widetilde{H}_{SR}(t), \left[\widetilde{H}_{SR}(t'), \widetilde{\rho}(t')R_0\right]\right]. \tag{1.22}$$

This last approximation is called Born approximation.

Markov approximation

One of the most significant complications of the last equation is that the evolution of ρ at time t is dependent on the whole story of the system. It is reasonable that the evolution of the system can depend on past history. Since S and R are interacting, the state of R at a later time t can contain information of the state of S at an earlier time t'. If the information of past history of S is quickly removed from R, then a good approximation is to replace $\rho(t')$ by $\rho(t)$ inside the integral of equation (1.22):

$$\dot{\widetilde{\rho}}(t) = -\frac{1}{\hbar^2}\int_0^t dt' Tr_R\left[\widetilde{H}_{SR}(t), \left[\widetilde{H}_{SR}(t'), \widetilde{\rho}(t)R_0\right]\right]. \tag{1.23}$$

This is called the Markov approximation. Let us now be more specific on what we meant by quickly in the previous paragraph. For the Markov approximation to be valid, we need the correlation time of the reservoir to be much smaller than the timescale governing the dynamics of the system S. To see that this is the case, an analysis similar to the one in [4] section 1.3 should be performed for each particular system under study.

To further simplify the equation, we now consider that the interaction Hamiltonian can be written as

$$\hat{H}_{SR} = \hbar\sum_i \hat{s}_i\hat{\Gamma}_i, \tag{1.24}$$

where $\hat{s}_i$ and $\hat{\Gamma}_i$ are operators respectively associated to the system S and the reservoir R. In this way, equation (1.23) takes the form

$$\begin{aligned}\dot{\widetilde{\rho}}(t) = -\sum_{i,j}\int_0^t dt' \{&[\widetilde{s}_i(t)\widetilde{s}_j(t')\widetilde{\rho}(t') - \widetilde{s}_j(t')\widetilde{\rho}(t')\widetilde{s}_i(t)]\left\langle\widetilde{\Gamma}_i(t)\widetilde{\Gamma}_j(t')\right\rangle_R \\ &+ [\widetilde{\rho}(t')\widetilde{s}_j(t')\widetilde{s}_i(t) - \widetilde{s}_i(t)\widetilde{\rho}(t')\widetilde{s}_j(t')]\left\langle\widetilde{\Gamma}_j(t')\widetilde{\Gamma}_i(t)\right\rangle_R\}.\end{aligned} \tag{1.25}$$

We can arrive to a simpler form by specifying the systems S and R and their interaction (1.24). We will do this in the next section for the case in which S is a two-level atom, and R is a set of electromagnetic modes.

1.4 Two-level atom

Let us now consider an atom interacting with a classical electromagnetic field [3]. Assume the field is a monochromatic wave with frequency ω and polarization $\hat{\epsilon}$

$$\mathbf{E} = \hat{\epsilon} E_0 \cos\omega t. \tag{1.26}$$

Using the dipole approximation, we have ignored the spatial dependence of the field. We observe that we can separate the field in its positive and negative parts:

$$\mathbf{E} = \hat{\epsilon}(E_0^{(+)} e^{i\omega t} + E_0^{(-)} e^{-i\omega t}) \equiv \mathbf{E}^{(+)} + \mathbf{E}^{(-)}. \tag{1.27}$$

Now suppose that the atom can be represented by only two levels, $|1\rangle$ and $|2\rangle$ (this is an approximation that will be validated later). Let the respective energies be $E_1 = 0$ and $E_2 = \hbar\omega_A$. We define $\Delta = \omega - \omega_A$ to be the detuning of the field from the $|1\rangle \to |2\rangle$ transition frequency. In the following, we will assume that the field is nearly resonant with the atomic transition (i.e. $\Delta \ll \omega_A$). The Hamiltonian of the system in the dipole approximation is then,

$$\begin{aligned} \hat{H} &= \hat{H}_A + \hat{H}_{AF} \\ &= \hbar\omega_A \hat{\sigma}_{22} - e\mathbf{E}\cdot\hat{\mathbf{r}}. \end{aligned} \tag{1.28}$$

In the last expression, we have adopted the notation $\hat{\sigma}_{ij} \equiv |i\rangle\langle j|$, and $\hat{\mathbf{r}}$ represents the position of the electron in the atom relative to its center of mass. If both $|1\rangle$ and $|2\rangle$ have well defined parity then $\langle i|\hat{\mathbf{r}}|i\rangle = 0$. Multiplying $\hat{H}_{AF}$ from both sides by $\mathbb{I} = \hat{\sigma}_{11} + \hat{\sigma}_{22}$ we obtain

$$\begin{aligned} \hat{H} &= \hbar\omega_A \hat{\sigma}_{22} - e\mathbf{E}\cdot\mathbf{d}_{21}(\hat{\sigma}_{21} + \hat{\sigma}_{12}) \\ \mathbf{d}_{12} &= -e\langle 1|\hat{\mathbf{r}}|2\rangle. \end{aligned} \tag{1.29}$$

In the interaction picture, the Hamiltonian is

$$\tilde{H}_{AF} = -e\mathbf{d}_{21}\cdot\left(\mathbf{E}^{(+)} + \mathbf{E}^{(-)}\right)\left(\hat{\sigma}_{12}e^{-i\omega_A t} + \hat{\sigma}_{21}e^{i\omega_A t}\right). \tag{1.30}$$

The above product has two terms containing $e^{\pm i(\omega+\omega_A)t}$, and two terms with $e^{\pm i(\omega-\omega_A)t}$. Neglecting terms that have fast oscillations corresponds to ignoring the former terms. This is called the rotating wave approximation (RWA). The resulting simplified Hamiltonian is

$$\tilde{H}_{AF} = -e\mathbf{d}_{21}\cdot\left(\mathbf{E}^{(+)}\hat{\sigma}_{12}e^{-i\omega_A t} + \mathbf{E}^{(-)}\hat{\sigma}_{21}e^{i\omega_A t}\right). \tag{1.31}$$

RWA is valid if we are interested in the dynamics of the system occurring at the timescale of defined by the detuning, $\frac{1}{\Delta}$ for $\Delta << \omega_A$. The neglected terms evolve at a shorter timescale $\sim \frac{1}{2\omega_A}$.

Incidentally, the same argumentation is useful to determine when it is suitable to approximate an atom as a two-level system. If our field is nearly-resonant to just one transition of the atom, then adding a level that is not related to this transition will contribute to the Hamiltonian only with fast-oscillating terms. In practice, we also need to consider the properties of the field we use to excite the atom and that the atoms have fine and hyperfine structure (figure 1.1).

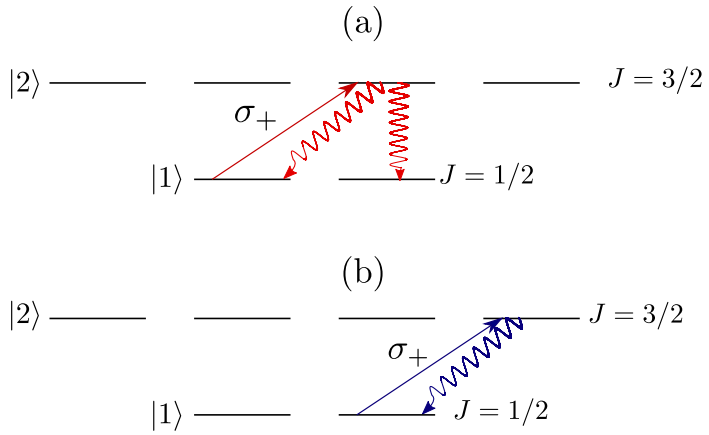

Figure 1.1: a) Example of a configuration where the two-level approximation is not suitable. The decay of the upper level can populate an initially unpopulated ground state. (b) Example of a configuration where the two-level approximation is appropriate.

Finally, defining the Rabi frequency as $\Omega = -\frac{\langle 1|\hat{\epsilon}\cdot\mathbf{d}|2\rangle E_0}{\hbar}$, the Hamiltonian of the two-level atom interacting with a classical field in the Schrödinger picture is

$$\hat{H} = \hbar\omega_A\hat{\sigma}_{22} + \frac{\hbar\Omega}{2}\left(\hat{\sigma}_{21}e^{-i\omega t} + \hat{\sigma}_{12}e^{i\omega t}\right). \tag{1.32}$$

The timescale for the evolution that is imposed by the final Hamiltonian (1.32) is $\frac{1}{\Omega}$. This means that, for our procedure to be consistent, we also need $\Omega \ll \omega_A$.

This Hamiltonian gives rise to the well-known Rabi oscillations of the populations of ground and excited state. For instance, if the atom is initially in the ground state, the probabilities of finding it in the ground and excited state at a later time t are respectively (figure 1.2)

$$\begin{aligned} \mathrm{P}_1(t) &= \cos^2\left(\frac{\Omega t}{2}\right), \\ \mathrm{P}_2(t) &= \sin^2\left(\frac{\Omega t}{2}\right). \end{aligned} \tag{1.33}$$

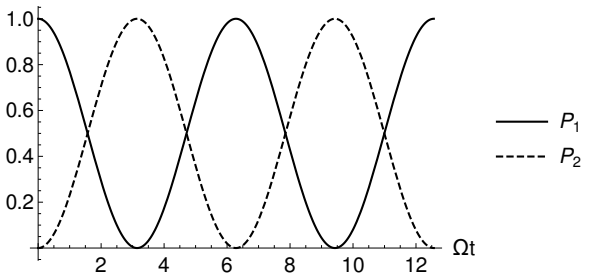

Figure 1.2: Rabi oscillations in a two-level atom when the initial state is $|1\rangle$.

1.4.1 Decay of a two-level atom

In this section, we review the master equation to describe the decay of a two-level system [4]. We model the reservoir as a quantized multimode electromagnetic field. The parts of the Hamiltonian of section 1.3 take the particular form

$$\begin{aligned} \hat{H}_S &= \hbar\omega_A\hat{\sigma}_{22}, \\ \hat{H}_R &= \sum_{\mathbf{k},\lambda}\hbar\omega_k\hat{a}^\dagger_{\mathbf{k}\lambda}\hat{a}_{\mathbf{k}\lambda}, \\ \hat{H}_{SR} &= \sum_{\mathbf{k},\lambda}\hbar\Omega^*_{\mathbf{k}\lambda}\hat{a}^\dagger_{\mathbf{k}\lambda}\hat{\sigma}_{21} + \text{h.c.} \end{aligned} \tag{1.34}$$

The sums in the last equation are performed over the different wavevectors $\mathbf{k}$ and wavelengths λ that describe the modes of the electromagnetic field interacting with the atom. Just as in equation (1.32), the Rabi frequencies are defined to be

$$\Omega_{\mathbf{k}\lambda} = -ie^{i\mathbf{k}\cdot\mathbf{r}_A}\sqrt{\frac{\omega_k}{2\hbar\epsilon_0 V}}\boldsymbol{\epsilon}_{\mathbf{k}\lambda}\cdot\mathbf{d}_{21}. \tag{1.35}$$

$\boldsymbol{\epsilon}_{\mathbf{k}\lambda}$, ω_k, $\hat{a}^\dagger_{\mathbf{k}\lambda}$ and $\hat{a}_{\mathbf{k}\lambda}$ are respectively the polarization vector, frequency, creation and annihilation operator associated with the mode $(\mathbf{k},\omega_k)$. $\mathbf{r}_A$ is the position of the atom,

and V is the quantization volume for the electromagnetic field[3].
Note that the Rabi frequencies characterizing the interaction of the atom with each mode is dependent on the wavevector $\mathbf{k}$ and wavelength λ.

The master equation describing the evolution of the two-level system in the Born-Markov approximation will be of the form Eq. (1.25). We identify

$$\begin{aligned}
\widetilde{s}_1(t) &= \hat{\sigma}_{12} e^{-i\omega_A t}, \\
\widetilde{s}_2(t) &= \hat{\sigma}_{21} e^{i\omega_A t}, \\
\widetilde{\Gamma}_1(t) &= \sum_{\mathbf{k},\lambda} \Omega^*_{\mathbf{k}\lambda} \hat{a}^\dagger_{\mathbf{k}\lambda} e^{i\omega_k t}, \\
\widetilde{\Gamma}_2(t) &= \sum_{\mathbf{k},\lambda} \Omega_{\mathbf{k}\lambda} \hat{a}_{\mathbf{k}\lambda} e^{-i\omega_k t}.
\end{aligned}$$

We also assume that the reservoir is in a thermal state with temperature T:

$$R_0 = \frac{e^{-H_R/k_B T}}{\mathrm{Tr}\left[e^{-H_R/k_B T}\right]} = \prod_j e^{-\hbar\omega_j \hat{a}^\dagger_j \hat{a}_j / k_B T} \left(1 - e^{-\hbar\omega_j/k_B T}\right).$$

We use the expression (1.25), replace the particular operators, and perform the integrals. The final master equation takes the form:

$$\begin{aligned}
\dot{\rho} = &-i\omega'_A \left[\hat{\sigma}_{22}, \rho\right] + \frac{\gamma}{2}(\bar{n}+1)(2\hat{\sigma}_{12}\rho\hat{\sigma}_{21} - \hat{\sigma}_{21}\hat{\sigma}_{12}\rho - \rho\hat{\sigma}_{21}\hat{\sigma}_{12}) \\
&+ \frac{\gamma\bar{n}}{2}\left(2\hat{\sigma}_{21}\rho\hat{\sigma}_{12} - \hat{\sigma}_{12}\hat{\sigma}_{21}\rho - \rho\hat{\sigma}_{12}\hat{\sigma}_{21}\right).
\end{aligned} \tag{1.36}$$

The transition frequency is modified by a Lamb shift $\omega'_A = \omega_A + \delta$. The shift δ and the decay rate γ can be expressed as integrals of the density mode function $g(\mathbf{k})$ as detailed in section 2.2 of [4]. $\bar{n}$ is the average occupation number at temperature T of the modes with frequency ω_A

$$\bar{n} = \frac{e^{-\hbar\omega_A/k_B T}}{1 - e^{-\hbar\omega_A/k_B T}}.$$

δ contains the Lamb shift. The integral that needs to be calculated to obtain δ diverges, so a renormalization process needs to be applied to obtain a finite value [6].

[3]Each mode of the electromagnetic field without sources is mathematically equivalent to a harmonic oscillator. The quantization of the field in free space is carried out dividing space into cubes of volume V (for details see chapter 2 of [5]).The electromagnetic field operator for the mode $(\mathbf{k}, \lambda)$ is then $\hat{\mathbf{E}}_{\mathbf{k}\lambda}(\mathbf{r}) = i\sqrt{\frac{\hbar\omega_k}{2\epsilon_0 V}}\boldsymbol{\epsilon}_{\mathbf{k}\lambda}\left[\hat{a}_{\mathbf{k}\lambda} e^{i\mathbf{k}\cdot\mathbf{r}} + \text{h.c.}\right]$ (and the total field is $\hat{\mathbf{E}} = \sum_{\mathbf{k},\lambda} \hat{\mathbf{E}}_{\mathbf{k}\lambda}$). The interaction term resulting from assuming that the atom-field interaction is dipolar (equation (1.8)) and this expression is $\hat{H}_{SR}$ in equation (1.34).

1.5 Three level atom

Now we consider the interaction between a three-level atom and two classical electromagnetic fields associated with a pair of laser beams. We label the levels of the atom as $|1\rangle$, $|2\rangle$ and $|3\rangle$, and we consider that one field is quasi-resonant to the transition $|1\rangle \rightarrow |2\rangle$ whereas the other field is quasi-resonant to the transition $|2\rangle \rightarrow |3\rangle$. Ω_1 will denote the Rabi frequency of the first laser and Ω_2 of the second.
There are three possible configurations for the levels mentioned above, illustrated in figure 1.3.

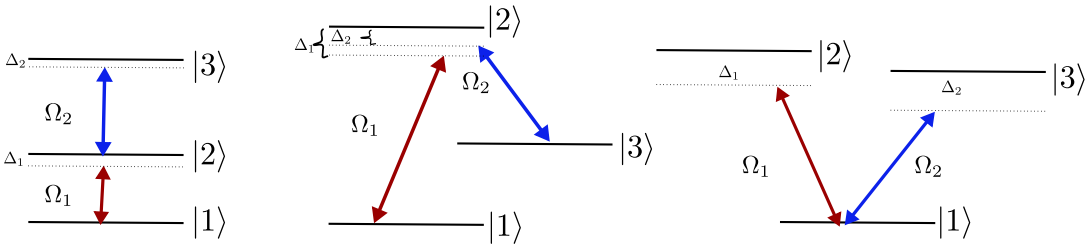

Figure 1.3: The three possible configurations of a three-level atom: (a) Ladder, (b)$\boldsymbol{\Lambda}$ and (c)$\boldsymbol{V}$ configuration.

The corresponding Hamiltonian describing the dynamics is

$$H = \hbar\omega_2\hat{\sigma}_{22} + \hbar\omega_3\hat{\sigma}_{33} + \hbar\frac{\Omega_1}{2}\left(\hat{\sigma}_{21}e^{i\omega_1 t} + \text{h.c.}\right) + \hbar\frac{\Omega_2}{2}\left(\hat{\sigma}_{32}e^{i\omega_2 t} + \text{h.c.}\right). \tag{1.37}$$

In the last equation $E_2 = \hbar\omega_2$, $E_3 = \hbar\omega_3$, and $E_1 = 0$. The lasers are detuned from the corresponding transitions by Δ_1 and Δ_2 ($\Delta_1 = |E_2 - E_1| - \hbar\omega_1$ and $\Delta_2 = |E_2 - E_3| - \hbar\omega_2$). We will focus on the ladder configuration since it is the relevant one for experiments involving Rydberg atoms. Note however that all the results following are analogous to the other two configurations up to some modifications.

1.5.1 Dressed state picture and Autler-Townes splitting

To eliminate the fast oscillations, we use the rotating frame defined by

$$\hat{H}_0 = \hbar\begin{pmatrix} 0 & 0 & 0 \\ 0 & \omega_1 & 0 \\ 0 & 0 & \omega_1 + \omega_2 \end{pmatrix}.$$

In this frame, the Hamiltonian (1.37) can be expressed as (where $\hat{U} = e^{\frac{i\hat{H}_0 t}{\hbar}}$)

$$\begin{aligned}\hat{H}_{3\text{ lev}} &= \hat{U}\hat{H}\hat{U}^\dagger + i\hbar(\partial_t\hat{U})\hat{U}^\dagger \\ &= \Delta_1\hat{\sigma}_{22} + (\Delta_1+\Delta_2)\hat{\sigma}_{33} + \hbar\frac{\Omega_1}{2}\left(\hat{\sigma}_{21}+\text{h.c.}\right) + \hbar\frac{\Omega_2}{2}\left(\hat{\sigma}_{32}+\text{h.c.}\right).\end{aligned} \tag{1.38}$$

It turns out that if we have two-photon resonance ($\Delta_2 = -\Delta_1$), the eigenvectors and eigenvalues of Hamiltonian (1.38) have a compact form. If we define θ and ϕ by [7]:

$$\begin{aligned}\tan\theta &= \frac{\Omega_1}{\Omega_2}, \\ \tan 2\phi &= \frac{\sqrt{\Omega_1^2+\Omega_2^2}}{\Delta_1},\end{aligned} \tag{1.39}$$

then the eigenvectors of Hamiltonian (1.38) are

$$\begin{aligned}|a_+\rangle &= \sin\theta\sin\phi\,|1\rangle + \cos\phi\,|2\rangle + \cos\theta\sin\phi\,|3\rangle, \\ |a_0\rangle &= \cos\theta\,|1\rangle - \sin\theta\,|3\rangle, \\ |a_-\rangle &= \sin\theta\cos\phi\,|1\rangle - \sin\phi\,|2\rangle + \cos\theta\cos\phi\,|3\rangle.\end{aligned} \tag{1.40}$$

and the respective eigenvalues are

$$\begin{aligned}E_+ &= \frac{\hbar}{2}\left(\Delta_1 + \sqrt{\Delta_1^2+\Omega_1^2+\Omega_2^2}\right), \\ E_- &= \frac{\hbar}{2}\left(\Delta_1 - \sqrt{\Delta_1^2+\Omega_1^2+\Omega_2^2}\right), \\ E_0 &= 0.\end{aligned} \tag{1.41}$$

In particular, state $|a_0\rangle$ is called dark state since this state is not coupled to light. The energy separation between energies E_+ and E_- is the origin of the Autler-Townes splitting [8]. The original line of absorption for the probe laser is split into two lines, each belonging to the states $|a_+\rangle$ and $|a_-\rangle$. From the expressions of the energies we see that the splitting becomes more noticeable as the laser intensities increase.

1.5.2 Decay of a three-level atom

Consider a three-level atom described by the Hamiltonian

$$\hat{H} = \sum_{i=1}^{3} E_i \hat{\sigma}_{ii}, \tag{1.42}$$

where E_i are the energies of the three levels. We assume that $|1\rangle \to |2\rangle$ and $|2\rangle \to |3\rangle$ are the only dipole-allowed transitions. By a process analogous to the section 1.4.1, we can deduce that the master equation in the Born-Markov approximation describing the decay of the atom is [9]

$$\begin{aligned}\dot{\rho} = &-\frac{i}{\hbar}\left[\hat{H}, \rho\right] \\ &+ \sum_{i,j} \gamma_i \left[(\bar{n}_i + 1)\left(2\hat{S}_j \rho \hat{S}_i^\dagger - \rho \hat{S}_i^\dagger \hat{S}_j - \hat{S}_i^\dagger \hat{S}_j \rho\right) + \bar{n}_i \left(2\hat{S}_j^\dagger \rho \hat{S}_i - \rho \hat{S}_i \hat{S}_j - \hat{S}_i \hat{S}_j^\dagger \rho\right)\right],\end{aligned} \tag{1.43}$$

where

$$\hat{S}_1 = \hat{\sigma}_{12} \qquad \hat{S}_2 = \hat{\sigma}_{23}.$$

If the frequencies $\omega_{12} \equiv \frac{|E_2 - E_1|}{\hbar}$ and $\omega_{23} \equiv \frac{|E_3 - E_2|}{\hbar}$ are such that $|\omega_{12} - \omega_{23}|\tau \gg 1$, where τ is the timescale of evolution of the atom, then we can ignore the terms $i \neq j$ and the master equation reduces to

$$\begin{aligned}\dot{\rho} = &-\frac{i}{\hbar}\left[\hat{H}, \rho\right] \\ &+ \sum_{i} \gamma_i \left[(\bar{n}_i + 1)\left(2\hat{S}_i \rho \hat{S}_i^\dagger - \rho \hat{S}_i^\dagger \hat{S}_i - \hat{S}_i^\dagger \hat{S}_i \rho\right) + \bar{n}_i \left(2\hat{S}_i^\dagger \rho \hat{S}_i - \rho \hat{S}_i \hat{S}_i - \hat{S}_i \hat{S}_i^\dagger \rho\right)\right],\end{aligned} \tag{1.44}$$

where γ_2 and γ_3 are the decay rates of levels $|2\rangle$ and $|3\rangle$. $\bar{n}_2$ and $\bar{n}_3$ are the number of thermal photons at frequencies ω_{12} and ω_{23}. If we consider a group of N atoms that decay independently one from another, the master equation that governs the evolution of the whole atomic system is

$$\begin{aligned}\dot{\rho} = &-\frac{i}{\hbar}\left[\hat{H}, \rho\right] \\ &+ \sum_{\mu} \sum_{i} \gamma_i (\bar{n}_i + 1)\left(2\hat{S}_i^{(\mu)} \rho \hat{S}_i^{(\mu)\dagger} - \rho \hat{S}_i^{(\mu)\dagger} \hat{S}_i^{(\mu)} - \hat{S}_i^{(\mu)\dagger} \hat{S}_i^{(\mu)} \rho\right) \\ &+ \gamma_i \bar{n}_i \left(2\hat{S}_i^{(\mu)\dagger} \rho \hat{S}_i^{(\mu)} - \rho \hat{S}_i^{(\mu)\dagger} \hat{S}_i^{(\mu)} - \hat{S}_i^{(\mu)} \hat{S}_i^{(\mu)\dagger} \rho\right),\end{aligned} \tag{1.45}$$

where μ labels the atoms, and $S_i^{(\mu)}$ is an operator acting on the space of the atom μ.

Note that this type of equation could be obtained for atoms of more than three levels, as long as all its transition frequencies satisfy $|\omega_i - \omega_j|\tau \gg 1$.

1.5.3 Electromagnetic induced transparency

When we have a system with multiple pathways of excitation we can have Fano interference. The amplitude probabilities of the different pathways can interfere on a constructive or destructive way, and produce an enhancement or attenuation of certain properties of the system. Under certain conditions, the different routes to excitation on three-level atoms can destructively interfere and suppress the absorption of light. This is known as electromagnetic induced transparency (EIT) [7].

In order to describe EIT, let us consider an ensemble of three-level atoms in the ladder configuration interacting with two lasers as illustrated in figure 1.3. We will assume that $|2\rangle$ decays to $|1\rangle$ with decay rate Γ_2. The evolution of this ensemble is described by the master equation (equation (1.45))

$$\dot{\rho} = \frac{1}{i\hbar}\left[\hat{H}_{\text{int}}, \rho\right] + \frac{\Gamma_2}{2}\left(2\hat{\sigma}_{12}\rho\hat{\sigma}_{21} - \hat{\sigma}_{22}\rho - \rho\hat{\sigma}_{22}\right). \tag{1.46}$$

Incidentally, we note that the steady state of equation (1.46) if we have two-photon resonance is $\rho_{\text{st}} = |a_0\rangle\langle a_0|$. This observation will be useful later in chapter 4.

The polarization density of the medium $\mathbf{P}$ in the linear regime is characterized by the linear susceptibility χ,

$$\mathbf{P} = \epsilon_0 \chi \mathbf{E}. \tag{1.47}$$

In terms of elements of the density matrix,

$$\begin{aligned} \mathbf{P} &= \sum_i \frac{\langle e\mathbf{r}\rangle}{V} \\ &= \frac{N}{V}\left[\mathbf{d}_{23}\rho_{23}e^{-i\omega_{23}t} + \mathbf{d}_{12}\rho_{12}e^{-i\omega_{12}t} + c.c.\right]. \end{aligned} \tag{1.48}$$

In the first line, the sum is performed over all atoms, and V is the volume of the sample. In the second line, N is the number of atoms, and we have defined $\mathbf{d}_{ij} \equiv \langle i|e\mathbf{r}|j\rangle$. We have assumed that the intensity of the probe laser is homogeneous across the sample.

We can identify in (1.48) the part of the polarization due to the probe field (by keeping track of the terms that oscillate with ω_1). If we label the field associated to the probe laser as $\mathbf{E}_1$, then the polarization density caused by it is:

$$\mathbf{P}_1 \equiv \epsilon_0 \chi_1 \mathbf{E}_1. \tag{1.49}$$

Assuming that the probe field is weak ($\Omega_1 \ll \Omega_2$) and can be treated as a perturbative effect, in the steady state of the equation (1.46), the linear susceptibility χ_1 for the probe laser is found to be [7]

$$\chi_1 = \frac{|\mathbf{d}_{12}|N}{\epsilon_0 \hbar V} \frac{4(\Delta_1+\Delta_2)(\Omega_2^2 - 4(\Delta_1+\Delta_2)\Delta_1) + 8i\Gamma_2(\Delta_1+\Delta_2)^2}{|\Omega_2^2 + 2i(\Delta_1+\Delta_2)(\Gamma_2 + 2i\Delta_1)|^2}. \tag{1.50}$$

χ_1 depends on every parameter of the system but Ω_1. If χ_1 depended on Ω_1 then equation (1.49) would not reflect a linear relation between the polarization density induced by the probe laser and $\mathbf{E}_1$, since by definition $\Omega_1 = \frac{\mathbf{d}_{12}\cdot\mathbf{E}_1}{\hbar}$.

The absorption coefficient for the probe laser is $A = \mathrm{Im}(\chi_1)$. Note that, if the two-photon detuning $\Delta_1 + \Delta_2$ is zero, we have $A = 0$. This can be intuitively understood by noting that, if $\Delta_1 + \Delta_2 = 0$ and $\Omega_1 \ll \Omega_2$, the steady state is $|a_0\rangle \approx |1\rangle$ (from equation (1.40)). The only state that can contribute to the absorption is $|2\rangle$ (since it is the only state through which photons can be spontaneously emitted). The paths for excitation to $|2\rangle$ are $|1\rangle - |2\rangle$ and $|1\rangle - |2\rangle - |3\rangle - |2\rangle$. Since $\Omega_2 \ll \Omega_1$, both paths have similar probability. Their contributions to the amplitude probability of finding the atom in $|2\rangle$ when the system has reached its steady state must also be similar and cancel each other. In this way we can achieve complete cancellation of absorption[4].

The susceptibility (1.50) predicts both Autler-Townes splitting and EIT. In figure 1.4 we plot A for different values of the Rabi frequency of the coupling laser, Ω_2. It is possible to go from the conditions where Fano interference is not relevant (figure 1.4(a)) to the conditions where it is relevant(figure 1.4(b)) in a continuous manner [10]. On each case the separation of the peaks is roughly Ω_2, as predicted by equation (1.41) in the limit $\Omega_1 \ll \Omega_2$.

[4] A less hand-waving argument for explaining $A = 0$ and its connection with quantum interference comes from building an effective non-hermitian Hamiltonian to describe the system, dissipation included. Expressing the Hamiltonian in the basis of states dressed with the coupling laser one can appreciate that the mathematical formulation of this problem is exactly the same to the Fano problem of autoionization, and the conditions for interference can be identified. For details, see section III B of [7] and references therein.

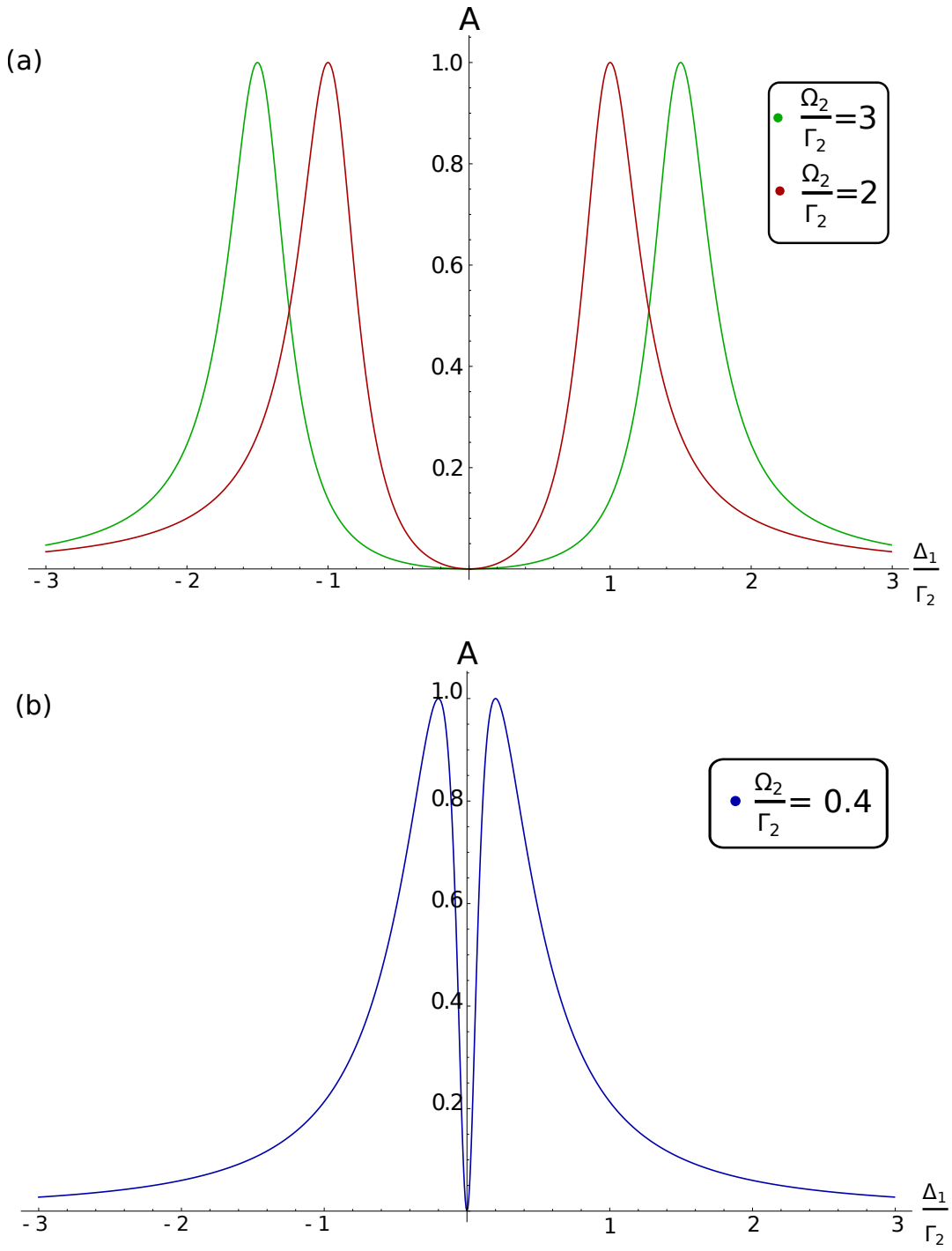

Figure 1.4: Absorption for different values of Ω_2 when $\Delta_2 = 0$ and $\frac{|\mathbf{d}_{12}|N}{\epsilon_0 \hbar V} = 1$. (a) The form of the absorption can be well approximated by the sum of two Lorentzians located at symmetric points around zero. The separation between the peaks is roughly Ω_2. In this range of parameters, Autler-Townes splitting and EIT can be challenging to tell apart experimentally. (b) The effects of Fano interference become evident, since A=0 when $\Delta_1 = 0$. This cannot be reproduced with the sum of two Lorentzians.

1.6 Adiabatic elimination

Let us consider again a three-level atom in the ladder configuration illustrated in figure 1.3. In this section, we will see that if both lasers are far-off resonance and the two-photon transition is nearly resonant ($\Delta_1 + \Delta_2 \simeq 0$), it is possible to describe the atom with an effective master equation involving only levels $|1\rangle$ and $|3\rangle$. The procedure that will allow us to eliminate the level $|2\rangle$ from the description of the atom is called adiabatic elimination [11].

The master equation describing the atom is (1.46). The evolution equations for the populations and coherences are

$$\begin{aligned}
\dot{\rho}_{11} &= \gamma_2\rho_{22} + i\frac{\Omega_1}{2}\left(\rho_{12} - \rho_{21}\right), \\
\dot{\rho}_{12} &= \left(i\Delta_1 - \frac{\gamma_2}{2}\right)\rho_{12} + i\frac{\Omega_1}{2}\left(\rho_{11} - \rho_{22}\right) + i\frac{\Omega_2}{2}\rho_{13}, \\
\dot{\rho}_{13} &= \left(i(\Delta_1 + \Delta_2) - \frac{\gamma_3}{2}\right)\rho_{13} - i\frac{\Omega_1}{2}\left(\rho_{11} - \rho_{22}\right) + i\frac{\Omega_2}{2}\rho_{13}, \\
\dot{\rho}_{22} &= -\gamma_2\rho_{22} + \gamma_3\rho_{33} - i\frac{\Omega_1}{2}\left(\rho_{12} - \rho_{21}\right) + i\frac{\Omega_2}{2}\left(\rho_{23} - \rho_{32}\right), \\
\dot{\rho}_{23} &= \left(i\Delta_2 - \frac{\gamma_2 + \gamma_3}{2}\right)\rho_{23} + i\frac{\Omega_2}{2}\left(\rho_{22} - \rho_{33}\right) - i\frac{\Omega_1}{2}\rho_{13}, \\
\dot{\rho}_{33} &= -\gamma_3\rho_{33} - i\frac{\Omega_2}{2}\left(\rho_{23} - \rho_{32}\right).
\end{aligned} \tag{1.51}$$

If

$$|\Delta_1|,\, |\Delta_2| \gg \Omega_1,\, \Omega_2,\, |\Delta_1 + \Delta_2|,\, \gamma_2, \gamma_3, \tag{1.52}$$

the level 2 will be weakly coupled to levels 1 and 3. Due to this weak coupling, the density matrix elements that relate to level 2 will reach a stationary state faster than other matrix elements. Making $\dot{\rho}_{12} = \dot{\rho}_{22} = \dot{\rho}_{23} = 0$, we obtain three equations that allow us to express ρ_{12}, ρ_{23} and ρ_{22} in terms of the matrix elements concerning levels 1 and 3. We then plug these expressions back in the remaining evolution equations in (1.51). To the lowest order of $\frac{\Omega_i}{\Delta_j}$ and $\frac{\gamma_i}{\Delta_j}$, and assuming $\Delta_2 \simeq -\Delta_1$, the remaining equations read

$$\begin{aligned}
\dot{\rho}_{11} &= \gamma_{\text{eff}}\rho_{33} + i\frac{\Omega_{\text{eff}}}{2}\left(\rho_{13} - \rho_{31}\right), \\
\dot{\rho}_{13} &= \left[i(\Delta_1 + \Delta_2 - \Delta^{(1)} + \Delta^{(3)}) - \gamma_{\text{eff}}\right]\rho_{13} + i\frac{\Omega_{\text{eff}}}{2}(\rho_{11} - \rho_{33}), \\
\dot{\rho}_{33} &= -\gamma_{\text{eff}}\rho_{33} - i\frac{\Omega_{\text{eff}}}{2}(\rho_{13} - \rho_{31}),
\end{aligned} \tag{1.53}$$

with

$$\begin{aligned}
\gamma_{\text{eff}} &= \gamma_3 + \frac{(\gamma_2 + \gamma_3)\Omega_2^2}{(2\Delta_2)^2}, \\
\Omega_{\text{eff}} &= -\frac{\Omega_1\Omega_2}{2\Delta_1}, \\
\Delta^{(1)} &= -\frac{\Omega_1^2}{4\Delta_1}, \\
\Delta^{(3)} &= -\frac{\Omega_2^2}{4\Delta_1}.
\end{aligned}$$

We now note that (1.53) can be expressed as the following master equation

$$\begin{aligned}
\dot{\rho} = &- i\left[(\Delta_1 + \Delta_2 + \Delta^{(3)})\hat{\sigma}_{33} + \Delta^{(1)}\hat{\sigma}_{11} + \frac{\Omega_{\text{eff}}}{2}(\hat{\sigma}_{13} + \hat{\sigma}_{31}), \rho\right] \\
&+ \frac{\gamma_{\text{eff}}}{2}\left(2\hat{\sigma}_{13}\rho\hat{\sigma}_{31} - \hat{\sigma}_{31}\hat{\sigma}_{13}\rho - \rho\hat{\sigma}_{31}\hat{\sigma}_{13}\right).
\end{aligned} \tag{1.54}$$

Equation (1.54) means that, if the conditions (1.52) on the parameters are met, the three-level atom dynamics is equivalent to that of a two-level atom interacting with light, with a direct decay from the excited state $|3\rangle$ to the ground state $|1\rangle$.

Chapter 2

Rydberg atoms

An ensemble of controlled strongly interacting particles is highly desirable for the implementation of quantum information protocols and the simulation of quantum many-body systems. For instance, employing strongly interacting atomic systems, one can realize two-photon logical gates ([12], [13]) and simulate complex condensed matter systems (study thermalization or properties out of equilibrium [14] and many-body physics [15]). These systems are also interesting from the purest theoretical point of view since the interaction among the components of the system usually contributes in a non-trivial manner to the macroscopic response of the system.

Nowadays, several examples of such strongly interacting systems are experimentally available, such as polar molecules and ions [16]. The example that concerns this thesis is Rydberg atoms that interact via the Van der Waals or the dipole interaction. This system has advantages over other systems presenting strong interactions, such as tunability: the selection of the state in which each atom is in can modify the strength, type, and angular dependence of the interaction between two Rydberg atoms. The interaction can be further tuned by the presence of an external electromagnetic field.

One of the most significant consequences of the strong interaction between Rydberg atoms is the dipole blockade. Heuristically, let us consider a gas of Rydberg atoms interacting with a light beam resonant with a transition from the ground state to a Rydberg state. The strong interaction between two nearby excited atoms will take out of resonance states in which two atoms are on a Rydberg state. Consequently, we can approximately describe the system with an effective model of two levels, one in which all the atoms are in the ground state and one in which there is an excitation shared by all the atoms.

In this chapter, we will review how the field of Rydberg quantum optics has evolved during the years. An account of the experiments and theoretical studies that have steered the current research interests of the area will be given so that we can place the present thesis on context. Along with that, we will review the principal properties of

Rydberg atoms. In the end, we will introduce the Rydberg blockade and antiblockade, the phenomena that will concern us for the rest of the thesis.

2.1 Properties of Rydberg atoms

Rydberg atoms are atoms with one or more highly-excited electrons[1]. As we can see in Table 2.1, there are some properties that scale critically with the degree of excitation, thus making Rydberg atoms have exaggerated properties when compared to atoms in lower states.

Table 2.1: Scaling of different properties of Rb atoms with respect to the principal quantum number n. Values are taken from [16].

Property	Scaling	Ground state	43S
Binding energy	n^{-2}	4.18 eV	8.56 meV
Orbit radius	n^2	5.63 a_0	2384.2 a_0
Lifetime	n^3	26.2 ns	42.3 μs
C_6	n^{11}	4707 au	-1.697$\times 10^{19}$au
$\langle 5p\|er\|ns\rangle$	$n^{-1.5}$	4.23 e a_0	0.0103 ea_0
$\langle np\|er\|(n+1)s\rangle$	n^2	-	1069 e a_0

In Table 2.1 we can see that the size of the electron orbit scales as n^2. From the numerical values given in the same table, we can conclude that Rydberg atoms are gigantic compared to their ground state counterpart. An electron on a Rydberg state is loosely tied to the positive core, making the system highly sensitive to external perturbations, such as electromagnetic fields and other atoms. As a result of this, the strength of the interaction between Rydberg atoms[2], characterized by the coefficient C_6, scales as n^{11}.

We can easily understand the scaling of the lifetime: the overlap between the wavefunctions associated with the ground state and a Rydberg state is small, so Rydberg atoms decay slowly. From the numerical examples in the table, we can see that Rydberg

[1] To keep things simple, during this thesis, we will only talk about Rydberg atoms with just one highly excited electron.

[2] The interaction potential between two atoms without permanent electric dipole moment is

$$V(R) = \frac{C_6}{R^6}.$$

states are metastable when compared to the first excited states of the atom.[3]

2.2 Early measurements of Rydberg Atoms

In 1890 R. Rydberg studied the spectral lines of alkaline atoms. According to him, the different series of lines followed the structure

$$E_{n\alpha} = E_{\infty\alpha} - \frac{-Ry}{(n-\delta_\alpha)^2}. \tag{2.1}$$

where $\alpha = s, p, d$ is labeling the different series, and Ry is the Rydberg's constant. $E_{\infty\alpha}$ and δ_α are respectively the limit of the series and the so-called quantum defects.

In the expression (2.1) n is an integer parameter labeling the terms on each series. The physical interpretation for this parameter, previous to the formulation of Quantum Mechanics, was given in 1913 with the Bohr model of the atom. In this model, it is assumed that the atom consists on an electron orbiting circularly around a positive core. Bohr proposed that the angular momentum of the electron could only take integer values of $\hbar$ and that the electron could only give away radiation by transitioning between certain levels of energy. By working with this assumptions we can deduce that the radius of the orbit goes as $r \sim n^2$ and that the energy must go as $E \sim \frac{1}{n^2}$. Having these expressions, physicists at this time were already aware that high-excited atoms could feature exaggerated properties and that they could give origin to interesting physics. Notice that such interpretation is validated by a full quantum description of hydrogenic atoms. Then, the quantum defect can be interpreted as a measure of the discrepancy from hydrogen energies due to the shielding of the nuclear charge by the core electrons in an atom.

Before 1970, there were at least two reasons that made Rydberg atoms an active area for research [18]. First, Rydberg states are at the border between bound states and the continuum, and any process which can result in either excited bound states or ions and free electrons usually leads to the production of Rydberg states. Second, the exaggerated atomic properties of Rydberg atoms made it possible to realize experiments which otherwise would be difficult to do using normal atoms. However, high-precision light sources were not available back then, making the controlled excitation of atoms to high energy states impossible. The existence of such high energy states could only be appreciated in uncontrolled processes. For instance, in 1965, astronomers detected

[3] One might argue that, due to the strong electric dipole moment between adjacent Rydberg states, fast spontaneous decay to other high energy states. This process depends on other quantum numbers like the electronic angular momentum and its projection along the quantization axis; it is also hindered by the small number of vacuum modes in the microwave and terahertz regions under standard conditions [17].

microwave radiation coming from Orion that was evidence of the transition $n_{110} \rightarrow n_{109}$ of hydrogen atoms [19].

2.3 Experiments with light

With the construction of a narrowband tunable dye laser in 1972, precise excitation of atoms became available. This allowed studying the energetic structure of highly excited states of different atoms ([20],[21]) in great detail.

Rydberg atoms are much more sensitive to radiation fields than atoms with low energies. The controlled excitation of Rydberg atoms opened the door to the experimental study of the interaction between atoms and radiation fields. For instance, it became possible to study the interaction between two-level atoms and the field inside a cavity. Since the transition frequencies between two Rydberg states is in the microwave region, using Rydberg states for these experiments facilitated the task of building a near-resonant cavity. This was used by the group of Serge Haroche to probe few-photon fields inside a cavity [22]. It was also proposed by M. Lukin et al. that Rydberg atoms could be used in the processing of quantum information by means of Rydberg blockade [23].

2.3.1 Two-photon excitation scheme

The wavelength of the light needed to excite rubidium atoms directly from the ground state to a Rydberg state is of 279 nm [16], which is in the UV region. Producing UV radiation to excite atoms is expensive and complicated. This is the reason why a two-photon excitation process (figure 2.1) is generally used in most of the experiments with Rydberg atoms. First, light of 780 nm excites the atom from the ground state ($5s_{1/2}$, $F = 2$, $m_F = 2$) to the intermediate state ($5p_{3/2}$, $F = 3$, $m_F = 3$). From there, light of 480 nm excites the atom to a Rydberg state ($ns_{1/2}$, $J = 1/2$, $m_J = 1/2$).

The intensities and detunings of lasers can be chosen to adiabatically eliminate the intermediate level. This is used when one wants the atoms to behave like effective two-level systems, and simulate Ising-type spin models [24]. The parameters can also be tuned to EIT condition, to map the strong Rydberg interaction to photon interactions and nonlinearities [25].

In most of the theoretical work involving Rydberg atoms, the light-atom interaction is modeled using the dipole approximation reviewed in chapter 1. The gigantic size of Rydberg atoms raises the question of how valid is this treatment. For instance, a rubidium atom in 43S has a radius of ~ 100 nm, which is no longer negligible when compared with optical wavelengths. We will still use this description since, in the case

of plane-wave excitation, the rate of dipole-forbidden transitions 5s $\rightarrow$ nd is around 2000 times slower than the rate of dipole-allowed transitions 5s $\rightarrow$ np for $n \in [25, 59]$ [26]. If the light has spatial structure, the dipole-forbidden effects can become more evident. For instance, the excitation of ground state atoms to Rydberg states using Laguerre-Gauss beams was studied in [27]. In this case, the dipole-forbidden transition rates could be as 10 to 100 times slower than dipole-allowed rates.

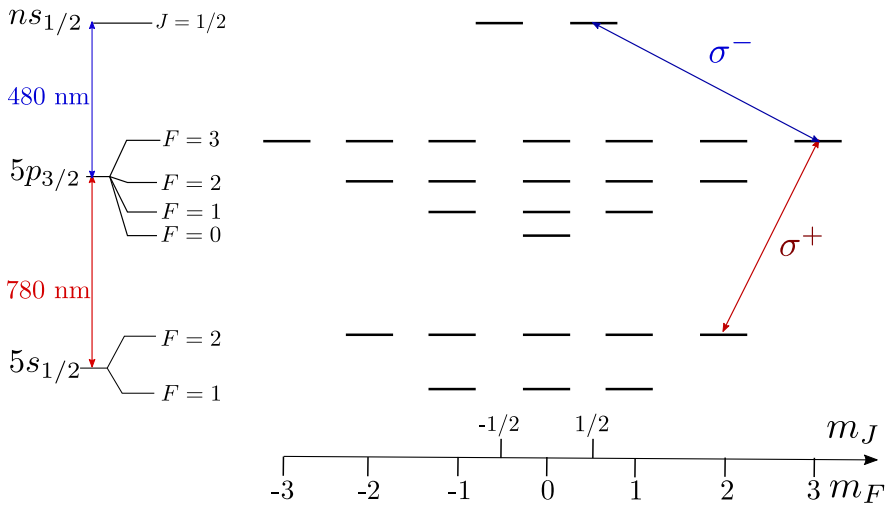

Figure 2.1: Detailed two-photon excitation scheme for ^{87}Rb.

2.4 Interaction between Rydberg atoms

Rydberg atoms interact strongly with one another, due to their large electric dipole moment. To roughly describe the interaction between one atom in a Rydberg state $|r\rangle$ and another one in a Rydberg state $|r'\rangle$, one can add to the Hamiltonian that describes the two atoms an interaction term $\hat{H}_{\text{int}}$ of the form

$$\hat{H}_{\text{int}} = V(\mathbf{R}) \left|rr'\right\rangle \left\langle rr'\right|, \tag{2.2}$$

where $V(\mathbf{R})$ is the interaction potential and $\mathbf{R}$ is the vector connecting atom 1 to atom 2. There are two types of potential of interaction that can be used to describe the interaction:

- Dipole-dipole interaction:

$$V(\mathbf{R}) = \frac{C_3}{R^3}. \tag{2.3}$$

- van der Waals interaction:

$$V(\mathbf{R}) = \frac{C_6}{R^6}. \tag{2.4}$$

C_3 and C_6 are numbers that quantify the strength of the interaction.

The most suitable type of interaction to use in expression (2.2) will be dictated by the degeneracy of the energy of the double state $E_{rr'} = E_r + E'_r$, or the Förster defect between pair states [28].

2.4.1 Förster resonances

The Förster defect between $|rr'\rangle$ and another pair state $|r_1 r_2\rangle$ is the difference between their energies,

$$\Delta(r, r', r_1, r_2) = |E_r + E_{r'} - E_{r_1} + E_{r_2}|.$$

As we will see in section 3.3, the interaction between atoms can be expressed at the lowest order as the dipole-dipole interaction

$$\hat{H}_{\text{int}}(\mathbf{R}) = \frac{\hat{\mathbf{d}}_1 \cdot \hat{\mathbf{d}}_2 - 3(\hat{R} \cdot \hat{\mathbf{d}}_1)(\hat{R} \cdot \hat{\mathbf{d}}_2)}{R^3}, \tag{2.5}$$

where $\hat{\mathbf{d}}_i$ is the dipole moment operator of atom i. $\hat{H}_{\text{int}}(\mathbf{R})$ induces either dipole-dipole (2.3) or van der Waals potential (2.4) depending on the value of the Förster defects between $|rr'\rangle$ and all the other pair states.

First, if $|rr'\rangle$ is such that $\Delta(r, r', r_1, r_2) \neq 0$ for all possible pair states, then we can apply the nondegenerate perturbation theory to estimate the form of the potential. If the states have definite parity, the first-order correction to the energy induced by (2.5) will be zero. The second correction takes the form

$$E^{(2)} = \sum_{r_1, r_2, \Delta(r,r',r_1,r_2) \neq 0} \frac{|\langle r_1 r_2 | \hat{H}_{\text{int}} | rr' \rangle|^2}{\Delta(r, r', r_1, r_2)} \sim \frac{1}{R^6}. \tag{2.6}$$

Then, the interaction potential associated with a pair state with non-zero Förster defects is of the van der Waals type (2.4).

Now assume that there exists a state $|r_1 r_2\rangle$ such that $\Delta(r, r', r_1, r_2) = 0$. The Hamiltonian restricted to the subspace $\{|rr'\rangle, |r_1 r_2\rangle\}$ and shifted by the energy $E_r + E_{r'}$ is

$$\hat{H} = \hbar \begin{pmatrix} 0 & \frac{A}{R^3} \\ \frac{A^*}{R^3} & 0 \end{pmatrix},$$

where $A = \langle rr'|\hat{\mathbf{d}}_1 \cdot \hat{\mathbf{d}}_2 - 3(\hat{R} \cdot \hat{\mathbf{d}}_1)(\hat{R} \cdot \hat{\mathbf{d}}_2)|r_1 r_2\rangle$. The eigenvalues of H are $\lambda_\pm = \pm\frac{|A|}{R^3}$. So, when the state of interest has a zero Förster defect the associated potential is of the dipole-dipole type (2.3).

We finish this parenthesis with two final remarks. Firstly, the condition of degeneracy for having a potential $V(R) \sim \frac{1}{R^3}$ can be met either naturally or using an electric field to shift levels ([29], [30]). Secondly, a more physical way of deriving the van der Waals interaction between two atoms with no permanent dipole moment is using the zero-point field, as in pages 101 to 104 of [5]. Intuitively, the two atoms have no permanent dipole moment. The zero-point field fluctuations can momentaneously induce a dipole moment in one of the atoms. The field produced by the induced moment can induce a dipole moment in the other atom. Thus, the atoms can interact.

The procedure for numerically obtaining the potential $V(\mathbf{R})$ for particular pair states $|rr'\rangle$ is discussed in chapter 3.

2.5 Rydberg blockade

Arguably, one of the most important consequences of the strong interaction between Rydberg atoms is the Rydberg blockade. To explain it, let us consider two two-level atoms, as depicted in figure 2.2 (a). The two levels of each atom are $|g\rangle$ and $|r\rangle$, and $|r\rangle$ is a Rydberg state. Assume that atoms interact through a van der Waals potential of the form $V(R) = \frac{C_6}{R^6}$ only when both atoms are on the Rydberg state. We drive the transition $|g\rangle \to |r\rangle$ with a laser that is described by the Rabi frequency Ω. The Hamiltonian that describes the whole situation (in the RWA) is:

$$\begin{aligned} \hat{H} = {} & E_r |rg\rangle\langle rg| + E_r |gr\rangle\langle gr| + 2Er |rr\rangle\langle rr| + \frac{C_6}{R^6} |rr\rangle\langle rr| \\ & + (\frac{\Omega}{2} |rg\rangle\langle gg| + \frac{\Omega}{2} |gr\rangle\langle gg| + \text{h.c.}). \end{aligned} \tag{2.7}$$

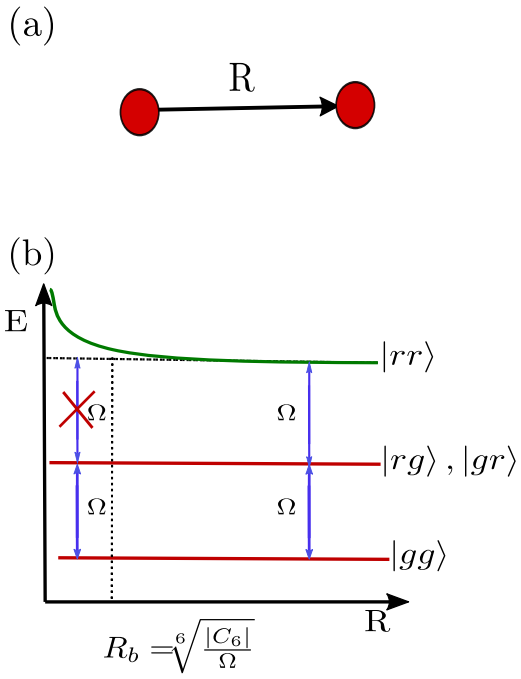

Figure 2.2: Intuitive explanation of Rydberg Blockade: (a) Two atoms separated by a distance **R**. (b) Energies of Hamiltonian (2.7) vs. R. When atoms are far apart, we can excite the system from $|gg\rangle$ to $|rr\rangle$ by means of two photons, since both transitions are resonant. On the other hand, as $R \to 0$, the level $|rr\rangle$ starts bending due to the interaction term in (2.7), taking out of resonance the upper transition.

As illustrated in figure 2.2 (b), only the level $|rr\rangle$ will be shifted due to the interaction. At a characteristic separation between atoms, the blockade radius R_b, excitation to the upmost level due to light starts to be strongly suppressed, and the system of two atoms will contain one excitation at most. The phenomenon just described here is called Rydberg blockade, and it will be a central topic in our study.

The Rydberg-Rydberg interaction was experimentally observed by the broadening of spectral lines in ^{87}Rb [31]. Coherent effects caused by blockade were first observed in [32], and Rydberg blockaded oscillations with two atoms were reported in 2009 [33].

2.6 Rydberg antiblockade

In addition to blockade, when we use the two-photon excitation scheme presented above, we are able to observe antiblockade, or the facilitation of double Rydberg excitation due to interatomic interaction. This effect was theoretically predicted [34], and experimentally observed in [35].

We consider two atoms being excited to a Rydberg state $|ns_{1/2}\rangle$ through two photons, as in figure 2.3. When both atoms are excited, they will interact through the potential $V(\mathbf{R})$,

$$H_{\text{int}} = V(\mathbf{R}) \left|ns_{1/2}, ns_{1/2}\right\rangle \left\langle ns_{1/2}, ns_{1/2}\right| . \tag{2.8}$$

In figure 2.4 (a) we plot the Rydberg population for a single atom in the stationary state vs. Δ_2 when $V(\mathbf{R}) = 0$. The laser inducing the lower transition splits the second level, and we observe a transient Autler-Townes splitting [34].

In figure 2.4 (b) and (c) we plot the Rydberg population and the double Rydberg population when $V(\mathbf{R}) = \frac{\Omega_1}{2}$. We observe that the possibility to excite both atoms to a Rydberg state is enhanced when the shift produced by the Rydberg interaction matches one of the Autler-Townes peaks.

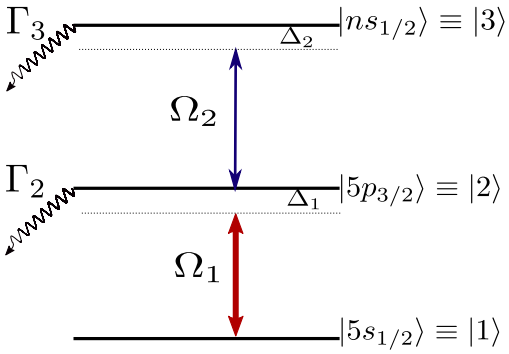

Figure 2.3: Excitation from ground state to a Rydberg level via the first laser, with Rabi frequency Ω_1 and detuning Δ_1, and the second laser with Rabi frequency and detuning Ω_2 and Δ_2. We assume that the decay rates of the two upper levels are respectively Γ_2 and Γ_3 and that the red laser is much more intense than the blue one ($\Omega_2 \ll \Omega_1$).

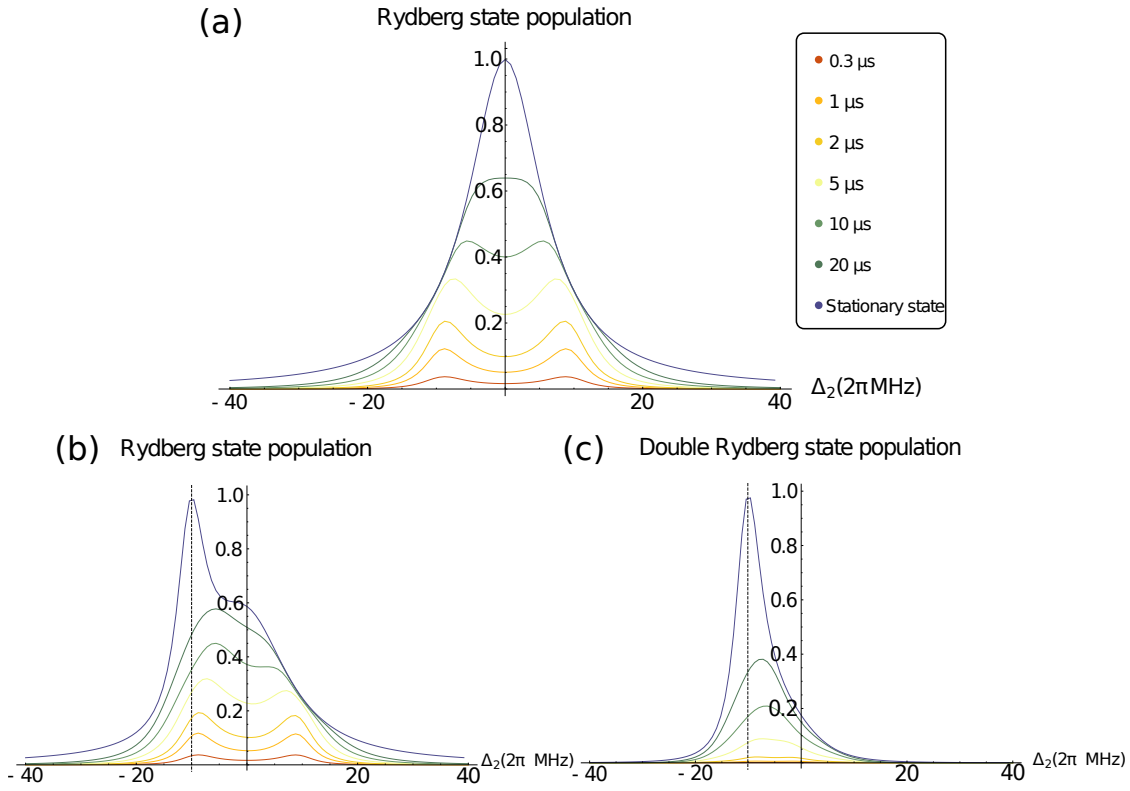

Figure 2.4: (a) Transient Autler-Townes peaks in the population of the Rydberg level in a single atom when the interaction between atoms is zero. (b) Rydberg state population of a single atom and (c) Population of the double excited state when the interaction between atoms is $V(\mathbf{R}) = \frac{\Omega_1}{2}$. The graphs were done for $\Delta_1 = 0$, $\Omega_1 = 20 \times 2\pi$ MHz, $\Omega_2 = 0.8 \times 2\pi$ MHz, $\Gamma_2 = 5 \times 2\pi$ MHz, and $\Gamma_3 = 0$. $\Delta_2 = \frac{\Omega_1}{2}$ is marked with the dark dashed line in (b) and (c).

2.7 Quantum optics with Rydberg atoms

Photons in vacuum do not interact with each other. This presents a severe problem for applications in which we would like to implement gates between photons.

If photons are on a medium, we can create effective interactions among them. Let us imagine first the case in which one photon is not able to significantly change the response of the system to a second photon. This will be the case if there is no interaction among the components of the medium. The photon then gets absorbed by an atom or molecule, but the rest of the components are still unperturbed. On the other hand, there are some media that present nonlinearities at the level of a few photons. That is, few photons are enough to produce a significant change in the response of the medium to incoming photons.

A staple example of a quantum system that can realize a nonlinearity is a single two-level atom (since the atom can only absorb a photon at a time). However, the atom-light coupling is not big enough to ensure that all photons will interact with the atom. One possible solution to this obstacle is to introduce the atom in a cavity.

Another possible candidate for the creation of a few photons nonlinearities is a Rydberg medium. The strong interaction between Rydberg atoms can be mapped to an interaction between photons via electromagnetic induced transparency [36]. For an in-depth review of this and other applications of Rydberg gases, the reader is advised to check [37] and [38].

Chapter 3

Calculation of Rydberg potentials

3.1 Introduction

In this chapter, we will review the procedure to numerically calculate Rydberg potentials. The work of this section is based on the tutorial [40] and was implemented using Matlab. There exists some open source projects targeting Rydberg atoms, such as the Python library ARC [39]. This library is a tool for performing calculations involving alkaline and alkaline earth metal atoms, such as energy diagrams, interaction potentials and Stark maps. The authors of [40] have also released pairinteraction, a software for calculating the interaction potentials discussed in this chapter.

First of all, we should clarify what we mean by a Rydberg potential. Let us think that we have two alkaline atoms. As it was stated in the last chapter, when both atoms are on a Rydberg state, the interaction among them is strong. As a result, the energy of the state in which both atoms are on a Rydberg state is a function of R, the separation between the atoms. See figure (2.2) for example: the energy of the level $|rr\rangle$ is a function $E_{rr}(R)$. This function is what we will call Rydberg potential. The dependence on R of E_{rr} is what ultimately originates the blockade. In order to fully characterize the two-body blockade, the fist natural step is to characterize the potential[1].

Our objective in this section is then to calculate the functions $E_{r_1r_2}(R)$. The subindex r_i contains the quantum numbers that completely describe the state of the atom i: $r_i \equiv (n_i, \ell_i, j_i, m_{j_i})$.

The steps that we will follow to calculate $E_{r_1r_2}(R)$ are:

- Step 1: Calculation of wavefunctions that describe Rydberg states on an alkaline

[1] Although this will not be used in the thesis, Rydberg potentials are also useful to predict the formation of macrodimers [41]: due to multipolar interactions, 2 Rydberg atoms can form a molecule with bond length exceeding $1\mu m$. The formation of such molecules is marked by minima in the Rydberg potentials.

atom.

- Step 2: Selection of significant basis.
- Step 3: Calculation of the energy via a variational calculation for different R.

3.2 Step 1: Wavefunctions of alkaline atoms

Since alkaline atoms are multielectronic atoms, there is not an exact and analytic wavefunction to describe them. However, alkaline atoms are special in the sense that they have only one valence electron. This allows us to approximately describe the atom as one electron and a positive core (composed by the nucleus and the closed electronic shells). This, in turn, allows us to describe the valence electron by a one-body wavefunction. The more excited the valence electron is, the more accurate this approximation is. If it is far away, effects caused by the fact that the atom has many electrons will be negligible.

We will denote the wavefunction describing the valence electron by $\psi_{n\ell m}$. As usual, ℓ represents the orbital angular momentum and m is its projection along the z axis. The wavefunction must satisfy the Schrödinger equation

$$\left(-\frac{\hbar^2}{2m}\nabla^2 + V(r)\right)\psi_{n\ell m} = E_{n\ell m}\psi_{n\ell m}, \tag{3.1}$$

where $V(r)$ describes the action of the positive core on the valence electron, and it is taken to be spherically symmetric. There are two ways in which one can obtain the wavefunctions that satisfy (3.1). The first option is to propose an effective potential that captures the effects of the positive core and to numerically solve the equation. The second option is to use the quantum defect theory to obtain analytical expressions that approximate the real wavefunctions. We next describe each approach and give a comparison between them.

3.2.1 Effective potential and numerical solution

One of the most used parametrizations for $V(r)$ is the one proposed in [1]

$$V_M(r) = -\frac{Z_{nl}(r)}{r} - \frac{\alpha_c}{2r^4}\left(1 - e^{-\left(\frac{r}{r_c}\right)^6}\right) + V_{so}, \tag{3.2}$$

$$Z_{nl}(r) = 1 + (Z-1)e^{-a_1 r} - r(a_3 + a_4 r)e^{-a_2 r},$$

where $V_{so} = \alpha\frac{\mathbf{L}\cdot\mathbf{S}}{r^3}$ is the spin-orbit coupling and Z is the nuclear charge.

We will refer to the potential (3.2) as Marinescu potential. The first term is a Coulomb potential. The function $Z_{nl}(r)$ seeks to model the fact that the positive core is not a point and has a charge distribution and a spatial structure.

The second term takes into account that the closed shells can be deformed in the presence of the valence electron[2]. α_c is the dipole polarizability of the positive core. The factor $\left(1 - e^{-\left(\frac{r}{r_c}\right)^6}\right)$ serves to cut off the unphysical behavior of this term as $r \to 0$.

The parameters a_i and r_c are adjusted so that the energy spectrum of potential (3.2) agrees with the measured spectrum of different alkaline atoms. The values of these parameters for Rb are listed in Table 3.1. They were taken from [1]. $\alpha_c = 9.0760$ and $\alpha = \frac{1}{137}$ is the fine structure constant.

Table 3.1: Parameters of Marinescu potential for Rb

	$\ell = 0$	$\ell = 1$	$\ell = 2$	$\ell \geq 3$
a_1	3.696	4.441	3.787	2.399
a_2	1.649	1.928	1.570	1.768
a_3	-9.861	-16.796	-11.656	-12.071
a_4	0.196	-0.816	0.529	0.772
r_c	1.662	1.502	4.868	4.798

Since this is a central potential, we separate the Schrödinger equation in spherical coordinates. We already know that the angular solution will be spherical harmonics. In order to completely know the wavefunctions and the energies of the problem we need to solve the radial equation

$$\frac{d^2u}{dr^2} + 2\left(E - V_M(r) - \frac{\ell(\ell+1)}{2r^2}\right)u = 0. \tag{3.3}$$

In the last equation we have used $\mu = 1$, $\hbar = 1$ and $u = rR$. R is the radial part of the wavefunction $\psi_{n\ell m}(r, \theta, \phi) = R_{n\ell}(r)Y_{\ell,m}(\theta, \phi)$.

Using the parameters in Table 3.1, we numerically solved the equation (3.3) using the Matrix Numerov method (which is reviewed on Appendix A). We obtained the wavefunctions and energies for principal quantum number between 40 and 80, with

- $\ell = 0$, $j = 1/2$

[2]The interaction potential between a particle with polarizability α_c and an electron separated by $\mathbf{R}$ goes as $V_{\text{p-e}} = -\frac{\alpha_c}{2R^4}$. The electric field generated by the electron at the position of the particle is $\mathbf{E} = -\frac{1}{R^2}\hat{R}$. This field will generate a dipole moment in the particle, $\mathbf{p} = \alpha_c\mathbf{E} = -\alpha_c\frac{1}{R^2}\hat{R}$. The potential felt by the electron due to the induced dipole is $V = \frac{\mathbf{p}\cdot\hat{R}}{R^2} = -\frac{\alpha_c}{R^4}$.

- $\ell = 1$, $j = 1/2$, $3/2$
- $\ell = 2$, $j = 3/2$, $5/2$
- $\ell = 3$, $j = 5/2$, $7/2$

3.2.2 Quantum defect theory and Coulomb functions

An alternative to the numerical solution is to use the quantum defect formalism. The method consists in noting that, for large distances, the potential that describes alkaline atoms must go as an hydrogen-like potential $V \sim \frac{1}{r}$. In addition, the energy of a given level $(n\ell j)$ is modeled as

$$E_{n\ell j} = -\frac{Ry^*}{n^{*2}}. \tag{3.4}$$

Ry^* is the modified Rydberg constant $Ry^* = \frac{Ry}{1+m_e/m_{\text{atom}}}$ and $Ry = 13.6\text{eV}$. The effective principal quantum number is $n^* = n - \delta_\alpha$, in accordance with the series (2.1) measured by Rydberg for alkaline atoms. δ_α is named the defect.

If we insert $V_M \sim \frac{1}{r}$ and the energy (3.4) in the radial equation (3.3), the resultant equation is solved by the so-called Coulomb functions

$$u_{n^*l} = \left(\frac{1}{a_0}\right)^{3/2} \frac{1}{\sqrt{(n^*)^2\Gamma(n^*+l+1)\Gamma(n^*-l)}} W_{n^*,l+1/2}\left(\frac{2r}{n^* a_0}\right), \tag{3.5}$$

where $W_{k,n}$ is the Whittaker function, and Γ is the gamma function. These solutions are only accurate far from the origin, where the real potential resembles $\frac{1}{r}$, so they can be useful to describe Rydberg atoms ([42], [43]). Another limitation of the approximation is that the spin-orbit coupling has been included only indirectly through the energies. Expression (3.4) is also used to express the experimental measured spectra of alkaline atoms. The defect is parametrized as

$$\delta_{nlj} = \delta_0 + \frac{\delta_2}{(n-\delta_0)^2} + \frac{\delta_4}{(n-\delta_0)^4} + ... \tag{3.6}$$

The coefficients δ_i are obtained adjusting (3.4) to the experimental transition energies. We used the coefficients δ_i for Rb reported in [44] and given in Table 3.2.

Table 3.2: Parameters for quantum defects for Rb

	$ns_{1/2}$	$np_{1/2}$	$np_{3/2}$	$nd_{3/2}$	$nd_{5/2}$
δ_0	3.131	0.179	2.642	1.348	1.346
δ_2	0.178	0.290	0.295	-0.603	-0.596

3.2.3 Comparison between the two approaches

In the figure 3.1 we compare 3 of the wavefunctions obtained with Numerov with the Coulomb functions and the wavefunctions given by the ARC library [39].

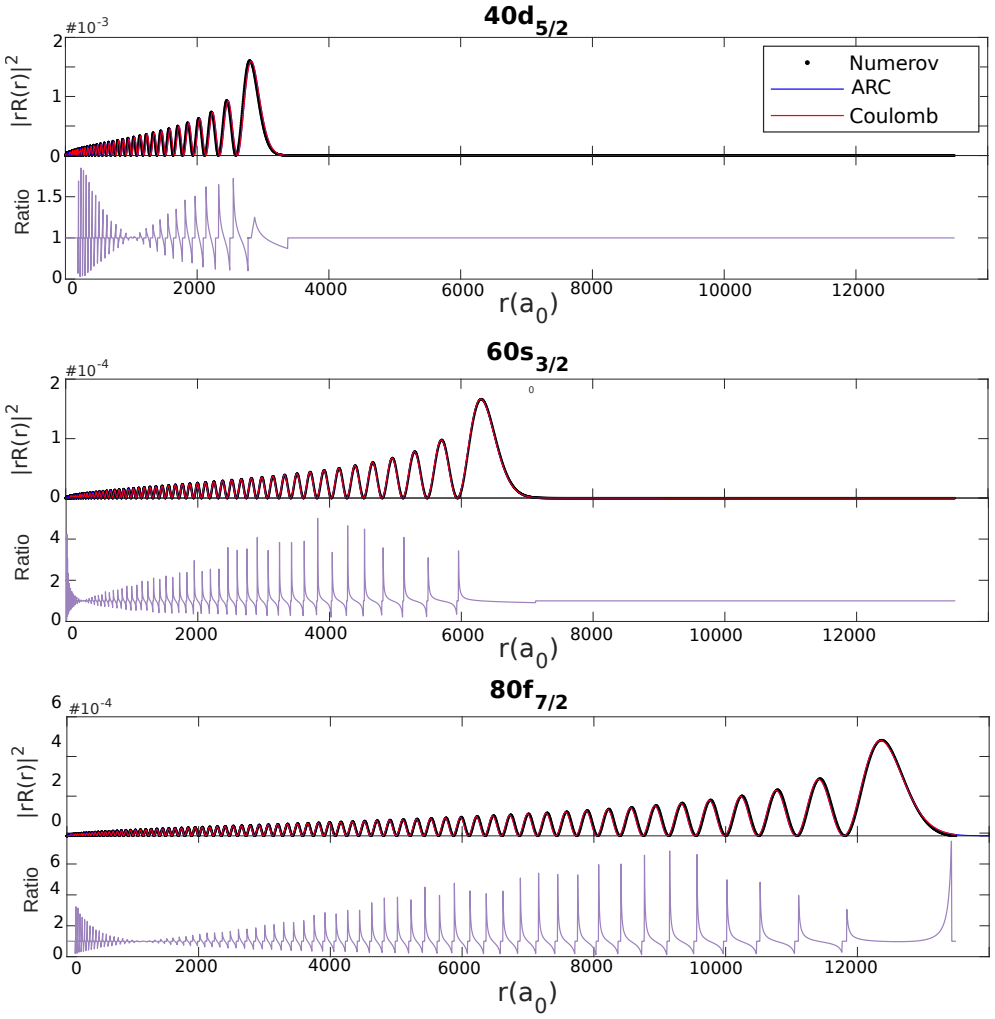

Figure 3.1: Comparison between Numerov, Coulomb and the wavefunctions obtained in ARC [39].The ratio between the Coulomb and Numerov radial probability densities, $\frac{|rR_{\text{coul}}|^2}{|rR_{\text{num}}|^2}$, is plotted in the lower graph on each case. The peaks in the ratio are located at the nodes of the wavefunction

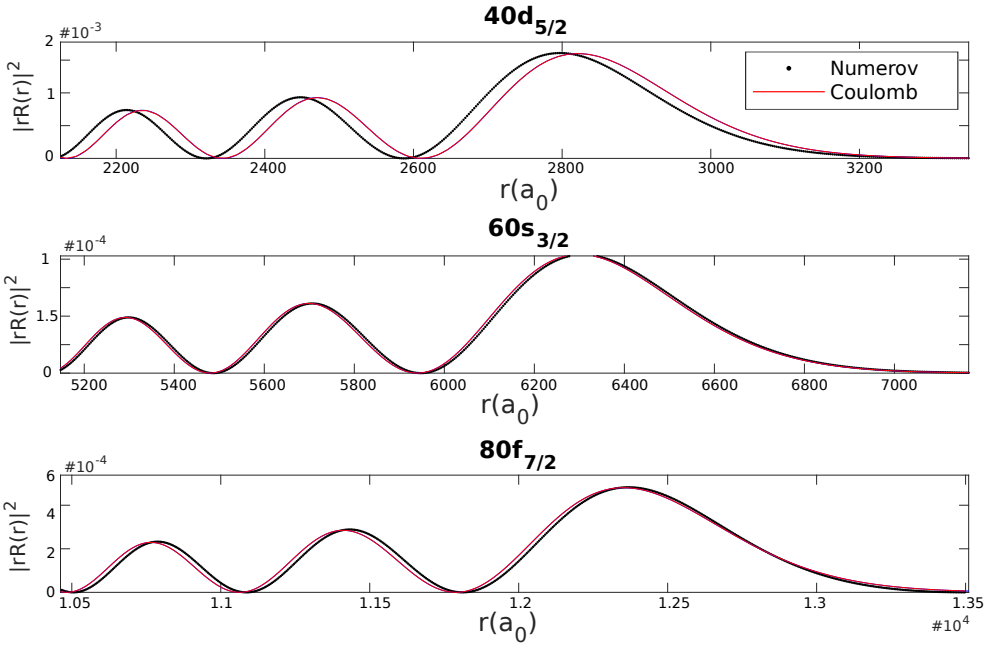

Figure 3.2: The two approaches have a noticeable differences for large r

We see that the two methods agree with the functions from the ARC library. For large r we get that both solutions are appreciably different (figure 3.2). This is expected, since spin-orbit coupling is not directly included in the Coulomb functions. In the next sections we will see how this difference affects the calculation of potentials.

3.3 Interaction between atoms

Now we are ready to take into account the interaction between atoms. Consider two atoms, as in figure 3.3. Each atom has an electron excited to a Rydberg state. Since the timescale of nuclei motion is much larger than the timescale for electronic motion, we can use the Born-Oppenheimer approximation and assume that the nuclei are fixed in space. Hence, $R = |\mathbf{R}|$ can be treated as a parameter of the system rather than as a degree of freedom.

The Hamiltonian describing the system can be written as

$$\hat{H} = \hat{H}_0 + \hat{H}_{\text{int}}, \tag{3.7}$$

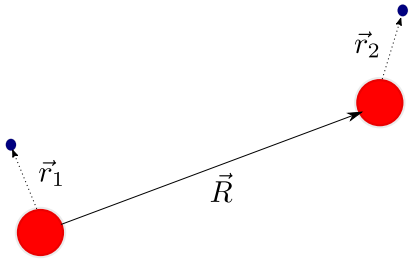

Figure 3.3: Two alkaline atoms separated by a distance R. $\mathbf{r}_i$ represents the relative position of each valence electron relative to the corresponding core.

where H_0 describes the atoms without interactions. We think that R is large enough so that the wavefunctions of the two electrons do not overlap appreciably. We also assume that R is small enough so that we can neglect retardation effects. The electrostatic interaction of the two atoms is given by

$$H_{\text{int}}(\mathbf{R}) = e^2 \left(\frac{1}{|\mathbf{R} + \mathbf{r}_2 - \mathbf{r}_1|} + \frac{1}{|\mathbf{R}|} - \frac{1}{|\mathbf{R} - \mathbf{r}_1|} - \frac{1}{|\mathbf{R} - \mathbf{r}_2|} \right). \tag{3.8}$$

Since the wavefunctions do not overlap we must have $R \gg r_1, r_2$. The interaction of two charge distributions with mass centers connected by a vector $\mathbf{R}$ can be expressed as a sum of multipole terms [45]. If both charge distributions are neutral, the most important contribution is the dipole-dipole interaction potential

$$\hat{H}_{\text{int}}(\mathbf{R}) = \frac{\hat{\mathbf{d}}_1 \cdot \hat{\mathbf{d}}_2 - 3(\hat{R} \cdot \hat{\mathbf{d}}_1)(\hat{R} \cdot \hat{\mathbf{d}}_2)}{R^3}, \tag{3.9}$$

where $\hat{\mathbf{d}}_i \equiv e\, \hat{\mathbf{r}}_i$ is the dipole moment operator of atom i and $\hat{R} = \frac{\mathbf{R}}{|\mathbf{R}|}$.

3.4 Matrix elements

Now we describe how to calculate matrix elements using pairs of the functions calculated in the last section. Let us suppose that we form the basis of N elements

$$\mathbf{B} = \{\psi_{r_{1i}}(\mathbf{r}_1)\psi_{r_{2i}}(\mathbf{r}_2)\}_{i=1}^{N}. \tag{3.10}$$

Each element of the basis is a product of a wavefunction describing atom 1, $\psi_{r_{1i}}(\mathbf{r}_1)$, and a wavefunction describing atom 2, $\psi_{r_{2i}}(\mathbf{r}_2)$ (we continue to use the notation $r_i \equiv (n_i, \ell_i, j_i, m_{j_i})$). Our objective is to calculate the matrix representation of the Hamiltonian (3.7) in this basis.

We note in the first place that $\hat{H}_0$ is diagonal in this basis. These diagonal elements are the sum of the energies of the two atoms without interaction

$$(\hat{H}_0)_{ii} = E_{r_{1i}} + E_{r_{2i}}.$$

We get those energies either from the Numerov results or the quantum defect formula. Since calculating the energies from expressions (3.4), (3.5) and parameters in Table 3.2 is numerically cheaper than storing and later retrieving the energy results of Numerov, we will use the quantum defect expression for energies in the program. Furthermore, we note from figure 3.4 that both results of energy agree quantitatively.

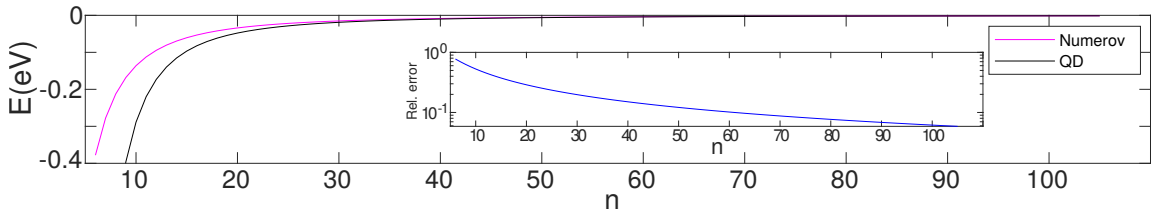

Figure 3.4: Numerov and quantum defect energies for $ns_{1/2}$ vs. n

In order to calculate the matrix elements of the interaction term $\hat{H}_{\text{int}}$ we will first calculate the elements $\langle n\ell jm|\hat{d}_q|n'\ell'j'm'\rangle$, where $\hat{d}_q$ is the q-component of the dipole moment on a given basis. We will use the spherical components

$$\begin{aligned} \hat{d}_0 &= \hat{d}_z, \\ \hat{d}_{\pm 1} &= \mp\frac{\hat{d}_x \pm i\hat{d}_y}{\sqrt{2}}. \end{aligned} \tag{3.11}$$

This will be convenient since we will be able to use the Wigner-Eckart theorem.

3.4.1 Wigner-Eckart theorem

We define an irreducible tensor of range κ as a set of $2\kappa + 1$ operators such that all operators have the same transformation properties as the spherical harmonics $Y_{\kappa q}$ under a rotation of the system of coordinates. We will denote these objects as $\hat{T}_{\kappa q}$. The Wigner-Eckart theorem allows us to express the matrix elements of these objects as

$$\langle n\ell sjm_j|\hat{T}_{\kappa q}|n'\ell's'j'm'_j\rangle = (-1)^{j-m_j}(nlsj||\hat{T}_{\kappa 0}||n'l's'j')\begin{pmatrix} j & \kappa & j' \\ -m_j & q & m'_j \end{pmatrix}. \tag{3.12}$$

$(nlsj||T_{\kappa 0}||n'l's'j')$ is the reduced matrix element,which does not depend neither on m_j and m'_j, nor on q. We put a zero in the subindex instead of a q to explicitly indicate

that this element does not depend on q. The factor (...) is called the Wigner $3j$ symbol (see Appendix B).

The spherical components of the dipole moment form a tensor with range one because we can express them as

$$\hat{d}_q = er\sqrt{\frac{4\pi}{3}}Y_{1q}. \tag{3.13}$$

This means we can apply Wigner-Eckart theorem and the elements we need to calculate will look like (3.12) with $\kappa = 1$. Thus we only need to compute the reduced matrix element $(lsj||\hat{d}_q||l's'j')$. According to [40], this quantity is

$$(nlsj||\hat{d}_q||n'l's'j') = (-1)^{\ell+s+j'+1}(nl||\hat{d}_q||nl')\sqrt{(2j+1)(2j'+1)}\begin{Bmatrix} l & j & s \\ j' & l' & 1 \end{Bmatrix}, \tag{3.14}$$

where $\{...\}$ is the Wigner $6j$ symbol (see Appendix B). $(l||\hat{d}_q||l')$ can be separated in an angular and a radial part

$$\begin{aligned}(nl||\hat{d}_q||n'l') &= \int_0^\infty dr R_{n\ell}(r)(er)R_{n'\ell'}(r)r^2(nl||\sqrt{\frac{4\pi}{3}}Y_{1q}||n'l') \\ &= (-1)^\ell\sqrt{(2\ell+1)(2\ell'+1)}\begin{pmatrix} l & 1 & l' \\ 0 & 0 & 0 \end{pmatrix}\int_0^\infty dr R_{n\ell}(r)(er)R_{n'\ell'}(r)r^2.\end{aligned}$$

In summary, the q component of $\mathbf{d}$ will have matrix elements of the form:

$$\begin{aligned}\langle n\ell jm|\hat{d}_q|n'\ell'j'm'\rangle &= \mu(n,\ell,j,n',\ell',j')C^q(j,m_j,j',m'_j), \\ C^q &= (-1)^{j'-1+m_j}\begin{pmatrix} j' & 1 & j \\ m'_j & q & -m_j \end{pmatrix}, \\ \mu &= (-1)^{j'+1+s}\sqrt{(2\ell+1)(2\ell'+1)(2j+1)(2j'+1)}\begin{pmatrix} l & 1 & l' \\ 0 & 0 & 0 \end{pmatrix} \\ &\times \begin{Bmatrix} j & 1 & j' \\ \ell' & s & \ell \end{Bmatrix}\int_0^\infty dr R_{n\ell}(r)(er)R_{n'\ell'}(r)r^2.\end{aligned} \tag{3.15}$$

On figure 3.5 we graph the radial part of the matrix element (μ) vs the difference of principal quantum numbers of the states involved.

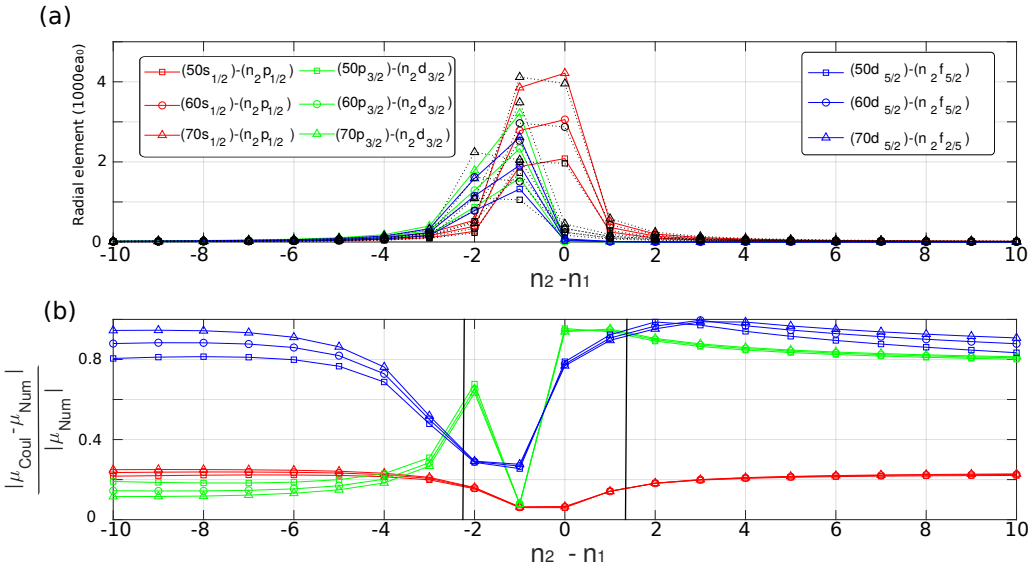

Figure 3.5: (a)Radial matrix element between some states. Data in color corresponds to the results obtained with Coulomb functions. Data in black corresponds to the results with Numerov. (b)Relative difference between color and black data.

The results obtained with Coulomb and Numerov have the same qualitative behavior: both go to zero if the difference between principal quantum numbers increases. We can understand this intuitively. If the two quantum numbers are not alike it means that the overlap between the corresponding wavefunctions will not be big[3]. As we shall see in next section, this observation is useful as a criteria to identify states that will not be relevant for the calculation of a potential.

However, if we quantitatively compare both sets we obtain that the difference is important in some regions and for some angular momenta (figure 3.5(b)). The relative error for the bigger and most relevant matrix elements are enclosed by the black rectangle. The quantitative differences stem from the differences in the wavefunctions for large r depicted in figure 3.2. Since Marinescu potential is more complete than Coulomb functions, in the sense that it includes spin-orbit coupling, we conclude that spin-orbit coupling is important to describe Rydberg atoms in the regions we are interested in (large r), so we will use exclusively Numerov wavefunctions for the next calculations.

[3]Look at the figure (3.1). The biggest contribution for the radial integral that appears in (3.15) will come from the biggest hump of each wavefunction. If the principal quantum numbers are alike it means that the humps have a big overlap. Conversely, if they are too different, the humps will have a negligible overlap and the integral's value will be small.

3.5 Step 2: Relevant basis and symmetries

3.5.1 Energy criterion

Let us suppose that we are calculating the potential for the pair of states $\psi_{n_1,\ell_1,j_1,m_{j_1}}$ and $\psi_{n_2,\ell_2,j_2,m_{j_2}}$ and we have chosen a basis like (3.10) to build the matrix representation of Hamiltonian (3.7).

$\hat{H}_{\rm int}$ will only contribute to non diagonal elements, since all the states have definite parity. The ij entry of the matrix representation will take the form

$$\begin{aligned}(\hat{H})_{ij} &= \langle r_{1i}, r_{2i}|\hat{H}_{\rm int}|r_{1j}, r_{2j}\rangle \\ &= \frac{1}{R^3}\left[\sum_{q=-1}^{1}\langle r_{1i}|\hat{d}_{1q}|r_{1j}\rangle\langle r_{2i}|\hat{d}_{2q}|r_{2j}\rangle - \sum_{q,p=-1}^{1} R_q R_p \langle r_{1i}|\hat{d}_{1q}|r_{1j}\rangle\langle r_{2i}|\hat{d}_{2p}|r_{2j}\rangle\right],\end{aligned} \tag{3.16}$$

where $q = \pm 1, 0$ label the components of vectors in the spherical basis. Thus, these entries contain products of the dipole matrix elements analyzed in the last section. As we have seen, the dipole matrix element $\langle n\ell jm|\hat{d}_q|n'\ell' j' m'\rangle$ tends to zero as the difference $|n - n'|$ increases. This means that the most relevant states to include on the basis are $\psi_{n_3,\ell_3,j_3,m_{j_3}}(\mathbf{r}_1)\psi_{n_4,\ell_4,j_4,m_{j_4}}(\mathbf{r}_2)$ where n_3 is close to n_1 and n_4 is close to n_2 or vice versa (states that do not have such quantum numbers will couple weakly to the state of interest and hence will not contribute to the potential). If the last condition is fulfilled it means that $E_{n_1\ell_1,j_1} + E_{n_2\ell_2,j_2} \simeq E_{n_3\ell_3,j_3} + E_{n_4\ell_4,j_4}$, so the first criterion to reduce the basis can be restated as:

Condition 1: $\psi_{n_3,\ell_3,j_3,m_{j_3}}(\mathbf{r}_1)\psi_{n_4,\ell_4,j_4,m_{j_4}}(\mathbf{r}_2)$ will be included on the relevant basis if $|E - E_{34}| < \Upsilon$, where E is the energy of the state of interest and E_{34} is the energy of state under consideration. Υ controls the number of states that will be included in the basis. A larger Υ means a larger basis, and thus a more accurate potential. The optimal value for Υ will ultimately depend on the range of distances for which we want to obtain the potential, and the degree of accuracy required. In the final version of the program used in this thesis, the user chooses Υ at the beginning of the program[4]. After obtaining the potential, he/she increases Υ and sees if there is a notable change in the obtained potential (through relative errors). The process is continued until an acceptable degree of convergence is reached. An upgraded version of the process would involve automatizing this convergence test.

[4]There is a lower bound for the sensitive initial choice of Υ one can make: Υ should not be smaller than the energetic separation of the target state from adjacent levels.

3.5.2 Symmetries

Once we have applied the energy criterion, we have a finite basis to work with. If the size of the basis obtained is N then we will have to calculate approximately N^2 matrix elements of $\hat{H}_{\text{int}}$. Taking into account extra arguments to reduce the dimension of the basis will reduce the number of required calculations by a power of two. With this motivation, we now turn to analyze the symmetries of an homonuclear diatomic system, and how to use them to further decrease the size of the relevant basis without decreasing the accuracy of the results.

The key argument is that two states with different symmetry properties, namely $|\psi_1\rangle$ and $|\psi_2\rangle$, will not be coupled by the Hamiltonian (that is $\langle\psi_1|\hat{H}|\psi_2\rangle = 0$). This induces a block diagonal structure on the matrix associated to the Hamiltonian, where each block corresponds to states with particular symmetry properties. In order to obtain the potential of a chosen state we only need to include states with the same symmetry properties on the basis.

The symmetry group of an homonuclear system is $D_{\infty h}$. The elements of this group are:

- C_ϕ: Rotation by the angle ϕ about the molecule axis.
- iC_2': Reflection across any plane that contains the molecule axis.

These symmetries have an associated conserved quantity. If we align the molecule axis to $\hat{z}$, then the conserved quantity associated to C_ϕ is the component along $\hat{z}$ of the sum of angular momentum. This means

$$\langle n_1\ell_1 s_1 j_1 m_{j_1} n_2\ell_2 s_2 j_2 m_{j_2}|\hat{H}|n_1'\ell_1' s_1' j_1' m_{j_1}' n_2'\ell_2' s_2' j_2' m_{j_2}'\rangle \neq 0 \Leftrightarrow m_{j_1} + m_{j_2} = m_{j_1}' + m_{j_2}'. \tag{3.17}$$

We can exploit the iC_2' symmetry by choosing the xz plane (so the symmetry transformation is $\mathbf{y} \to -\mathbf{y}$) and changing to the basis

$$\begin{aligned} |\psi\rangle_{+/-} = \frac{1}{\sqrt{2}}(& |n_1\ell_1 s_1 j_1 m_{j_1} n_2\ell_2 s_2 j_2 m_{j_2}\rangle \\ & + d(-1)^{l_1+l_2+m_{j_1}+m_{j_2}-j_1-j_2}\,|n_1\ell_1 s_1 j_1 - m_{j_1} n_2\ell_2 s_2 j_2 - m_{j_2}\rangle), \end{aligned} \tag{3.18}$$

where $d = \pm 1$. The Hamiltonian will not couple states + with states -. Note that this state only has well defined total angular momentum if $m_{j_1} + m_{j_2} = 0$. This is because C_ϕ and iC_2' do not commute. For the case $m_{j_1} + m_{j_2} = 0$ we can use both symmetries,

and for the case $m_{j_1} + m_{j_2} \neq 0$ we only use the rotation symmetry.

Another symmetry transformation of the system inversion: ($\mathbf{r}_i \to -\mathbf{r}_i$,$\mathbf{R} \to -\mathbf{R}$). A symmetrized basis that can be used to exploit this symmetry is

$$|\psi\rangle_{g/u} = \frac{1}{\sqrt{2}} \left(|n_1 \ell_1 s_1 j_1 m_{j_1} n_2 \ell_2 s_2 j_2 m_{j_2}\rangle - p(-1)^{l_1+l_2} |n_2 \ell_2 s_2 j_2 m_{j_2} n_1 \ell_1 s_1 j_1 m_{j_1}\rangle \right). \tag{3.19}$$

$|\psi\rangle_{g/u}$ is said to have gerade/ungerade symmetry. $p = \pm 1$ for g/u. The Hamiltonian will not couple gerade states with ungerade ones.

The last symmetry is permutation: $(1, 2) \to (2, 1)$. The basis to exploit this symmetry is

$$|\psi\rangle_{s/a} = \frac{1}{\sqrt{2}} \left(|n_1 \ell_1 s_1 j_1 m_{j_1} n_2 \ell_2 s_2 j_2 m_{j_2}\rangle - f\, |n_2 \ell_2 s_2 j_2 m_{j_2} n_1 \ell_1 s_1 j_1 m_{j_1}\rangle \right), \tag{3.20}$$

where $f = \pm 1$ for symmetric/antisymmetric. Since we have both permutation and inversion symmetry, we can realize by looking at equations (3.19) and (3.20) that $P = (-1)^{\ell_1+\ell_2}$ is also a conserved quantity of the system.

In summary, we further reduce the size of the basis to calculate the potential associated with $\psi_{n_1,\ell_1,j_1,m_{j_1}} \psi_{n_2,\ell_2,j_2,m_{j_2}}$ by:

- Choosing either the gerade or ungerade symmetry for the state for which we want the calculate the potential.
- Calculating $P = (-1)^{\ell_1+\ell_2}$ and $M = m_{j_1} + m_{j_2}$.
- Eliminating states from the basis that does not have the same P or M and symmetrizing the surviving states to match the g or u symmetry chosen for the relevant state.

All these steps amount to choose a block on the diagonal of the matrix depicted in figure 3.6.

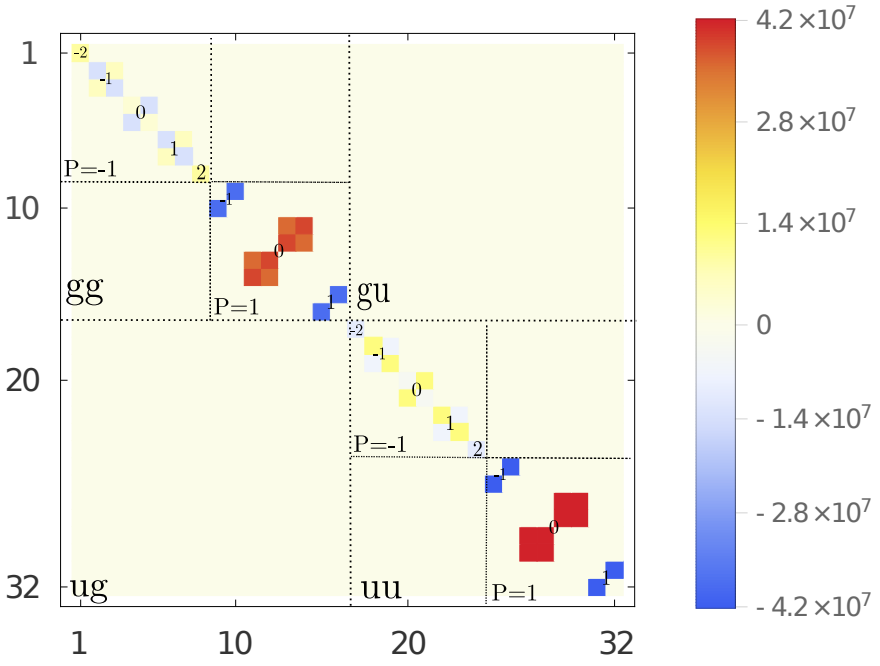

Figure 3.6: Example of the block structure induced by the symmetries of the system. The matrix is divided in gerade and ungerade blocks (gg and uu). Each sub-block is divided in blocks with different P and M.

Figure 3.7 demonstrates that the effort of taking into account the symmetries of the system pays off in the reduction of the size of the problem.

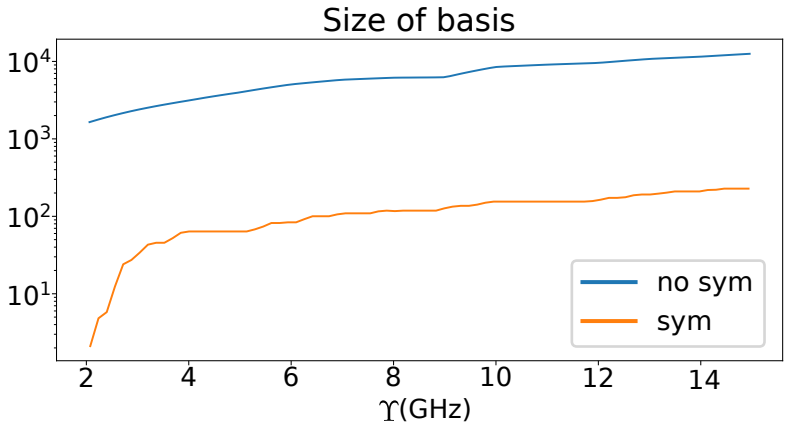

Figure 3.7: Size of the basis vs Υ with and without the use of symmetries when the target state is $116s_{1/2}116s_{1/2}$.

3.6 Step 3: Potentials

3.6.1 Symmetrized matrix elements

Now that we have limited the size of the basis, we are ready to construct the matrix representing the Hamiltonian (3.7).

To calculate the matrix elements we first have to symmetrize the states (gerade or ungerade). Alternatively, we can implement the symmetrization at the level of matrix elements. For this purpose, let us calculate $\langle\psi|d_{q_\alpha}d_{q_\beta}|\phi\rangle$ (which is the type of elements we have to calculate when constructing the matrix associated with $H_{\rm int}$) where $|\psi\rangle$ and $|\phi\rangle$ are states with g or u symmetry

$$
\begin{aligned}
|\psi\rangle &= \frac{1}{\sqrt{2}}\left(|\eta_1\eta_2\rangle - p_\psi(-1)^{l_1+l_2}\,|\eta_2\eta_1\rangle\right),\\
|\phi\rangle &= \frac{1}{\sqrt{2}}\left(|\eta_3\eta_4\rangle - p_\phi(-1)^{l_3+l_4}\,|\eta_3\eta_4\rangle\right),
\end{aligned}
$$

where $\{n_i, l_i, j_i, m_i\} \equiv \eta_i$. By a direct calculation we obtain

$$
\begin{aligned}
2\,\langle\psi|\hat{d}_{q_\alpha}\hat{d}_{q_\beta}|\phi\rangle = {}& \langle\eta_1|\hat{d}_{q_\alpha}|\eta_3\rangle\,\langle\eta_2|\hat{d}_{q_\beta}|\eta_4\rangle - p_\phi(-1)^{l_3+l_4}\,\langle\eta_1|\hat{d}_{q_\alpha}|\eta_4\rangle\,\langle\eta_2|\hat{d}_{q_\beta}|\eta_3\rangle\\
&- p_\psi(-1)^{l_1+l_2}\,\langle\eta_2|\hat{d}_{q_\alpha}|\eta_3\rangle\,\langle\eta_1|\hat{d}_{q_\beta}|\eta_4\rangle\\
&+ p_\psi p_\phi(-1)^{l_1+l_2+l_3+l_4}\,\langle\eta_2|\hat{d}_{q_\alpha}|\eta_4\rangle\,\langle\eta_1|\hat{d}_{q_\beta}|\eta_3\rangle\,.
\end{aligned}
\tag{3.21}
$$

3.6.2 Associated matrix

As we have previously mentioned, the Hamiltonian of the system is given by

$$\hat{H} = \hat{H}_0 + \hat{H}_{\rm int}.$$

$\hat{H}_0$ is diagonal in the chosen basis. The interaction Hamiltonian expressed in terms of the spherical components of the dipole moments of the two atoms is

$$
\begin{aligned}
\hat{H}_{\rm int} \equiv{}& \frac{\hat{\mathbf{d}}_1\cdot\hat{\mathbf{d}}_2 - 3(\hat{r}\cdot\hat{\mathbf{d}}_1)(\hat{r}\cdot\hat{\mathbf{d}}_2)}{r^3}\\
={}& \frac{\hat{d}_{1z}\hat{d}_{2z}(1-3\cos^2\theta) - \hat{d}_{1+}\hat{d}_{2-} - \hat{d}_{1-}\hat{d}_{2+}}{r^3}\\
&- \frac{3\sin^2\theta(\hat{d}_{1+}\hat{d}_{2+} + \hat{d}_{1-}\hat{d}_{2-} - \hat{d}_{1+}\hat{d}_{2-} - \hat{d}_{1-}\hat{d}_{2+})}{2r^3}\\
&- \frac{3\sin\theta\cos\theta(\hat{d}_{1-}\hat{d}_{2z} - \hat{d}_{1+}\hat{d}_{2z} + \hat{d}_{1z}\hat{d}_{2-} - \hat{d}_{1z}\hat{d}_{2+})}{\sqrt{2}r^3},
\end{aligned}
\tag{3.22}
$$

where θ is the angle between the quantization axis and the molecular axis. The matrix elements of each of the operators $\hat{d}_{q_\alpha}\hat{d}_{q_\beta}$ appearing on equation (3.22) can be calculated using the expression (3.21).

3.6.3 Potentials

We are ready to obtain the potential for a given state $\psi_{n_1,\ell_1,j_1,m_{j_1}}\psi_{n_2,\ell_2,j_2,m_{j_2}}$ for a range of separation between atoms $[R_{\min}, R_{\max}]$. For each R on that range, we build the matrix associated to the Hamiltonian and diagonalise it. On each step, we will choose the eigenvalue that matches the eigenvector with the biggest overlap with the state $\psi_{n_1,\ell_1,j_1,m_{j_1}}\psi_{n_2,\ell_2,j_2,m_{j_2}}$. The potential will be the curved formed by the selected points.

Figure 3.8 gives an example of the type of potentials obtained with the procedure described above.

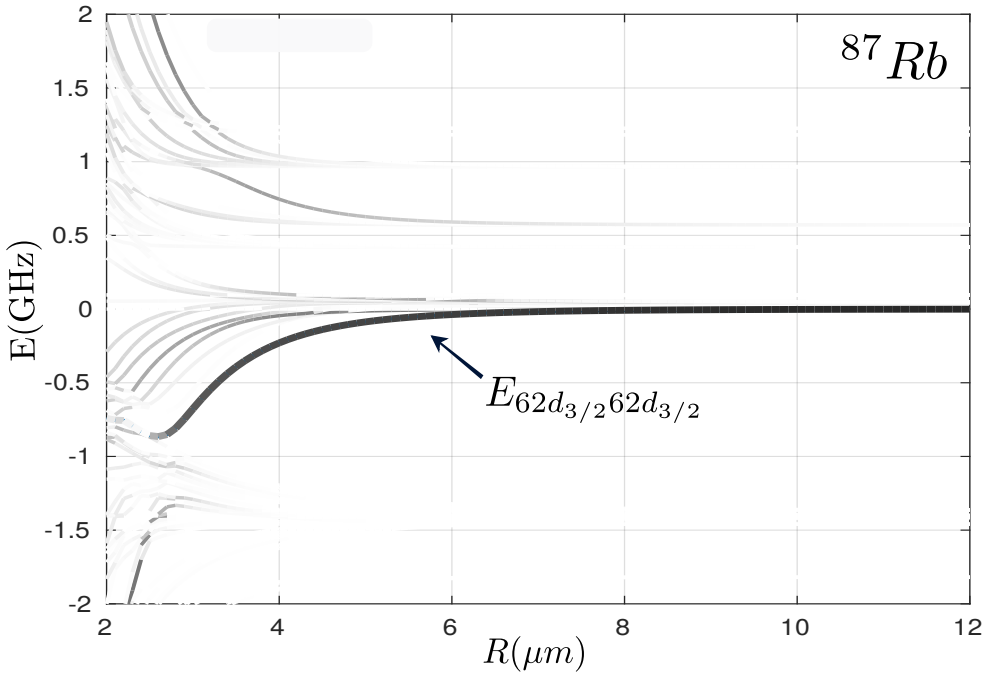

Figure 3.8: Results for the potential of the target state $|62d_{3/2}, 62d_{3/2}\rangle$. The overlap of the corresponding eigenvector with the target state is encoded in the darkness of the curve. The darkest curve corresponds to the potential for $|62d_{3/2}, 62d_{3/2}\rangle$.

What is the validity region for the results? There is no upper limit for the distance between atoms, since for $R \to \infty$ all the energy modifications due to interaction should disappear, and we see that this is indeed the case for our numerical results since

$\hat{H}_{\text{int}} \sim \frac{1}{R^3}$. The distances for which the numerical potentials described here are valid are bounded from below by the Le Roy radius [49]. This is the distance at which the wavefunctions of the valence electrons of each atom start to overlap, so we cannot longer consider that each atom belongs to a specific atom. The Le Roy radius of a pair of alkaline atoms in the same state (n, ℓ, j) is [49]

$$\mathscr{R}_{\text{LR}} = 4\sqrt{\langle n\ell j|\hat{r}^2|n\ell j\rangle}.$$

$\mathscr{R}_{\text{LR}} \sim n^2$, since the expected value of the radius grows as n^2. For $n \sim 60$, $\mathscr{R}_{\text{LR}}$ is approximately 0.18 μm. Clearly, there is another aspect that limits the validity of this potentials for short distances. In section 3.3 we have truncated the multipole expansion describing the interaction. For short distances the ignored terms could become important.

3.6.4 C_6 coefficient

If the state of interest is nondegenerate in the Förster resonance sense (see section 2.4.1), then the form of the interaction potential between two atoms can be approximated as

$$V(R) = \frac{C_6}{R^6}. \tag{3.23}$$

Assume that the state of interest is $|r_n r_n\rangle \equiv |n\ell_1 s_1 j_1 m_1, n\ell_2 s_2 j_2 m_2\rangle$ (i.e. that both atoms have the same principal quantum number). We approximate C_6 by the biggest contribution of expression (2.6), that comes from pair states where both atoms have $n-1$ as principal quantum number

$$C_6 \sim \frac{|\langle r_{n-1} r_{n-1}|\hat{H}_{\text{int}}|r_n r_n\rangle|^2}{\Delta E_{r_{n-1}r_{n-1}r_r r_n}}.$$

The level spacing between adjacent Rydberg levels goes as $\Delta E \sim n^{-3}$:

$$\Delta E_{r_{n-1}r_{n-1}r_r r_n} \sim |\frac{1}{n^2} - \frac{1}{(n-1)^2}| = |\frac{2n-1}{n^2(n-1)^2}| \sim \frac{1}{n^3}.$$

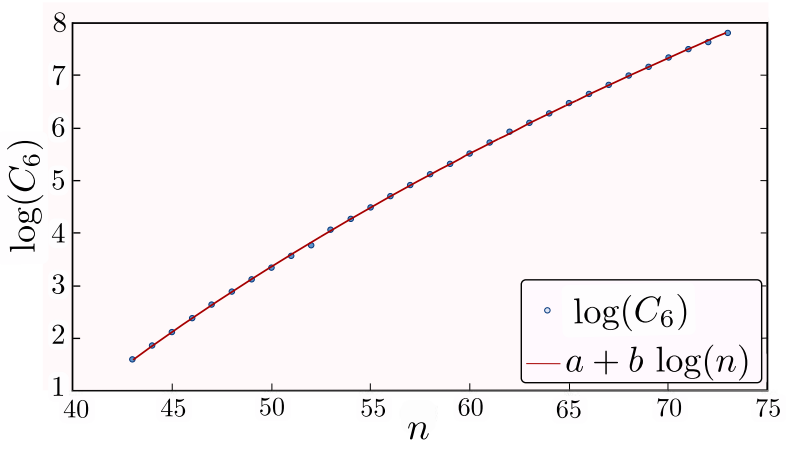

Figure 3.9: $\log(C_6)$ vs log(n). Blue dots are the numerical results and the red line corresponds to the fitted line. The slope of the fit, b=11.81, agrees acceptably with the expected behavior $C_6 \propto n^{11}$.

The numerator, on the other hand, goes as $|\langle r_{n-1}r_{n-1}|\hat{H}_{\text{int}}|r_n r_n\rangle|^2 \sim n^8$, since the transition dipole moment between neighboring levels goes as n^2. This all implies that $C_6 \sim n^{11}$.

We obtain the potentials for pair states of the form $|n\ell jm_j, n\ell jm_j\rangle$. Then, we fit to each curve a function of the type $\frac{C_6}{R^6}$. Figure 3.9 shows the C_6 coefficients obtained with this procedure (blue dots). We see that the behavior $C_6 \sim n^{11}$ agrees well with our numerical results.

3.7 Possible extensions

There are some directions one could take to make a more complete program:

- The addition of an external static electric field to the program would allow to tune the interaction potential (add angular dependence, or change the type of potential from $\sim \frac{1}{r^6}$ to $\sim \frac{1}{r^3}$ by creating a zero Förster defect). The presence of external fields could be implemented by adding H_E to the Hamiltonian, where

$$\hat{H}_E = (-e\hat{\mathbf{r}} \cdot \mathbf{E}) \otimes \mathbb{1} + \mathbb{1} \otimes (-e\hat{\mathbf{r}} \cdot \mathbf{E}). \tag{3.24}$$

  If we express the products in terms of the spherical components of the electric field and $\hat{\mathbf{r}}$, the matrix elements of this addition could be readily calculated with the tools we have. However, a serious complication is added: the electric field would break symmetries that are useful to reduce the dimension of our problem.

- Effects of interactions bigger than the dipole-dipole interaction of equation (3.8) could become important for gases with high density. The higher-order interactions can also be expressed in terms of spherical momenta, allowing to use the Wigner-Eckart theorem to calculate its matrix elements.

Chapter 4

Antiblockade with two Rydberg atoms

Having characterized the interaction between two Rydberg atoms, we now focus on studying the dynamics of two atoms with such interactions driven by lasers. Two ^{87}Rb atoms separated by a distance R are interacting with two lasers. The two lasers can excite each atom individually from the ground state $|5s_{1/2}\rangle$ to a Rydberg state $|60s_{1/2}\rangle$ via a two-photon transition, with $|5p_{3/2}\rangle$ as the intermediate state (figure 4.1(a)). From now on, we will call the ground state $|1\rangle$, the intermediate state $|2\rangle$, and the Rydberg level $|3\rangle$.

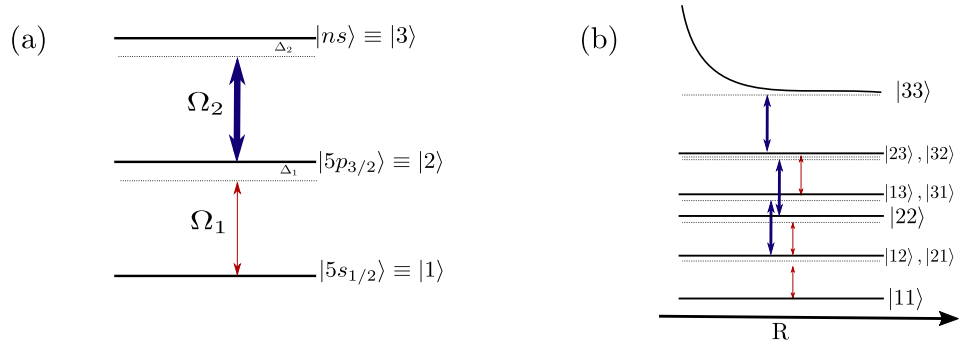

Figure 4.1: (a) Excitation scheme for one atom (b)Excitation scheme for two atoms. The dependence of the energy of the level 33 is due to the Rydberg interaction.

Let ω_1 be the frequency of the red laser and ω_2 be the frequency of the blue laser. The detuning between laser 1 and the transition $|1\rangle \rightarrow |2\rangle$ is $\Delta_1 = \omega_{12} - \omega_1$. Likewise, the detuning between the blue laser and the transition $|2\rangle \rightarrow |3\rangle$ is $\Delta_2 = \omega_{23} - \omega_2$.

The Hamiltonian describing the system is

$$\hat{H} = \sum_{im} \epsilon_i \hat{\sigma_{ii}}^{(m)} + \hat{H}_{dd} - \hat{\mathbf{d}}_1 \cdot [\mathbf{E}_1(\mathbf{x}_1, t) + \mathbf{E}_2(\mathbf{x}_1, t)] - \hat{\mathbf{d}}_2 \cdot [\mathbf{E}_1(\mathbf{x}_2, t) + \mathbf{E}_2(\mathbf{x}_2, t)] \,. \quad (4.1)$$

We denote $\hat{\sigma}_{ij}^{(m)} \equiv |i\rangle_m \langle j|_m$. ϵ_i is the energy of level i, $\hat{\mathbf{d}}_i$ is the electric dipole moment of atom i, $\mathbf{x}_i$ is its position, and $\mathbf{E}_i(\mathbf{x}, t)$ is the electric field of laser i. $\hat{H}_{dd}$ is the static dipole-dipole interaction between the two atoms

$$\hat{H}_{dd} = \frac{\hat{\mathbf{d}}_1 \cdot \hat{\mathbf{d}}_2 - 3(\hat{\mathbf{d}}_1 \cdot \hat{r})(\hat{\mathbf{d}}_2 \cdot \hat{r})}{R^3}. \tag{4.2}$$

4.1 Effective model

In chapter 3, we learned that the static dipole-dipole interaction between the two atoms:

- Admixes Rydberg states. At a given distance R between the atoms, the double-excited state $|33\rangle$ is actually a composition of pair states whose energy is close to the energy of the state of interest,

$$|33(R)\rangle = \sum_{\alpha\beta} c_{\alpha\beta}^{33}(R) \, |\alpha\beta\rangle \, . \tag{4.3}$$

  $c_{\alpha\beta}^{33}(R)$ are the coefficients quantifying the contribution of each basis element $|\alpha\beta\rangle$ to the state $|33(R)\rangle$. We must have

$$\lim_{R\to\infty} |33(R)\rangle = |33\rangle \, ,$$
$$\lim_{R\to\infty} c_{\alpha\beta}^{33}(R) = \delta_{3\alpha}\delta_{3\beta}.$$

  From the diagonalization we also obtain admixed states that asymptotically correspond to other pair states. We will denote these as $|\alpha\beta(R)\rangle$ ($|\alpha\beta(R)\rangle$ tends to $|\alpha\beta\rangle$ as atoms separate).

- Creates a shift of the order of GHz on the energy of the state with two Rydberg atoms. The energy of the double Rydberg state $|33\rangle$ goes as

$$\epsilon_{33}(R) = 2\epsilon_{33}^{\infty} + \Delta_{33}(R), \tag{4.4}$$

  where ϵ_{33}^{∞} denotes twice the energy of level $|3\rangle$ without interaction. Likewise, the energy of the other double Rydberg states will be

$$\epsilon_{\alpha\beta}(R) = 2\epsilon_{\alpha\beta}^{\infty} + \Delta_{\alpha\beta}(R).$$

In the figure 4.1(b), $|3\rangle$ was considered to be the only Rydberg level populated due to the excitation lasers. But in principle, other Rydberg states could be populated due to the admixing and the shifts produced by the interaction. What are the conditions

the system has to fulfill for the diagram to be a reasonable approximation?

In this section, we will deduce the effective model represented in figure 4.1(b), and we will identify the conditions for this to be an acceptable description of the system. First, we need to analyze the part of the Hamiltonian referring only to the atoms

$$\hat{H}_A = \sum_{im} \epsilon_i \hat{\sigma}_{ii}^{(m)} + \hat{H}_{dd}. \tag{4.5}$$

We proceed to review the approximations that can be used to simplify the system.

First approximation

The interaction term (4.2) can a priori mix all atomic states. That is, expressions like (4.3) should follow for all pair states of the system, and not just $|33\rangle$. The first approximation we will make consists in neglecting the admixing of pair states that do not have a double Rydberg excitation.

One atom on a low energy state and one atom on a Rydberg state, or two atoms on low energy states also have a non-zero dipole-dipole interaction. However, these interactions are negligible when compared to the Rydberg-Rydberg interactions. To see this, we consider the numerical values of the dipole matrix elements from Table 2.1:

$$\begin{aligned} \langle 43S|er|44S\rangle &= 1069ea_0, \\ \langle 43S|er|5P\rangle &= 0.0103ea_0, \\ \langle 5P|er|5S\rangle &= 4.23ea_0. \end{aligned}$$

The dipole matrix element between two Rydberg states is at least three orders of magnitude bigger than the dipole matrix element in the other two cases. In chapter 3, we restricted the basis (3.10) to contain just pair states where both atoms were in Rydberg states. Assume that in the calculation described in chapter 3, we included in the basis pair states where one of the atoms is in either $|1\rangle$ or $|2\rangle$. The matrix representing $\hat{H}_A$ would have a structure like the one illustrated in figure 4.2. The section corresponding to pair states with at most one Rydberg excitation would be approximately diagonal, while the section corresponding to two Rydberg excitations would be of the form of figure 3.6.

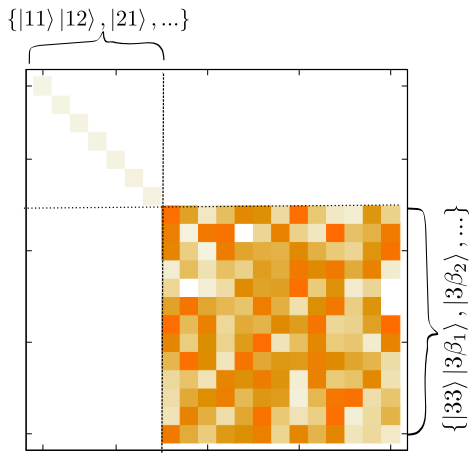

Figure 4.2: Structure of of the matrix representation of $\hat{H}_A$ in the basis $\{|1\rangle, |2\rangle, |3\rangle, |\beta_1\rangle, ...\} \bigotimes \{|1\rangle, |2\rangle, |3\rangle, |\beta_1\rangle, ...\}$. $\{|\beta_i\rangle\}$ are other Rydberg states, in addition to $|3\rangle$. The section corresponding to pair states where with at most one Rydberg excitation is approximately diagonal, so the admixing of pair states of this nature is negligible.

Therefore, the first approximation that we consider is to neglect interactions that do not occur between the Rydberg states. We will assume that the energies of the pair states where at least one of the two atoms is not in a Rydberg state do not change in a significant proportion for the separation range under consideration, and that these states will not admix with other states. Hence, the natural basis for expressing our problem when the distance between atoms is R is

$$\mathscr{B} = \{|11\rangle, |12\rangle, |13\rangle, |21\rangle, |22\rangle, |23\rangle, |31\rangle, |32\rangle\} \cup \{|\alpha\beta(R)\rangle\}_{\alpha,\beta}.$$

In this basis the Hamiltonian takes the form

$$\begin{aligned}\hat{H} = \epsilon_2 \left(\hat{\sigma}_{22}^{(1)} + \hat{\sigma}_{22}^{(2)}\right) + \sum_{\alpha\beta} (\epsilon_\alpha + \epsilon_\beta) \left(\hat{\sigma}_{\alpha\alpha}^{(1)} + \hat{\sigma}_{\beta\beta}^{(2)}\right) \\ + \sum_{\alpha\beta} \Delta_{\alpha\beta}(R) |\alpha\beta(R)\rangle \langle\alpha\beta(R)| - (\hat{\mathbf{d}}_1 + \hat{\mathbf{d}}_2) \cdot (\mathbf{E}_1 + \mathbf{E}_2).\end{aligned} \tag{4.6}$$

Not all the Rydberg levels will enter into the dynamics induced by light. For this to be true, we need that the detuning of laser two and the shifts $\Delta_{\alpha\beta}(R)$ caused by interaction do not combine in a way that allows for an accidental excitation of a double Rydberg state that is not $|33(R)\rangle$. This can be guaranteed if both Δ_2 and $\Delta_{\alpha\beta}(R)$ are much smaller than the characteristic separation of Rydberg states around 60s. This separation is of the order of GHz. In figure 4.3, we plot the shift for 60s60s, following the same color code of the last chapter. We see that for $4\mu m \leq R$ the shift induced is

not appreciable in the scale of GHz.

As long as our atoms are separated by a distance larger than $4\mu m$, double Rydberg states that are not $|33\rangle$ should not enter into the dynamics of the system, and we can reduce the Hamiltonian to

$$\begin{aligned}\hat{H} = \epsilon_2 \left(\hat{\sigma}_{22}^{(1)} + \hat{\sigma}_{22}^{(2)}\right) + \epsilon_3(\hat{\sigma}_{33}^{(1)} + \hat{\sigma}_{33}^{(2)}) + \Delta_{33}(R)\,|33(R)\rangle\,\langle 33(R)| \\ - \hat{\mathbf{d}}_1 \cdot [\mathbf{E}_1(\mathbf{x}_1, t) + \mathbf{E}_2(\mathbf{x}_1, t)] - \hat{\mathbf{d}}_2 \cdot [\mathbf{E}_1(\mathbf{x}_2, t) + \mathbf{E}_2(\mathbf{x}_2, t)]\,.\end{aligned} \tag{4.7}$$

and the relevant basis is

$$\mathscr{B} = \{|11\rangle\,, |12\rangle\,, |13\rangle\,, |21\rangle\,, |22\rangle\,, |23\rangle\,, |31\rangle\,, |32\rangle\,, |33(R)\rangle\}. \tag{4.8}$$

In the next section, we check the validity of the last approximation under realistic density conditions for a cloud of atoms.

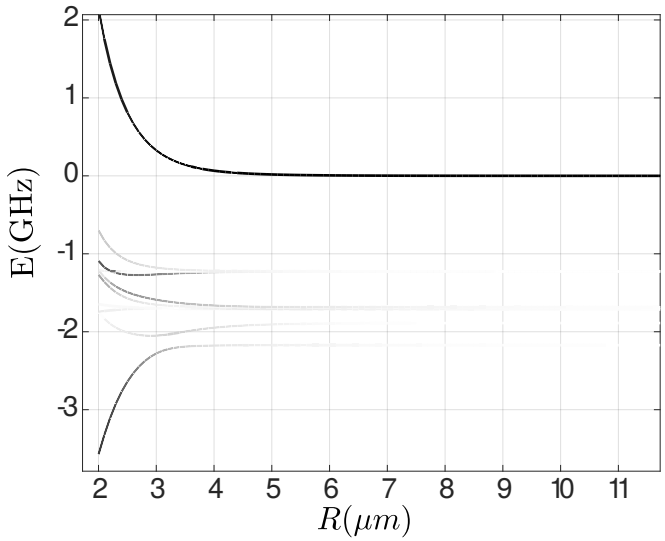

Figure 4.3: The dark curve corresponds to the potential for 60s60s. Lighter curves represent the energy curves for other eigenstates. If we adjust a vdW potential C_6/R^6 to the curve we obtain $C_6 = 251.869\text{GHz}\mu\text{m}^6$.

Second approximation

To test the validity of reducing the basis, we perform an analysis of the probability of finding a pair of atoms closer than $4\mu m$ on a cloud of 10^4 atoms. We assume that the radius of the cloud is 3.33μm.

We consider that each component of the position of each atom follows a Gaussian distribution of the form

$$P(x_i) = \frac{1}{\sqrt{2\pi\sigma^2}} e^{-\frac{x_i^2}{2\sigma^2}}.$$

If we have N atoms within the cloud, then we have $\frac{N(N-1)}{2}$ different pairs of atoms and distances between pairs. These distances have the distribution

$$P_d(d) = \int_{\text{A.S.}} dV_1 \int_{\text{A.S.}} dV_2 \delta(\sqrt{(x_1-x_2)^2+(y_1-y_2)^2+(z_1-z_2)^2} - d) \prod_{\substack{i=1,2 \\ \chi=x,y,z}} P(\chi_i),$$

where $dV_i \equiv dx_i dy_i dz_i$ and the subscript A.S. means that the integral is over all the space. In order to do this integral we change to the variables $x_r = x_1 - x_2$ and $x = x_1 + x_2$ for each component. Writing explicitly each $P(\chi_i)$ and taking into account that for each transformation, the jacobian is $J = \frac{1}{2}$, we get

$$P_d(d) = \frac{1}{(4\pi\sigma^2)^3} \int_{-\infty}^{\infty} dx_r \int_{-\infty}^{\infty} dx ... \delta(\sqrt{x_r^2+y_r^2+z_r^2} - d) e^{-\frac{x_r^2+x^2+y_r^2+y^2+z_r^2+z^2}{4\sigma^2}}.$$

Here we have used the notation ... to indicate that identical integrals are performed for variables y and z.. The integrals on x, y, and z can be done trivially. We then have

$$P_d(d) = \frac{1}{(2\pi^{3/2}\sigma)^3} \int_{-\infty}^{\infty} dx_r ... \delta(\sqrt{x_r^2+y_r^2+z_r^2} - d) e^{-\frac{x_r^2+y_r^2+z_r^2}{4\sigma^2}}.$$

Next we change to spherical coordinates

$$\begin{aligned} P_d(d) &= \frac{1}{(2\pi^{3/2}\sigma)^3} \int_0^{2\pi} d\phi \int_0^{\pi} d\theta \sin\theta \int_0^{\infty} R^2 dR \delta(R-d) e^{-\frac{R^2}{4\sigma^2}} \\ &= \frac{1}{2\sqrt{\pi}\sigma^3} d^2 e^{-\frac{d^2}{4\sigma^2}}. \end{aligned} \tag{4.9}$$

In figure 4.4 we plot the histogram of distances between atoms from a cloud of 10^4 atoms generated with Gaussian distributions for each coordinate, and the distribution (4.9). We observe that the average is above the limit set for the approximation to be valid.

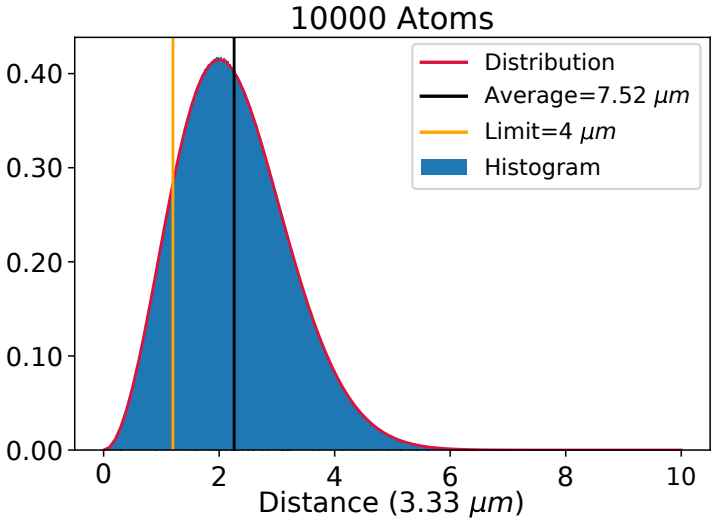

Figure 4.4: Distribution of the separation between atoms in the cloud.

Using the distribution, we find that only around 13% of the pairs of atoms have $R \leq 4\mu m$. From this, we conclude that at least for the case where $|33\rangle = |60s60s\rangle$, the approximation is reasonable. This could become false if instead of 60s60s we have states with bigger principal quantum numbers.

Taking the second approximation to be valid, the Hamiltonian describing the dynamics induced by light is indeed (4.7). The next step is to express the part of the Hamiltonian (4.7) that describes the interaction with light in terms of basis (4.8).

Hamiltonian in the coupled basis

We assume that the electric field of laser 1 is the same at the positions of both atoms $\mathbf{E}_1(\mathbf{x}_1, t) \simeq \mathbf{E}_1(\mathbf{x}_2, t) \equiv \mathbf{E}_1(t)$. We further assume that both lasers can be represented by plane waves. Since laser 1 is resonant with just the lower transition, its interaction with the atoms can be expressed as

$$\hat{H}_1 = -\mathbf{E}_1(t) \cdot (\hat{\mathbf{d}}_1 + \hat{\mathbf{d}}_2) = \frac{\hbar\Omega_1}{2} \sum_{j=1,2} \left(\hat{\sigma}_{12}^{(j)} e^{i\omega_1 t} + \hat{\sigma}_{21}^{(j)} e^{-i\omega_1 t} \right). \tag{4.10}$$

in the rotating wave approximation. The Rabi frequency for the first laser is

$$\Omega_1 = -\frac{\langle 1|\hat{\mathbf{d}}|2\rangle \cdot \mathbf{E}_1}{\hbar}. \tag{4.11}$$

Likewise, we assume the field of laser 2 to be the same at the positions of both atoms. To write the term describing the interaction of the second laser with the atoms, we insert two identities on each side of it:

$$\begin{aligned}\hat{H}_2 &= -\mathbf{E}_2(t)\cdot(\hat{\mathbf{d}}_1+\hat{\mathbf{d}}_2)\\ &= [|11\rangle\langle 11| + |12\rangle\langle 12| + |13\rangle\langle 13| + |21\rangle\langle 21| + |22\rangle\langle 22| + |23\rangle\langle 23|\\ &+ |31\rangle\langle 31| + |32\rangle\langle 32| + |33(R)\rangle\langle 33(R)|][-\mathbf{E}_2\cdot(\hat{\mathbf{d}}_1+\hat{\mathbf{d}}_2)]\\ &[|11\rangle\langle 11| + |12\rangle\langle 12| + |13\rangle\langle 13| + |21\rangle\langle 21| + |22\rangle\langle 22| + |23\rangle\langle 23|\\ &+ |31\rangle\langle 31| + |32\rangle\langle 32| + |33(R)\rangle\langle 33(R)|].\end{aligned}$$

Since the second laser is quasi-resonant only to the transition $|2\rangle \rightarrow |3\rangle$, most of the terms will oscillate with a frequency far from ω_2 and hence can be neglected. The surviving terms are

$$\begin{aligned}\hat{H}_2 &= -\mathbf{E}_2(t)\cdot\mathbf{d}[|12\rangle\langle 13| + |21\rangle\langle 31| + |22\rangle\langle 23| + |22\rangle\langle 32| + \text{h.c}]\\ &- \mathbf{E}_2(t)\cdot[|33(R)\rangle\langle 33(R)|\,(\hat{\mathbf{d}}_1+\hat{\mathbf{d}}_2)(|32\rangle\langle 32| + |23\rangle\langle 23|) + \text{h.c}]\\ &- \mathbf{E}_2(t)\cdot|33(R)\rangle\langle 33(R)|\,(\hat{\mathbf{d}}_1+\hat{\mathbf{d}}_2)\,|33(R)\rangle\langle 33(R)|\,.\end{aligned}$$

In order to calculate the last two terms in the above expression we need to know the coefficients $c^{33}_{\alpha\beta}(R)$ that appear in the expansion of $|33(R)\rangle$ in equation 4.3. In figure 4.5 we plot those coefficients when $3 = 60s_{1/2}$.

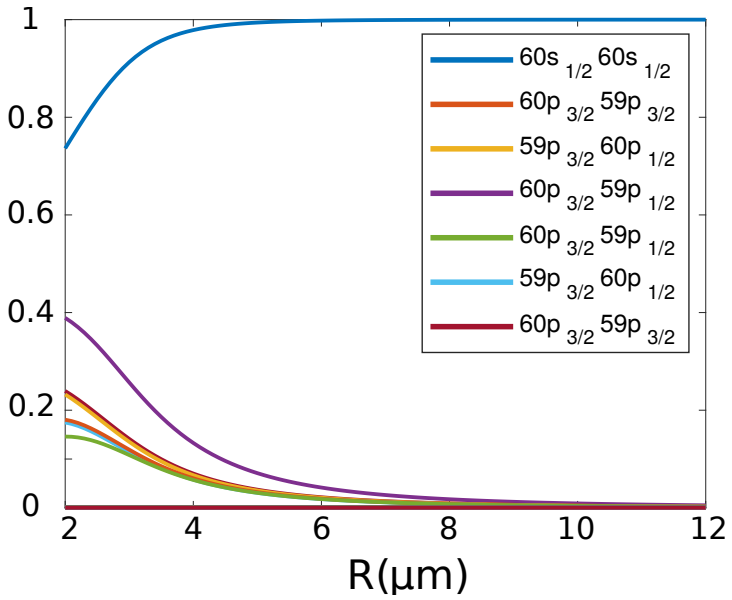

Figure 4.5: The most important composition coefficients of the state $|33(R)\rangle$ vs. R. The principal component corresponds to the state $60s_{1/2}60s_{1/2}$, as expected.

We see that, apart from $|33\rangle$, the most important contributions to $|33(R)\rangle$ come from np-mp states, so we can approximate $|33(R)\rangle$ as

$$|33(R)\rangle = \sum_{\alpha\beta} c^{33}_{\alpha\beta}(R)\,|\alpha\beta\rangle \simeq C_{33}(R)\,|33\rangle + \sum_{ij} C_{ij}(R)\,|p_i p_j\rangle\,. \tag{4.12}$$

This behavior is expected since p-p states directly couple to $|33\rangle$ through H_{dd}. s-s, d-d and s-d states couple only to second order, so their contribution is weaker.
Knowing this, let us calculate one of the remaining terms. We will adopt the notation $c^{33}_{\alpha\beta}(R) \equiv c_{\alpha\beta}$. Taking into account that $|2\rangle$ is odd under a parity transformation and that $|3\rangle$ is even we have

$$|33(R)\rangle\langle 33(R)|\,(\hat{\mathbf{d}}_1+\hat{\mathbf{d}}_2)\,|32\rangle\langle 32| = \sum_{\alpha\beta\gamma\delta} c_{\alpha\beta}c^*_{\gamma\delta}\,\langle\gamma\delta|\hat{\mathbf{d}}_1+\hat{\mathbf{d}}_2|32\rangle\,|\alpha\beta\rangle\langle 32|\,.$$

$|\gamma\delta\rangle$ can be either a p-p Rydberg state or $|33\rangle$. If it is a p-p state we get that

$$\langle\gamma\delta|\hat{\mathbf{d}}_1+\hat{\mathbf{d}}_2|32\rangle = \langle np, mp|\hat{\mathbf{d}}_1|32\rangle = \langle np|\hat{\mathbf{d}}_1|3\rangle\langle mp|2\rangle = 0,$$

since $\hat{\mathbf{d}}_2$ cannot couple states of the same parity. $|\gamma\delta\rangle$ represents a pair of Rydberg states with $m \neq 2$ and hence this term is zero.

So the only non-zero contributions to the sum come from $\gamma = 3, \delta = 3$:

$$|33(R)\rangle\langle 33(R)|\,(\hat{\mathbf{d}}_1+\hat{\mathbf{d}}_2)\,|32\rangle\langle 32| = \sum_{\alpha\beta} c_{\alpha\beta}c^*_{33}\,|\alpha\beta\rangle\langle 32|\,.$$

$|\alpha\beta\rangle\langle 32|$ will oscillate as $e^{it(E_\alpha+E_\beta-E_3-E_2)}$. Assuming this as a fast oscillation except in the case when $\alpha = 3, \beta = 3$, we approximate the last result as

$$|33(R)\rangle\langle 33(R)|\,(\hat{\mathbf{d}}_1+\hat{\mathbf{d}}_2)\,|32\rangle\langle 32| \simeq |c_{33}|^2\,|33\rangle\langle 32|\,. \tag{4.13}$$

Using the same reasoning we get

$$|33(R)\rangle\langle 33(R)|\,(\hat{\mathbf{d}}_1+\hat{\mathbf{d}}_2)\,|23\rangle\langle 23| \simeq |c_{33}|^2\,|23\rangle\langle 23|\,. \tag{4.14}$$

The last term can be written as:

$$|33(R)\rangle\langle 33(R)|\,(\hat{\mathbf{d}}_1+\hat{\mathbf{d}}_2)\,|33(R)\rangle\langle 33(R)| = \textstyle\sum_{\alpha\beta\gamma\delta\zeta\eta\mu\nu} c_{\alpha\beta}c_{\gamma\delta}c^*_{\zeta\eta}c^*_{\mu\nu}\,\langle\zeta\eta|\mathbf{d}_1+\mathbf{d}_2|\alpha\beta\rangle\,|\gamma\delta\rangle\langle\mu\nu|\,.$$

The operator $|\gamma\delta\rangle\langle\mu\nu|$ will rotate at a frequency of $\frac{1}{\hbar}(\epsilon_\gamma+\epsilon_\delta-\epsilon_\mu-\epsilon_\nu)$, that will be of the order of GHz (because all the levels involved are Rydberg levels)[1]. On the other hand, the frequency of the laser is of the order of THz. This means we can neglect this last term. So the term describing the interaction of atoms with the second laser is (applying the RWA in the surviving terms)

[1]This is not true for the case where $\gamma = \mu$ and $\delta = \nu$. These terms will only cause shifts. In particular, they will not induce a non-desired transition to double Rydberg states different from $|33\rangle$.

$$\begin{aligned}\hat{H}_2 = &\frac{\hbar\Omega_2}{2}\left[(|12\rangle\langle 13| + |21\rangle\langle 31| + |22\rangle\langle 23| + |22\rangle\langle 32|)e^{i\omega_2 t} + \text{h.c}\right] \\ &+ \frac{\hbar\Omega_2 c_{33}^2}{2}\left[(|32\rangle\langle 33| + |23\rangle\langle 33|)e^{i\omega_2 t} + \text{h.c.}\right].\end{aligned} \tag{4.15}$$

The complete Hamiltonian is

$$\begin{aligned}\hat{H} = &\epsilon_2\left(\hat{\sigma}_{22}^{(1)} + \hat{\sigma}_{22}^{(2)}\right) + \epsilon_3(\hat{\sigma}_{33}^{(1)} + \hat{\sigma}_{33}^{(2)}) + \Delta_{33}(R)c_{33}(R)^2\,|33\rangle\langle 33| \\ &+ \frac{\hbar\Omega_1}{2}\sum_{j=1,2}\left(\hat{\sigma}_{12}^{(j)}e^{i\omega_1 t} + \text{h.c}\right) + \hat{H}_2.\end{aligned} \tag{4.16}$$

Note that under the approximation $c_{33} \simeq 1$ the Hamiltonian reduces to

$$\begin{aligned}\hat{H} = &\epsilon_2\left(\hat{\sigma}_{22}^{(1)} + \hat{\sigma}_{22}^{(2)}\right) + \epsilon_3(\hat{\sigma}_{33}^{(1)} + \hat{\sigma}_{33}^{(2)}) + \Delta_{33}(R)\,|33\rangle\langle 33| \\ &+ \frac{\hbar\Omega_1}{2}\sum_{j=1,2}\left(\hat{\sigma}_{12}^{(j)}e^{i\omega_1 t} + \text{h.c}\right) + +\frac{\hbar\Omega_2}{2}\sum_{j=1,2}\left(\hat{\sigma}_{23}^{(j)}e^{i\omega_2 t} + \text{h.c.}\right).\end{aligned} \tag{4.17}$$

We will use Hamiltonian (4.17) in next sections, keeping in mind that it is useful as long as $c_{33} \simeq 1$. This happens for $R \geq 4\mu$m (figure 4.5). Results of using (4.17) for $R \leq 4\mu$m need to be validated by comparing them with the results obtained by using Hamiltonian (4.16).

4.2 Rotating Frame

We now express the Hamiltonian (4.17) in the rotating frame defined by

$$\begin{aligned}\hat{H}_0 = &\hbar\begin{pmatrix}0 & 0 & 0\\ 0 & \omega_1 & 0\\ 0 & 0 & \omega_1+\omega_2\end{pmatrix}\otimes\mathbb{I} \\ &+\mathbb{I}\otimes\hbar\begin{pmatrix}0 & 0 & 0\\ 0 & \omega_1 & 0\\ 0 & 0 & \omega_1+\omega_2\end{pmatrix}.\end{aligned}$$

On this frame, the Hamiltonian 4.17 can be expressed as (where $\hat{U} = e^{\frac{i\hat{H}_0 t}{\hbar}}$)

$$\begin{aligned}\bar{H} &= \hat{U}\hat{H}\hat{U}^\dagger + i\hbar(\partial_t\hat{U})\hat{U}^\dagger \\ &= \Delta_1\left(\hat{\sigma}_{22}^{(1)} + \hat{\sigma}_{22}^{(2)}\right) + (\Delta_1+\Delta_2)\left(\hat{\sigma}_{33}^{(1)} + \hat{\sigma}_{33}^{(2)}\right) + \Delta_{33}(R)\,|33\rangle\langle 33| \\ &+ \frac{\hbar\Omega_1}{2}\sum_{j=1,2}\left(\hat{\sigma}_{12}^{(j)} + \text{h.c}\right) + \frac{\hbar\Omega_2}{2}\sum_{j=1,2}\left(\hat{\sigma}_{23}^{(j)} + \text{h.c.}\right).\end{aligned} \tag{4.18}$$

From now on, we will denote $\bar{H}$ simply by $\hat{H}$, taking under consideration that this is expressed in the rotating frame.

4.3 Master equation and simulations

If we consider that $|3\rangle$ decays to level $|2\rangle$ with rate γ_3, and that $|2\rangle$ decays to $|1\rangle$ with rate γ_2, then the master equation that describes the system is (equation (1.45) deduced in the first chapter)

$$\begin{aligned}\dot{\rho} &= -\frac{i}{\hbar}\left[\hat{H},\rho\right] + \mathscr{L}[\rho] \\ \mathscr{L}[\rho] &= \sum_m \frac{\gamma_2}{2}\left(2\hat{\sigma}_{12}^{(m)}\rho\hat{\sigma}_{21}^{(m)} - \hat{\sigma}_{21}^{(m)}\hat{\sigma}_{12}^{(m)}\rho - \rho\hat{\sigma}_{21}^{(m)}\hat{\sigma}_{12}^{(m)}\right) \\ &\quad + \sum_m \frac{\gamma_3}{2}\left(2\hat{\sigma}_{23}^{(m)}\rho\hat{\sigma}_{32}^{(m)} - \hat{\sigma}_{32}^{(m)}\hat{\sigma}_{23}^{(m)}\rho - \rho\hat{\sigma}_{32}^{(m)}\hat{\sigma}_{23}^{(m)}\right).\end{aligned} \tag{4.19}$$

We have set $\bar{n} = 0$ for both decays, since at temperatures equal or lower to the room temperature, the average number of optical photons is negligible.

We used realistic numerical parameters for the system ([35],[47]):

- $\Omega_2 = 2\pi \times 20$ MHz.
- $\Delta_1 = 2\pi \times 100$ MHz, $\Delta_2 = -2\pi \times 100$ MHz.
- The lifetime for 43S in ^{87}Rb is 42.3 μs, so that $\gamma_3 \simeq 0.02$ MHz.
- The lifetime for 5P in ^{87}Rb is 26.2 ns, so that $\gamma_2 \simeq 38$ MHz.

4.3.1 Connected correlation, populations and coherences in the steady state

The steady state of equation (4.19) is the solution of

$$\dot{\rho} = 0. \tag{4.20}$$

This poses a set of coupled algebraic equations for the elements of the density matrix ρ_{ij}. We use Mathematica to obtain the solution. Once we have the steady state ρ_{st}, we calculate the expected values of populations and coherences for each atom. Besides, we calculate the connected correlation, defined as [50]

$$\langle\hat{\sigma}_{33}^{(1)}\hat{\sigma}_{33}^{(2)}\rangle_C = \frac{\langle\hat{\sigma}_{33}^{(1)}\hat{\sigma}_{33}^{(2)}\rangle}{\langle\hat{\sigma}_{33}^{(1)}\rangle\langle\hat{\sigma}_{33}^{(2)}\rangle} - 1. \tag{4.21}$$

This quantity will be useful to define the blockade radius: if the atoms are separated a distance such that the dipolar interaction is negligible, then the atoms are expected to be completely uncorrelated, and $\langle\hat{\sigma}_{33}^{(1)}\hat{\sigma}_{33}^{(2)}\rangle \simeq \langle\hat{\sigma}_{33}^{(1)}\rangle\langle\hat{\sigma}_{33}^{(2)}\rangle$. So $\langle\hat{\sigma}_{33}^{(1)}\hat{\sigma}_{33}^{(2)}\rangle_C \to 0$ when $R \to \infty$. If, on the other hand, the atoms are close to one another and the shift generated by dipolar interaction is important we expect to have Rydberg blockade.

This means we cannot have the two atoms simultaneously excited. Because of this, we expect that as $R \to 0$, $\langle \hat{\sigma}_{33}^{(1)} \hat{\sigma}_{33}^{(2)} \rangle_C \to -1$. The region of the R parameter between these two behaviors will contain the blockade radius.

In figures 4.6, 4.7 and 4.8 we show the results for the connected correlation, the populations and the coherences vs the separation between atoms. Interestingly, if we use Hamiltonian (4.16) instead of Hamiltonian (4.17) (that is, if we take into account that c_{33} depends on the distance), we obtain the same results for the range of distances explored ($R \in [2\mu\text{m}, 12\mu\text{m}]$). In spite of this, we restrict the analysis to $R \geq 4\mu$m since, as we have mentioned, it is the range at which we can safely neglect the effect of Rydberg states other than $|3\rangle$ on the dynamics of the system.

In figure 4.6 we observe an unusual behavior for the correlation function as we lower the ratio $\frac{\Omega_1}{\Omega_2}$. The three cases in the figure obey our intuition asymptotically: as $R \to \infty$ the three of them tend to 0, signaling an uncorrelated evolution between the atoms. At $R \to 0$ the correlation goes to -1, indicating that the double excitation has been inhibited. In the intermediate region, we see a hump with a dip in between. A positive correlation means that the double excitation is favored over a single excitation, signaling an antiblockade. The dip in the middle of the hump is a destruction of this condition.

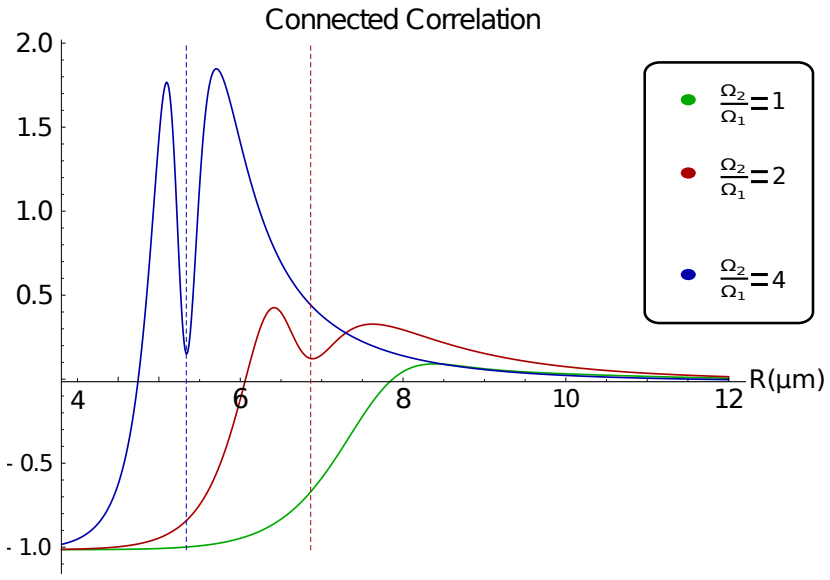

Figure 4.6: Connected correlation for different ratios of the two Rabi frequencies. The structure in the intermediate region appears on a continuous manner as we vary $\frac{\Omega_1}{\Omega_2}$. The blue and red dashed lines indicate the position of the respective dip in the correlation.

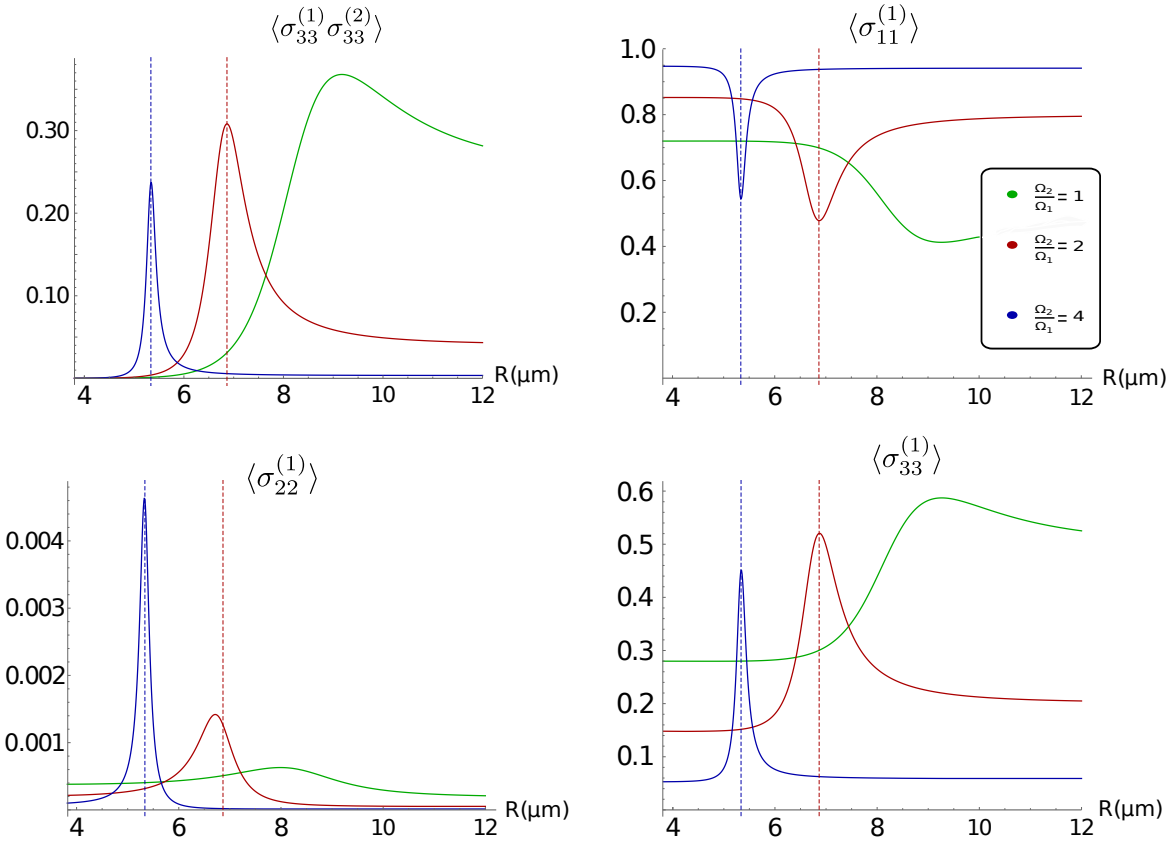

Figure 4.7: Population of the double excited state, first, second and third state of an individual atom. All the plots follow the color code of $\langle \hat{\sigma}_{11}^{(1)} \rangle$. The blue and red dashed lines indicate the position of the dip in the respective correlation.

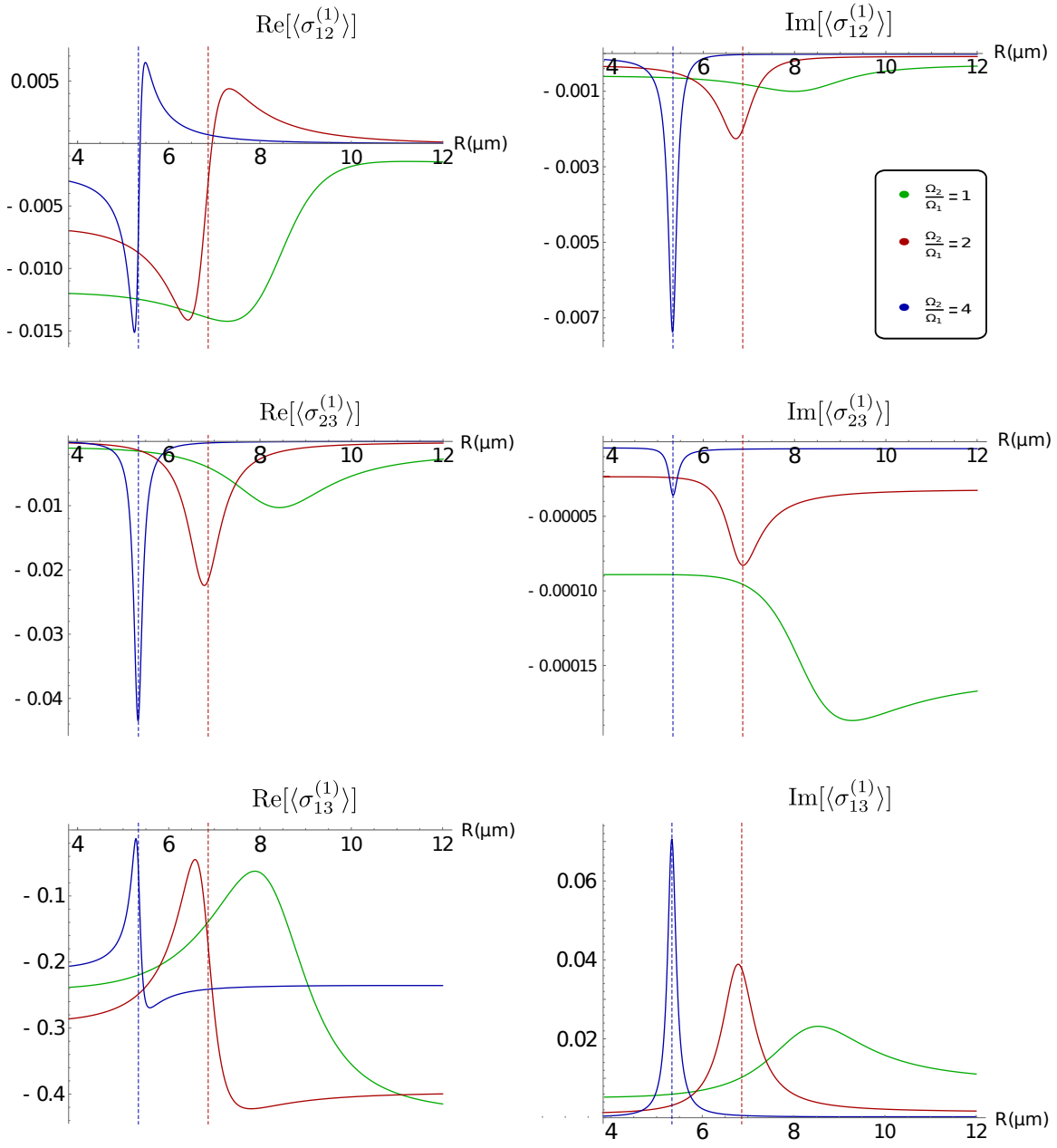

Figure 4.8: Coherences of individual atoms. All the plots follow the color code of $\mathrm{Im}\langle\hat{\sigma}_{12}^{(1)}\rangle$. The blue and red dashed lines indicate the position of the dip in the respective correlation.

In figures 4.7 and 4.8 we see that this dip is accompanied by singular behavior in the populations and coherences of the atom. The dip in the correlation coincides with a dip in the population of the ground state, and a peak in both the populations of the intermediate and Rydberg level (although the population of the intermediate level remains always negligible when compared with the other two populations). At the same

R, the imaginary parts of the coherences present dips. The coherences of individual atoms give information on the electric linear susceptibility of a medium formed by such atoms (see for example equation (1.48)), and thus on the absorption coefficient and refractive index incoming light sees in the medium.

4.3.2 Avoided Crossings

The region of positive correlation occurs around an avoided crossing in the Hamiltonian (4.18) describing the unitary evolution of the system, as noted in figure (4.9).
In the limit $R \to \infty$ the interaction between atoms Δ goes to zero, and we recover

$$\hat{H} = \hat{H}_{3\text{ lev}} \otimes \mathbb{I} + \mathbb{I} \otimes \hat{H}_{3\text{ lev}}, \tag{4.22}$$

where $\hat{H}_{3\text{ lev}}$ is the three-level atom Hamiltonian of chapter 1. For the case of two-photon-resonance the eigenvectors of Hamiltonian (4.22) describing the atoms dressed with light are $|a_i a_j\rangle$ with $i, j = 0, +, -$. From the parameters we have chosen, and expressions for mixing angles and eigenstates, (1.41) and (1.40), we see that $|a_0\rangle \approx |1\rangle$, $|a_+\rangle \approx |2\rangle$ and $|a_-\rangle \approx |3\rangle$.

In figure (4.9) we label different eigenvalues according to the eigenvalue they tend to as $R \to \infty$. From this figure, we observe that eigenvalues appreciably depend on R only when they have a significant contribution of the state $|33\rangle$. In the following, we denote $|a_i a_j\rangle_R$ to be the eigenvector of the system of atoms separated by R that asymptotically corresponds to $|a_i a_j\rangle$.

When atoms are far apart, the only eigenvalue that seems to depend on R is the one corresponding to $|a_- a_-\rangle_R$. The dependence of this curve on R leads to an avoided crossing with the energy curves of $|a_- a_0\rangle_{\pm R}$ at $R \approx 6\mu$m. $|a_- a_0\rangle_{-R}$ is decoupled from states that are symmetric under the exchange of both atoms, so its energy curve will continue to be flat. On the other hand, there will be a mixture between eigenstates corresponding to $|a_- a_0\rangle_{+R}$ and $|a_- a_-\rangle_R$. The energy curve of $|a_- a_0\rangle_{+R}$ goes upwards and makes another avoided crossing with $|a_0 a_0\rangle_R$. At this avoided crossing $|a_0 a_0\rangle_R$ and $|a_- a_0\rangle_{+R}$ admix. This has consequences on the stationary state since $|a_0 a_0\rangle$ is approximately the stationary state of the system without interactions

$$\rho_{\text{st}\infty} \simeq |a_0 a_0\rangle \langle a_0 a_0| .$$

This is due to the fact that $\gamma_2 \gg \gamma_3$ (we saw in chapter 1 that for $\gamma_3 = 0$f the stationary state of one three-level atom is $|a_0\rangle \langle a_0|$). Around the avoided crossing, we should expect an increase in the contribution of $|33\rangle$ in the stationary state. In other words, we should expect the double excitation to be favored and an increase in the connected correlation.

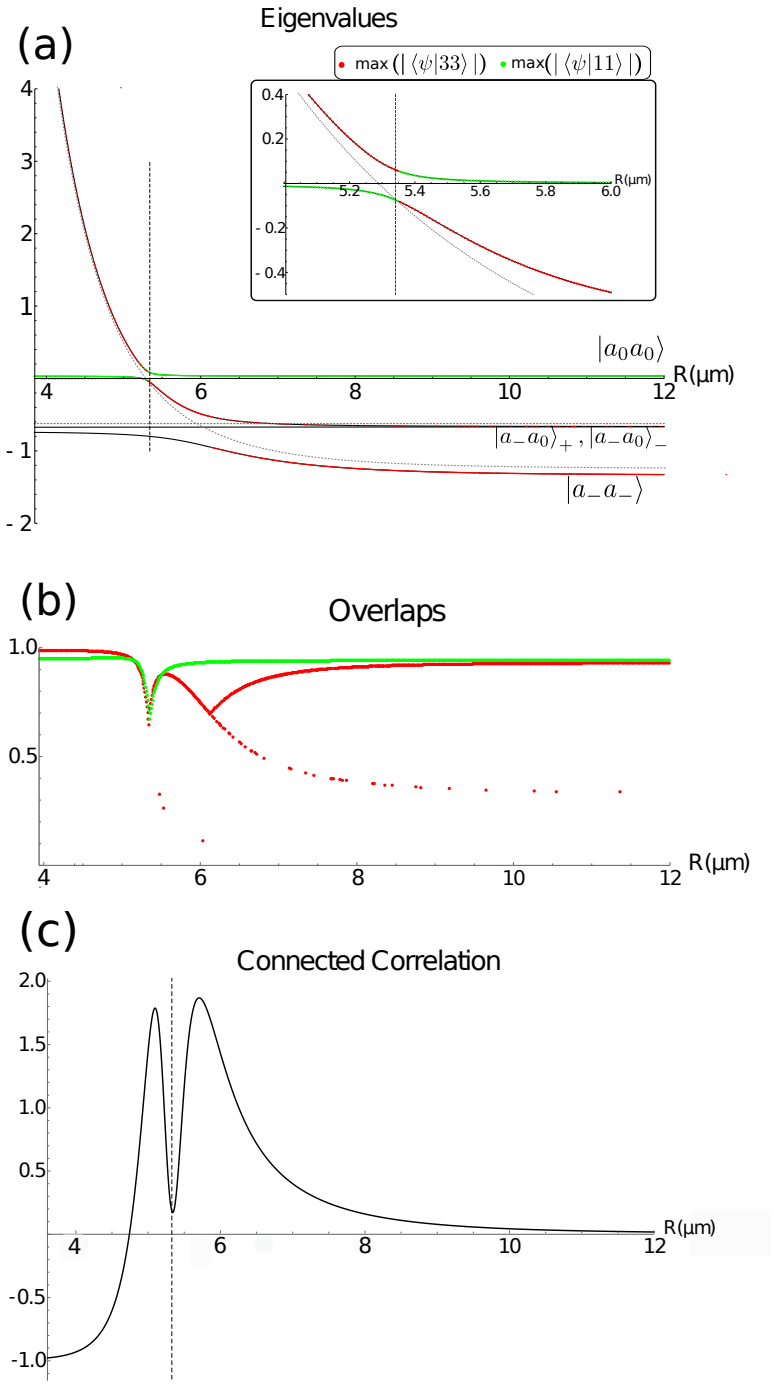

Figure 4.9: Avoided crossing in the spectrum of Hamiltonian coincides with the dip in the center of the hump in the correlation. The dashed line indicates both the position of the avoided crossing and the dip (5.34 μm) (a) Eigenvalues of Hamiltonian vs. R (black). The red dots signal the eigenvalue whose eigenvector ψ has the maximum overlap with state $|33\rangle$. Similarly, green dots signal maximum overlap with $|11\rangle$. The gray curves correspond to eigenvalues when $\Omega_1 = 0$. (b) Value of maximum overlap with $|33\rangle$ (red) and $|11\rangle$ (green). (c) Connected correlation. (a), (b) and (c) were made with $\frac{\Omega_2}{\Omega_1} = 4$.

This explanation also gives us a way to estimate the position of the region at which we have positive connected correlation. If we assume that when eigenvalues vary with R, they do it with a $\frac{C_6}{R^6}$ dependence, then R_d, the position of the avoided crossing and the dip, must satisfy

$$E_{--} = \Delta_1 - \sqrt{\Delta_1^2 + \Omega_1^2 + \Omega_2^2} = \frac{C_6}{R_d^6}. \tag{4.23}$$

Besides this, we see that we are able to approximate the stationary state of the system from one and the other side of the avoided crossing by the corresponding eigenvector with the greatest overlap with $|a_0 a_0\rangle$ (figure 4.10). The results for double-excited state population and the connected correlation can be well-approximated in this way at points far from the avoided crossing. The discrepancy near the avoided crossing means that other eigenstates have a non-negligible contribution to the stationary state.

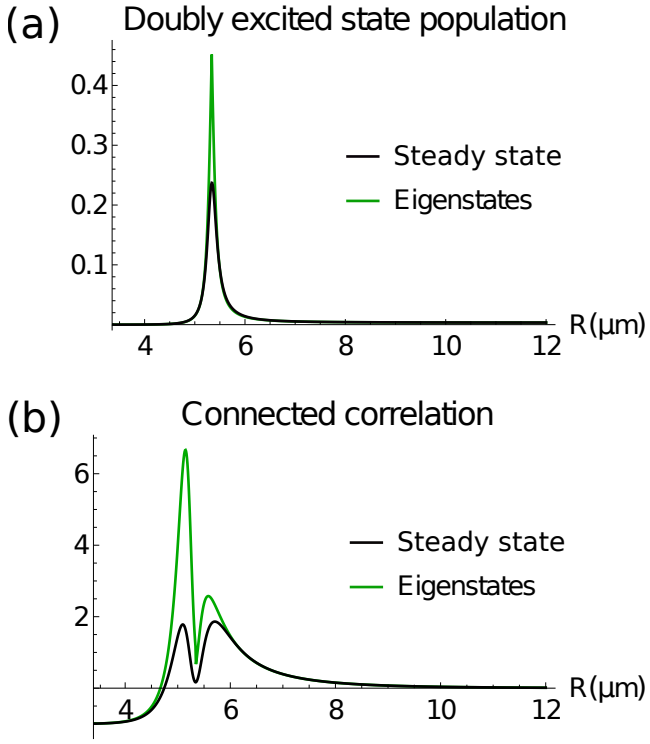

Figure 4.10: Green curve corresponds to the steady state results. The black one is obtained from the eigenvectors of $\hat{H}$ as described above. (a) Double-excited state population and (b) Connected correlation.

A word on the dip

The above discussion on the avoided crossing and its connection to the facilitation of excitation seems to suggest that the distance R_d at which the avoided crossing occurs should also be the distance at which we observe the maximum antiblockade. In other

words, the presence of the dip at R_d in the correlation seems counterintuitive in light of the interpretation we have given to the avoided crossing.

In order to further explore this, we notice that we have ignored the state $|a_-a_0\rangle_+$ altogether. The avoided crossing at R_d =5.34 μm implies admixing of non only $|a_0a_0\rangle_R$ and $|a_-a_-\rangle_R$, but also of $|a_0a_0\rangle_R$ with $|a_0a_-\rangle_{+R}$. This hints that the steady state $\rho_{\rm st}$ should also have a significant contribution from $|a_0a_-\rangle_{+R}$. This suspicion is confirmed by computing the fidelities of $\rho_{\rm st}$ with $|a_0a_0\rangle$, $|a_0a_-\rangle$ and $|a_-a_-\rangle$ (figure 4.11). In fact, we see that $F(\rho_{\rm st}, |a_-a_-\rangle) \simeq F(\rho_{\rm st}, |a_0a_-\rangle)_+$ in all the range of distances considered. This makes us realize that, even tough the avoided crossing argument is useful to identify the location of the intermediate structure, it does not fully explain the physics behind it. In particular, it does not provide an explanation for frustration of antiblockade (the dip).

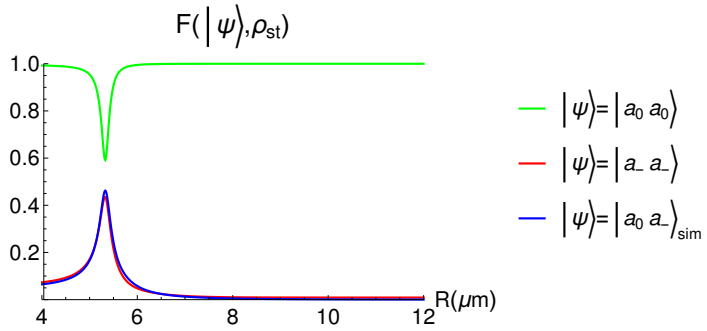

Figure 4.11: Fidelities of $\rho_{\rm st}$ with $|a_0a_0\rangle_R$, $|a_0a_-\rangle_{+R}$ and $|a_-a_-\rangle_R$.

4.4 Adiabatic elimination

In most of the theoretical work involving Rydberg atoms excited using the two-photon scheme, the adiabatic elimination of the second level is performed (see for example [34], [46] and [47]). An interesting question is: Do the blockade and antiblockade regions observed in last section survive the adiabatic elimination?

We perform the elimination of the second level on each atom, as outlined in chapter 1. After the elimination, each atom is now a two-level system (with levels $|1\rangle$ and $|3\rangle$). An effective field interacts with the atoms, with Rabi frequency and detuning given by

$$\begin{aligned} \Omega_{\rm eff} &= -\frac{\Omega_1\Omega_2}{2\Delta_1}, \\ \Delta_{\rm eff} &= \Delta_1 + \Delta_2 + \frac{\Omega_1^2 - \Omega_2^2}{4\Delta_1}. \end{aligned} \tag{4.24}$$

The decay of the upper level is $\gamma_{\rm eff} = \gamma_3 + \frac{(\gamma_2+\gamma_3)\Omega_2^2}{(2\Delta_2)^2}$. After performing the elimination,

we calculate the connected correlation in the stationary state of the system, and see that the features observed in last section survive the elimination (figure 4.12).

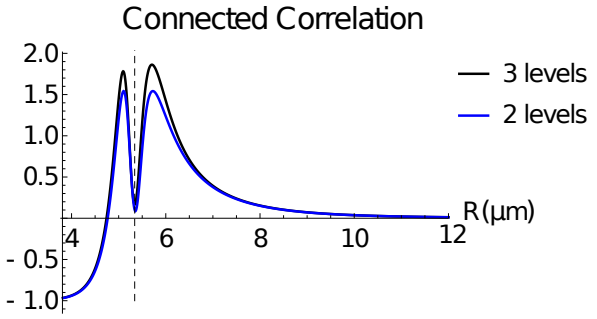

Figure 4.12: Comparison between the connected correlation obtained before (black) and after (blue) performing adiabatic elimination.

4.5 Four-photon transition

Seeking to further characterize the region of positive correlation, we now turn to study possible correlations in the rates of excitations of different states. The expectation value for the polarization in the stationary state,

$$\langle \hat{\mathbf{P}} \rangle = \frac{1}{V} \langle \hat{\mathbf{d}}_1 + \hat{\mathbf{d}}_2 \rangle,$$

gives information on the linear susceptibility of a medium composed by pairs of interacting atoms. The process in which the two atoms are excited from the ground state to the Rydberg state involves the absorption of four photons. To characterize it, we need to calculate the expectation value of $\langle \hat{\mathbf{P}}^4 \rangle = \langle (\hat{\mathbf{P}} \cdot \hat{\mathbf{P}})(\hat{\mathbf{P}} \cdot \hat{\mathbf{P}}) \rangle$.

We relabel the states as

$$\begin{aligned} &|11\rangle \to |1\rangle,\ |21\rangle \to |4\rangle\,,\ |31\rangle \to |7\rangle\,, \\ &|12\rangle \to |2\rangle,\ |22\rangle \to |5\rangle\,,\ |32\rangle \to |8\rangle\,, \\ &|13\rangle \to |3\rangle,\ |23\rangle \to |6\rangle\,,\ |33\rangle \to |9\rangle \end{aligned}$$

to lighten the notation, and make $\mathbf{d}_{12} \equiv \langle 5s_{1/2}|e\hat{\mathbf{r}}|5p_{3/2}\rangle$, $\mathbf{d}_{23} \equiv \langle 5p_{3/2}|e\hat{\mathbf{r}}|60s_{1/2}\rangle$. $\langle \hat{\mathbf{P}} \rangle$ and $\langle \hat{\mathbf{P}} \cdot \hat{\mathbf{P}} \rangle$ in terms of the density matrix elements are

$$\begin{aligned} \langle \hat{\mathbf{P}} \rangle = \frac{Ne}{V} \{ &\mathbf{d}_{12}^{(1)} (\rho_{41} + \rho_{52} + \rho_{63}) + \mathbf{d}_{12}^{(2)} (\rho_{21} + \rho_{54} + \rho_{87}) \\ &+ \mathbf{d}_{23}^{(1)} (\rho_{74} + \rho_{85} + \rho_{96}) + \mathbf{d}_{23}^{(2)} (\rho_{32} + \rho_{65} + \rho_{98}) + \text{h.c.} \}, \end{aligned}$$

$$
\begin{aligned}
\langle \hat{P}^2 \rangle &= \langle \hat{\mathbf{P}} \cdot \hat{\mathbf{P}} \rangle \\
&= \frac{e^2 N^2}{V^2} \{ [(\mathbf{d}_{12}^{(1)} \cdot \mathbf{d}_{12}^{(1)*})(\rho_{11} + \rho_{22} + \rho_{33} + \rho_{44} + \rho_{55} + \rho_{66}) \\
&+ (\mathbf{d}_{12}^{(2)} \cdot \mathbf{d}_{12}^{(2)*})(\rho_{11} + \rho_{44} + \rho_{77} + \rho_{22} + \rho_{55} + \rho_{88}) \\
&+ (\mathbf{d}_{23}^{(1)} \cdot \mathbf{d}_{23}^{(1)*})(\rho_{44} + \rho_{55} + \rho_{66} + \rho_{77} + \rho_{88} + \rho_{99}) \\
&+ (\mathbf{d}_{23}^{(2)} \cdot \mathbf{d}_{23}^{(2)*})(\rho_{22} + \rho_{33} + \rho_{55} + \rho_{66} + \rho_{88} + \rho_{99}) \\
&+ [2(\mathbf{d}_{12}^{(1)} \cdot \mathbf{d}_{12}^{(2)})\rho_{51} + 2(\mathbf{d}_{23}^{(1)} \cdot \mathbf{d}_{12}^{(2)*})\rho_{75} \\
&+ 2(\mathbf{d}_{12}^{(1)} \cdot \mathbf{d}_{23}^{(2)})\rho_{62} + 2(\mathbf{d}_{12}^{(1)} \cdot \mathbf{d}_{12}^{(2)*})\rho_{42} \\
&+ 2(\mathbf{d}_{12}^{(1)} \cdot \mathbf{d}_{23}^{(2)*})\rho_{53} + 2(\mathbf{d}_{23}^{(1)} \cdot \mathbf{d}_{12}^{(2)})\rho_{84} \\
&+ 2(\mathbf{d}_{23}^{(1)} \cdot \mathbf{d}_{23}^{(2)*})\rho_{95} + 2(\mathbf{d}_{23}^{(1)} \cdot \mathbf{d}_{23}^{(2)*})\rho_{86} \\
&+ (\mathbf{d}_{12}^{(1)} \cdot \mathbf{d}_{23}^{(1)})(\rho_{71} + \rho_{82} + \rho_{93}) + (\mathbf{d}_{12}^{(2)} \cdot \mathbf{d}_{23}^{(2)})(\rho_{31} + \rho_{64} + \rho_{97}) + \text{c.c.}] \}.
\end{aligned}
\tag{4.25}
$$

We have adopted the notation $\mathbf{d}_{12}^{(k)}$ to indicate that the matrix element was taken on the atom k. $\langle \hat{\mathbf{P}} \rangle$ contains all the possible transitions of one photon in the system. Likewise, $\langle \hat{P}^2 \rangle$ and $\langle \hat{P}^4 \rangle$ contain all the possible transitions of two and four photons, respectively. For instance, the first term in the last line in the expression (4.25) for $\langle \hat{P}^2 \rangle$ describes the process where atom 2 undergoes a transition $|1\rangle \rightarrow |2\rangle$ and then a transition $|2\rangle \rightarrow |3\rangle$. The quantity that characterizes such a process is then $(\rho_{31} + \rho_{64} + \rho_{97})$. Similarly, the last term of the expression (4.25) corresponds to the same process in atom 1.

In particular, the part of $\langle \hat{P}^4 \rangle$ that corresponds to the two atoms absorbing two photons each is

$$
\langle \hat{P}_{4ph}^4 \rangle = \frac{e^4 N^4}{V^4} \rho_{91} \{ 2(\mathbf{d}_{12}^{(1)} \cdot \mathbf{d}_{23}^{(1)})(\mathbf{d}_{12}^{(2)} \cdot \mathbf{d}_{23}^{(2)}) + 4(\mathbf{d}_{12}^{(1)} \cdot \mathbf{d}_{12}^{(2)})(\mathbf{d}_{23}^{(1)} \cdot \mathbf{d}_{23}^{(2)}) \}. \tag{4.26}
$$

The matrix element that characterizes the transition from ground state to double Rydberg state is $\rho_{91} = \rho_{33\_11}$. In figure 4.13 we plot this coherence along with the coherences that correspond to the excitation of a single atom to the Rydberg state. We see that at the point of the avoided crossing ρ_{33_11} is enhanced: the real and imaginary part of ρ_{33_11} have a larger value at the resonance condition than the coherences associated with the transition $|1\rangle \rightarrow |3\rangle$ of a single atom.

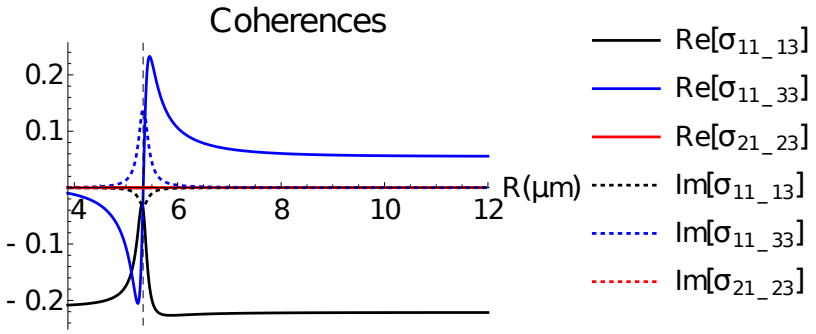

Figure 4.13: Real (solid lines) and imaginary parts (dashed lines) of coherences related with the transition $|1\rangle \rightarrow |3\rangle$ in the second atom. At the avoided crossing region the coherence related to $|11\rangle \rightarrow |33\rangle$ (blue lines) is enhanced. This signals the presence of antiblockade.

Furthermore, we can define a new connected correlation,

$$\langle P^4 \rangle_c \equiv |\rho_{91}| - |(\rho_{71} + \rho_{82} + \rho_{93})(\rho_{31} + \rho_{64} + \rho_{97})|. \tag{4.27}$$

As we have said before, ρ_{91} describes the transition where both atoms make the transition $|1\rangle \rightarrow |3\rangle$. On the other hand, $(\rho_{71} + \rho_{82} + \rho_{93})$ describes atom 1 going from $|1\rangle \rightarrow |3\rangle$ regardless of what atom 2 does, and $(\rho_{31} + \rho_{64} + \rho_{97})$ describes atom 2 going from $|1\rangle \rightarrow |3\rangle$ regardless of what atom 1 does. If the excitation of both atoms is independent, then $|\rho_{91}| \simeq |(\rho_{71} + \rho_{82} + \rho_{93})(\rho_{31} + \rho_{64} + \rho_{97})|$ and $\langle P^4 \rangle_c \simeq 0$. $\langle P^4 \rangle_c \neq 0$ signals parameter regions where the excitation of each atom to a Rydberg state interfere with one another (either constructively or destructively). In figure 4.14 we see that the correlation goes to zero for large interatomic distances, as expected. For distances $5 \lesssim R \lesssim 8$ we see a positive correlation and hence a facilitation of double excitation. For $R \lesssim 5$ the facilitation disappears and the correlation becomes negative. This is in agreement with figure 4.9, that identifies $4 \leq R \lesssim 5$ as the region of Rydberg blockade.

Note that the analysis of the avoided crossings above is useful to both determine the position of the antiblockade region and gain intuition on the stationary state of the system at different interatomic distances. Nevertheless, the analysis of correlation (4.27) is necessary to realize that blockade and antiblockade regions are caused by the interference between excitation channels.

We also observe that, whereas adiabatic elimination simplifies the problem, it blurs the physical interpretation of different channels of excitation interfering with one another. Without elimination, ρ_{91} represents a four-photon transition, where each photon is attributable to one of the two fields present in the model. If we were to define the correlation (4.27) in the model after elimination, the process in which both atoms go from the ground state to the Rydberg state would be an effective two-photon process, where each photon does not belong exclusively to either of the fields.

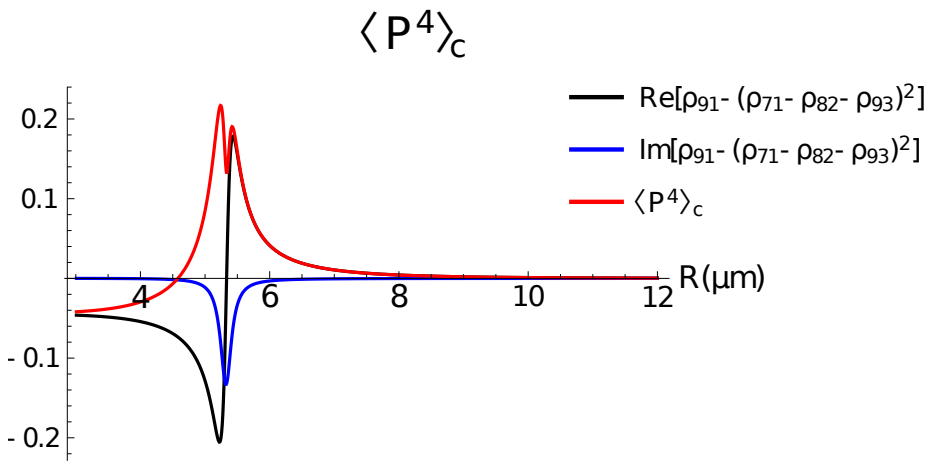

Figure 4.14: Four-photon connected correlation for the parameters of figure 4.9. Its behavior agrees qualitatively with the connected correlation for population (figure 4.6).

Chapter 5

Conclusions

We numerically calculated the potentials of interaction for rubidium Rydberg atoms. For this, we used an effective potential to model alkaline atoms, and symmetry arguments to build a significant basis for the calculation. Additionally, a study of the connected correlation, population and coherences of two atoms interacting through such a potential was performed. We draw the following conclusions:

- The interaction potentials obtained reproduce the $C_6 \propto n^{11}$ intuitively expected.
- Due to the truncation of the multipole expansion for the interaction, the Le Roy radius and the fact that admixing of states due to interaction becomes important at small distances, the validity of this analysis is bounded from below in distances. The minimum value of the interatomic distance depends on the degree of excitation of the atoms. The state studied in this thesis was $|60s_{1/2}60s_{1/2}\rangle$, and the lower bound of validity was estimated at $R \simeq 4\mu$m.
- Studying the connected correlation, we are able to identify interatomic distance ranges for having blockade and antiblockade in two ^{87}Rb atoms, using realistic values for the Rabi frequencies and detunings.
- The position of the antiblockade region corresponds to the position of an avoided crossing in the eigenvalues of the Hamiltonian describing the unitary evolution of the system. The avoided crossing is the result of the light-induced energy structure of the atomic system and the interaction between atoms.
- The processes that correspond to the excitation of each atom from the ground state to the Rydberg state can interfere constructively or destructively. Antiblockade and blockade are respectively associated with constructive and destructive interference.

There are some questions associated with this work that remain unexplored:

- The code for calculating Rydberg potentials could be extended to the case of three atoms. The effect of a third atom on the correlation could be explored.

- In the case of a dense gas, the mixing of Rydberg levels due to interaction discussed at the beginning of chapter 4 could play an important role. This could contribute to the creation of the so-called Rydberg contaminants [25] (atoms in Rydberg states different to the one we wanted to excite originally).

- The adiabatic elimination of the second level means we could reduce the dimension of the density matrix and produce a simpler set of equations to be solved for obtaining the steady state. This could be explored to gain further intuition on the cause of appearance of the dip.

- Extend the study to arrays of atoms with lattice constant belonging to the blockade or antiblockade region and see how it affects or relates to the antiferromagnetic and bistable phases of arrays of Rydberg atoms [48] .

Appendix A

Matrix Numerov method

Our objective is to solve the Schrödinger equation in one dimension. This can be done with the usual Numerov method, where one guesses the energy and then integrates the equation from the initial boundary to the final one. The guess of the energy is refined until one is able to fulfill both boundary conditions. This method can become inefficient if one is interested in solving the Schrödinger equation for multiple energies, as is our case.

An attractive alternative to this procedure is the matrix Numerov method [51]. This method consists in discretizing the wavefunction and converting the problem to a matrix eigenvalue problem. Let the interval where we want to solve for the wavefunctions be $[x_I, x_F]$. We pick an equispaced lattice of points $\{x_i\}$ belonging to this interval and describe a wavefunction with a vector whose components are the values of the wavefunction at these points. The operators that form the Schrödinger equation become matrices in this approach.

The Schrödinger equation in 1D has the form

$$\psi''(x) = -2m\frac{(E - V(x))}{\hbar^2}\psi(x).$$

By expanding $\psi''(x)$ using second-order finite differences, we are left with the expression

$$\frac{-\hbar^2}{2m}B^{-1}A\boldsymbol{\psi} + V\boldsymbol{\psi} = E\boldsymbol{\psi}, \tag{A.1}$$

where $\boldsymbol{\psi} \equiv (\psi(x_I), \psi(x_1), ..., \psi(x_F))$, $V = \text{diag}(V(x_I), ...V(x_F))$, and A and B are simple matrices whose expressions can be found in [51]. The important observation to make is that A.1 is an eigenvalue problem. By diagonalizing the matrix on the left side we obtain a set of eigenvectors and eigenvalues. Conveniently, by increasing the number of points on the lattice we can achieve more precision in the obtained wavefunctions and get more eigenenergies and wavefunctions. The error in the method goes as $\sim d^4$, where d is the step size.

A.1 Solution of the radial Schrödinger equation

The equation we are interested in solving is

$$\frac{d^2u}{dr^2} + 2\left(E - V_M - \frac{\ell(\ell+1)}{2r^2}\right)u = 0, \tag{A.2}$$

where V_M is the Marinescu potential. In particular, we are interested in solving the problem for high-energy states. There are two main reasons why it is not straightforward to solve this equation with the method we just reviewed:

- We expect the wavefunctions that are solution of the equation (A.2) to have a similar behavior to the radial hydrogen wavefunctions. In figure A.1, near the origin, we can observe the hydrogen radial wavefunction for a high energy state. This wavefunction has an increasing density of oscillations as we approach to the origin. Thus, in order to solve the problem efficiently, it would be desirable to have a lattice that mimics this behavior: more points as we approach to the origin.

- We have a singularity in the potential at $r = 0$. This can be fixed by restricting the interval where we solve the equation to $[r_{\min}, r_{\max}]$, and making $r_{\min}$ a small non-zero number.

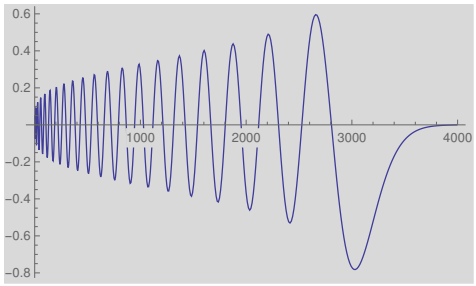

Figure A.1: Hydrogen radial wavefunction with $n = 40$. Image taken from [52]

The first point is fixed by considering an equispaced lattice $\{s_i\}$ and making a new non-equispaced lattice $\{r_i\}$ with $r_i = s_i^2$. The lattice $\{r_i\}$ will then have a bigger density of points near the origin. Next, we first make the change variable $r = s^2$ in equation (A.2), so we obtain the equation we should solve for the equispaced lattice s. In order to obtain an equation with the form $\psi''(s) = f(s)\psi(s)$ and apply the method on last section directly, we make $u(r) = J(s(r))\psi(s(r))$ [52]. J will be used to eliminate factors that contain the first derivative of χ. The second derivative in (A.2) is then

$$\frac{d^2u}{dr^2} = \frac{\psi(s)J''(s)}{4s^2} - \frac{\psi(s)J'(s)}{4s^3} + \left(\frac{J'(s)}{2s^2} - \frac{J(s)}{4s^3}\right)\chi'(s) + \frac{J(s)\psi''(s)}{4s^2}. \tag{A.3}$$

So we need $\frac{J'(s)}{2s^2} - \frac{J(s)}{4s^3} = 0$. The solution to that equation is $J(s) = \sqrt{s}$. So, making $u(s) = \sqrt{s}\chi(s)$, the equation that $\chi(s)$ satisfies is

$$\chi''(s) = 8s^2 \left(\frac{3}{32s^4} + V_{\text{eff}}\left(s^2\right) - E, \right) \chi(s) \tag{A.4}$$

with $V_{\text{eff}}(s^2) = V(s^2) + \frac{\ell(\ell+1)}{2s^4}$. The equation A.4 has the form $\psi''(s) = f(s)\psi(s)$, so we can apply the method described in the first section.

A.2 Example: Hydrogen atom

As a check, we apply the method to the case of hydrogen atom (making $V(r) = \frac{1}{r}$) and compare the results with the exact wavefunctions. This is shown in figures A.2 and A.3. There we see that the numerical method and the non-equispaced lattice produces results that agree reasonably well with the exact wavefunctions, even for high-excited states.

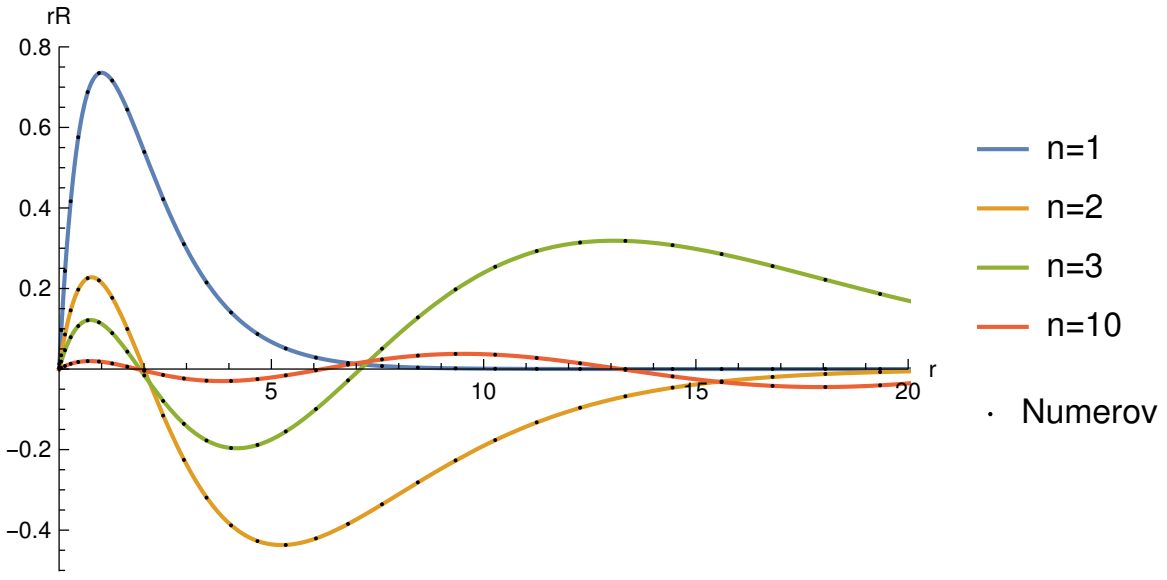

Figure A.2: Comparison between Numerov and analytical wavefunctions.

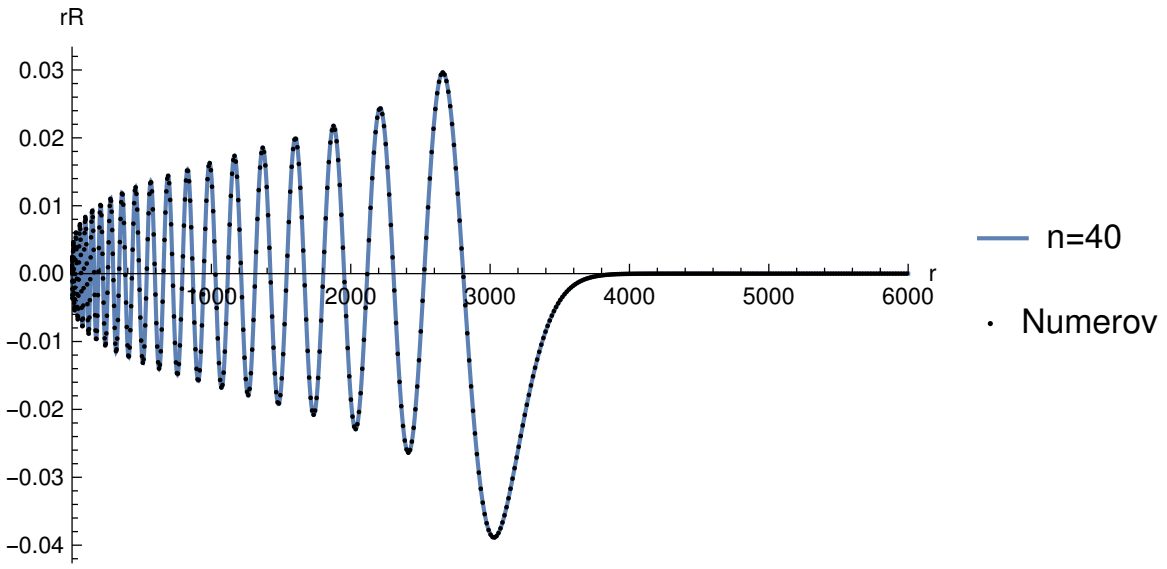

Figure A.3: Comparison between Numerov and analytical wavefunctions.

Appendix B

Wigner Symbols

The 3j and 6j Wigner symbols appear in the context of the sum of angular momenta. Here we review its definitions, properties, and methods of calculation.

B.1 3j symbols

If we have a system composed of two particles, each with an angular momentum $\mathbf{j}_1$ and $\mathbf{j}_2$, we define the total angular momentum as

$$\hat{\mathbf{j}} = \hat{\mathbf{j}}_1 + \hat{\mathbf{j}}_2. \tag{B.1}$$

There are two possible basis to represent the system:

- The decoupled basis $\{|j_1, j_2, m_1, m_2\rangle\}$ of simultaneous eigenstates of $\{\hat{\mathbf{j}}_1^2, \hat{\mathbf{j}}_2^2, \hat{j}_{1z}, \hat{j}_{2z}\}$.
- The coupled basis $\{|j_1, j_2, J, M\rangle\}$ of simultaneous eigenstates of $\{\hat{\mathbf{j}}_1^2, \hat{\mathbf{j}}_2^2, \hat{\mathbf{j}}^2, \hat{j}_z\}$.

The unitary transformation connecting the two basis is defined in terms of the Clebsch-Gordan coefficients $\langle j1, j2, m_1, m_2|J, M\rangle$ [53]

$$|j_1, j_2, J, M\rangle = \sum_{m_1, m_2} \langle j_1, j_2, m_1, m_2|J, M\rangle \, |j_1, j_2, m_1, m_2\rangle \, . \tag{B.2}$$

The 3j Wigner symbols are defined by

$$\begin{pmatrix} j_1 & j_2 & J \\ m_1 & m_2 & -M \end{pmatrix} = \frac{(-1)^{j_1 - j_2 - M}}{\sqrt{2J+1}} \langle j_1, j_2, m_1, m_2|j_1, j_2, J, M\rangle \, . \tag{B.3}$$

B.1.1 Properties

Some of their properties are:

1.
$$\begin{pmatrix} j_1 & j_2 & J \\ m_1 & m_2 & -M \end{pmatrix} \neq 0 \iff m_1 + m_2 = M \text{ and } |j_1 - j_2| \leq J \leq j_1 + j_2.$$

The last condition is referred to as the triangular inequality. These selection rules can be directly deduced from the properties of the Clebsch-Gordan coefficients.

2. They are invariant under a cyclic permutation of the three columns.
$$\begin{pmatrix} j_1 & j_2 & J \\ m_1 & m_2 & -M \end{pmatrix} = \begin{pmatrix} J & j_1 & j_2 \\ -M & m_1 & m_2 \end{pmatrix}.$$

B.1.2 Methods for calculation

By using the ladder operators
$$\hat{J}_\pm = \hat{j}_{1\pm} + \hat{j}_{2\pm},$$
$$\hat{J}_\pm |JM\rangle = \sqrt{J(J+1) - M(M\pm 1)}\, |JM\rangle\,,$$
we can deduce recurrence relations relating different Clebsch-Gordan coefficients. For instance,
$$\begin{aligned}\sqrt{J(J+1) - M(M+1)}\, \langle j_1, j_2, m_1, m_2 | j_1, j_2, J, M\rangle =& \sqrt{j_1(j_1+1) - m_1(m_1+1)}\, \langle j_1, j_2, m_1+1, m_2 | j_1, j_2, J, M+1\rangle \\ &+ \sqrt{j_2(j_2+1) - m_2(m_2+1)}\, \langle j_1, j_2, m_1, m_2+1 | j_1, j_2, J, M+1\rangle\,.\end{aligned}$$

An analogous expression for $\langle j_1, j_2, m_1, m_2 | j_1, j_2, J, M\rangle$ exists in terms of coefficients with $\Delta M = -1$. A recurrence relation connecting coefficients with $\Delta J = \pm 1$ is also available [53].
The only element present in the expansion (B.2) for the coupled basis element with $J_{\max} = M_{\max} = j_1 + j_2$ is $|j_1, j_2, j_1, j_2\rangle$. From this and the definition (B.3) we can see that
$$\langle j_1, j_2, j_1, j_2 | j_1, j_2, j_1 + j_2, j_1 + j_2\rangle = 1. \tag{B.4}$$
Starting with (B.4) with particular numerical numbers for j_1 and j_2 and using the recurrence relations, it is straightforward to obtain the rest of the 3j Wigner symbols for those particular j_i. There is also a closed expression known as the Racah formula [53]
$$\begin{aligned}\begin{pmatrix} a & b & c \\ \alpha & \beta & \gamma \end{pmatrix} =& (-1)^{a-b-\gamma} \sqrt{\Delta(abc)} \sqrt{(a+\alpha)!(a-\alpha)!(b+\beta)!(b-\beta)!(c+\gamma)!(c-\gamma)!} \\ &\times \sum_t (-1)^t \left[t!(c-b+t+\alpha)!(c-a+t+\beta)!(a+b-c-t)!(a-t-\alpha)!(b-t-\beta)!\right],\end{aligned}$$

where

$$\Delta(abc) = \frac{(a+b-c)!(b+c-a)!(c+a-b)!}{(a+b+c+1)!}.$$

is the triangular coefficient, and t in the sum takes all the values for which all the factorials inside make sense. The program for Rydberg potentials calculates the Wigner 3j symbols using the Racah formula (the implementation was taken from [54]).

B.2 6j symbols

When we consider a system formed by three particles, each with an angular momentum $\hat{\mathbf{j}}_i$ $(i = 1, 2, 3)$, we have three different ways to construct the coupled basis. We choose any two of the angular momenta and add them. Then, we couple the remaining one. Each choice will produce a different basis. We will denote as $|(j_1 j_2) J_{12}, j_3, J\rangle$ the basis that was obtained by adding $\hat{\mathbf{j}}_1$ and $\hat{\mathbf{j}}_2$, and then adding $\hat{\mathbf{j}}_3$. Similarly $|j_1, (j_2 j_3) J_{23}, J\rangle$ represents the basis resulting from adding $\hat{\mathbf{j}}_2$ and $\hat{\mathbf{j}}_3$, and then adding $\hat{\mathbf{j}}_1$. The coefficients of the unitary transformation between these two basis define the 6j Wigner symbols [53]

$$\begin{Bmatrix} j_1 & j_2 & J_{12} \\ j_3 & J & J_{23} \end{Bmatrix} = \frac{(-1)^{j_1+j_2+j_3+J}}{\sqrt{(2J_{12}+1)(2J_{23}+1)}} \langle |j_1, (j_2 j_3) J_{23}, J\rangle \, |j_1, (j_2 j_3) J_{23}, J\rangle \,. \tag{B.5}$$

B.2.1 Properties

1. $\begin{Bmatrix} j_1 & j_2 & j_3 \\ J_1 & J_2 & J_3 \end{Bmatrix} \neq 0$ only if the 4 triads $(j_1 j_2 j_3)$, $(j_1 J_2 J_3)$, $(J_1 j_2 J_3)$ and $(J_1 J_2 j_3)$ satisfy the triangular inequality.

2. They are invariant under the permutation of any pair of its columns.

$$\begin{Bmatrix} j_1 & j_2 & J_{12} \\ j_3 & J & J_{23} \end{Bmatrix} = \begin{Bmatrix} j_2 & j_1 & j_3 \\ J_2 & J_1 & J_3 \end{Bmatrix}.$$

3. They can be expressed as a sum of 3j Wigner symbols

$$\frac{1}{(2j_3+1)} \begin{Bmatrix} j_1 & j_2 & j_3 \\ j_3 & J & J_3 \end{Bmatrix} = \sum_{M_1,M_2,M_3,m_1,m_2} (-1)^{\zeta} \begin{pmatrix} J_1 & J_2 & j_3 \\ M_1 & -M_2 & m_3 \end{pmatrix} \begin{pmatrix} J_2 & J_3 & j_1 \\ M_2 & -M_3 & m_1 \end{pmatrix} \times \begin{pmatrix} J_3 & J_1 & j_2 \\ M_3 & -M_1 & m_2 \end{pmatrix} \begin{pmatrix} j_1 & j_2 & j_3 \\ m_1 & m_2 & m_3 \end{pmatrix},$$

where $\zeta \equiv (-1)^{J_1+J_2+J_3+M_1+M_2+M_3}$.

The last property, along with the method for calculating 3j Wigner symbols gives a priori method for calculating 6j Wigner symbols (for particular values of j_i and J_i we compute all the 3j Wigner symbols involved and then perform the sum).

There is also a Racah formula for 6j Wigner symbols [55]

$$\begin{Bmatrix} j_1 & j_2 & j_3 \\ J_1 & J_2 & J_3 \end{Bmatrix} = \sqrt{\Delta(j_1 j_2 j_3)\Delta(j_1 J_2 J_3)\Delta(J_1 j_2 J_3)\Delta(J_1 J_2 J_3)} \sum_t \frac{(-1)^t (t+1)!}{f(t)}, \quad \text{(B.6)}$$

where $\Delta(abc)$ is the triangular coefficient and

$$f(t) = (t - j_1 - j_2 - j_3)!(t - j_1 - J_2 - J_3)!(t - J_1 - j_2 - J_3)!(t - J_1 - J_2 - j_3)!$$
$$(j_1 + j_2 + J_1 + J_2 - t)!(j_2 + j_3 + J_2 + J_3 - t)!(j_1 + j_3 + J_1 + J_3 - t)!.$$

The sum takes all the values of t for which $f(t)$ makes sense. The program for Rydberg potentials calculates the Wigner 6j using this formula (implemented in the script found in [56]).

References

[1] M. Marinescu,H. Sadeghpour and A.Dalgarno, Dispersion coefficients for alkali-metal dimers, Phys. Rev. A 49 982 (1994).

[2] M. O. Scully and M.S. Zubairy, Quantum Optics (Cambridge University Press, 1997)

[3] D. Steck, Quantum and Atom Optics, available online at http://steck.us/teaching (revision 0.13.1, 29 April 2020).

[4] H. Carmichael, Statistical Methods in Quantum Optics 1: Master Equations and Fokker-Planck Equations (Springer-Verlag Berlin Heidelberg, 1999).

[5] P. Milonni, The Quantum Vacuum, (Academic Press, 1993)

[6] H. A. Bethe, The Electromagnetic Shift of Energy Levels, Phys. Rev. 72, 339 (1947).

[7] M. Fleischhauer, A. Imamoglu, and J. Marangos, Electromagnetically induced transparency: Optics in coherent media, Rev. Mod. Phys. 77, 633 (2005).

[8] C.N. Cohen-Tannoudji, The Autler-Townes Effect Revisited. In: Chiao R.Y. (eds) Amazing Light. Springer, New York, NY (1996).

[9] R. Puri, Mathematical Methods of Quantum Optics (Springer, 2001)

[10] P. Anisimov, J. Dowling and B. Sanders, Objectively Discerning Autler-Townes Splitting from Electromagnetically Induced Transparency, Phys. Rev. Lett. 107, 163604 (2011).

[11] E. Brion, L. H. Pedersen and K Molmer, Adiabatic elimination in a lambda system, J. of Phys. A, 40, 5 (2007).

[12] M. Saffman, T. G. Walker and K. Molmer, Quantum information with Rydberg atoms, Rev. of Mod. Phys., 82 (2010).

[13] D. Tiarks, S. Schmidt-Eberle, T. Stolz, G. Rempe and S. Dürr, A photonphoton quantum gate based on Rydberg interactions,Nature Physics 15 (2019).

[14] P. Hauke and M. Heyl, Many-body localization and quantum ergodicity in disordered long-range Ising models, Phys. Rev. B 92, 134204 (2015).

[15] A. Browaeys and T. Lahaye, Many-body physics with individually controlled Rydberg atoms, Nat. Phys. 16, 132142 (2020).

[16] R. Löw, H. Weimer, J. Nipper, J.Balewski1,B. Butscher, H. P. Büchler and T. Pfau, An experimental and theoretical guide to strongly interacting Rydberg gases, J. Phys. B: At. Mol. Opt. Phys. 45, 113001 (2012).

[17] N. Sibalic and C.S. Adams, Rydberg Physics, 2018. IOP Publishing Ltd.

[18] T. F. Gallagher: Rydberg Atoms (Cambridge Univ.Press, Cambridge 1994).

[19] B. Höglund and P. G. Mezger, Hydrogen Emission Line $n_{110} \rightarrow n_{109}$: Detection at 5009 Megahertz in Galactic H II Regions, Science 150, 3694 (1965).

[20] C. Fabret, P. Goy and S. Haroche, Millimetre resonances in Na Rydberg levels detected by field ionization : quantum defects and Stark-effect studies, J. Phys. B: Atom. Molec. Phys., 10, 6 (1977).

[21] S. Svanberg, P. Tsekeris and W. Happer, Hyperfine-Structure Studies of Highly Excited D and F Levels in Alkali Atoms Using a cw Tunable Dye Laser, Phys. Rev. Lett., 30,18 (1973).

[22] M. Raimond, M. Brune, and S. Haroche, Colloquium: Manipulating quantum entanglement with atoms and photons in a cavity, Rev. Mod. Phys.73, 565 (2001).

[23] M. D. Lukin, M. Fleischhauer, R. Cote, L. M. Duan, D.Jaksch, J. I. Cirac, and P. Zoller, Dipole Blockade and Quantum Information Processing in Mesoscopic Atomic Ensembles, Phys. Rev. Lett.87,037901 (2001).

[24] H. Bernien,S. Schwartz,A. Keesling et al, Probing many-body dynamics on a 51-atom quantum simulator. Nature 551, 579584 (2017).

[25] P. Bienias, J. Douglas, A. Paris-Mandoki,P. Titum, I. Mirgorodskiy, C. Tresp, E. Zeuthen, M. J. Gullans, M. Manzoni, S. Hofferberth, D. Chang, and A. V.Gorshkov, Photon propagation through dissipative Rydberg media at large input rates, arXiv:1807.07586 (2018).

[26] D. Tong, S. M. Farooqi, E. G. M. van Kempen, Z. Pavlovic, J. Stanojevic, R. Ct, E. E. Eyler, and P. L. Gould, Observation of electric quadrupole transitions to Rydberg nd states of ultracold rubidium atoms, Phys. Rev. A, 79, 052509 (2009).

[27] J. D. Rodrigues, L. G. Marcassa and J. T. Mendona, Excitation of high orbital angular momentum Rydberg states with LaguerreGauss beams, J. Phys. B: At. Mol. Opt. Phys. 49, (2016).

[28] T. Walker and M. Saffman, Zeros of Rydberg-Rydberg Föster Interactions, J. Phys. B: At. Mol. Opt. Phys. 38, (2005)

[29] H. Gorniaczyk, C. Tresp, P. Bienias, A. Paris-Mandoki, W. Li, I. Mirgorodskiy, H. P. Bchler, I. Lesanovsky, and S. Hofferberth, Enhancement of Rydberg-mediated single-photon nonlinearities by electrically tuned Frster resonances, Nat Commun 7, 12480 (2016).

[30] J. Nipper, J. B. Balewski, A. T. Krupp, B. Butscher, R. Lw, and T. Pfau, Highly Resolved Measurements of Stark-Tuned Frster Resonances between Rydberg Atoms,Phys. Rev. Lett. 108, 113001 (2012).

[31] J. Raimond,G. Vitrant and S. Haroche, Spectral line broadening due to the interaction between very excited atoms: 'the dense Rydberg gas', J. Phys. B: At. Mol. Phys. 14 L655 (1981).

[32] R. Heidemann, U. Raitzsch, V. Bendkowsky, B. Butscher, R. Löw, L. Santos, and T. Pfau, Evidence for Coherent Collective Rydberg Excitation in the Strong Blockade Regime, Phys. Rev. Lett. 99, 163601 (2007).

[33] E. Urban, T. Johnson, T. Henage, L. Isenhower, D. Yavuz, T. Walker and M. Saffman, Observation of Rydberg blockade between two atoms, Nature Physics 5, 110114 (2009).

[34] C. Ates, T. Pohl, T. Pattard and J. M. Rost, Antiblockade in Rydberg Excitation of an Ultracold Lattice Gas, Phys. Rev. Lett. 98, 023002 (2007).

[35] T. Amthor, C. Giese, C. Hofman, and M. Weidemüller, Evidence of Antiblockade in an Ultracold Rydberg Gas, Phys. Rev. Lett. 104, 013001 (2010).

[36] O. Firstenberg, C. S. Adams, and S. Hofferberth, Nonlinear quantum optics mediated by Rydberg interactions, J. Phys. B: At. Mol. Opt. Phys. 49, 152003 (2016).

[37] J. Lim, H. Lee, and J. Ahn, Review of cold Rydberg atoms and their applications, Journal of the Korean Physical Society 63, 867876 (2013).

[38] C. Adams, J. Pritchard, J. Shaffer,Rydberg atom quantum technologies, J. Phys. B: Atom. Molec. Phys., 53 012002 (2019).

[39] N. Sibalic, J. .D.Pritchard, C.S.Adams and K.J.Weatherill, ARC: An open-source library for calculating properties of alkali Rydberg atoms, Comp. Phys. Comm., 220, 319 (2017).

[40] S.Weber, C. Tresp, H. Menke, A. Urvoy, O. Firstenberg, H. Bchler and S. Hofferberth, Calculation of Rydberg interaction potentials, J. Phys. B: At. Mol. Opt. Phys. 50 133001 (2017).

[41] X. Han, S. Bai, Y.Jiao, L. Hao, Y. Xue, J. Zhao, S. Jia and G. Raithel, Adiabatic potentials of cesium (nDJ)2 RydbergRydberg macrodimers, Phys. Rev. A 97, 031403(2019).

[42] M. Eiles, Trilobites, butterflies, and other exotic specimens of long-range Rydberg molecules, J. Phys. B: Atom. Molec. Phys., 52, 11 (2019).

[43] M. Seaton, Quantum defect theory, Rep. Prog. Phys., 46, (1983).

[44] W. Li, I. Mourachko, M. W. Noel, and T. F. Gallagher, Millimeter-wave spectroscopy of cold Rb Rydberg atoms in a magneto-optical trap: Quantum defects of the ns, np, and nd series, Phys. Rev. A, 67, 052502 (2003).

[45] A. Dalgarno and W. D. Davidson, The Calculation of Van der Waals Interactions, Adv. At. Mol. Phys. 2 132 (1966).

[46] T. L. Nguyen, Study of dipole-dipole interaction between Rydberg atoms - Toward quantum simulation with Rydberg atoms, 2016. Universit Pierre et Marie Curie UPMC Paris VI.

[47] A. Paris-Mandoki, C. Braun, J. Kumlin, C. Tresp, I. Mirgorodskiy, F. Christaller, H. P. Büchler, and S. Hofferberth, Free-Space Quantum Electrodynamics with a Single Rydberg Superatom, Phys. Rev. 7, 041010 (2017).

[48] A. Hu, T. E. Lee, and C. W. Clark, Spatial correlations of one dimensional driven-dissipative systems of Rydberg atoms, Phys. Rev. A 88 (2013).

[49] R. Le Roy, Long-Range Potential Coefficients From RKR Turning Points, Can. J. Phys. 52 (1974).

[50] J. T. Young, T. Boulier, E. Magnan, E. A. Goldschmidt, R. M. Wilson, S. L. Rolston, J. V. Porto, and A. V. Gorshkov, Dissipation induced dipole blockade and anti-blockade in driven Rydberg systems, Phys. Rev. A 97, 023424 (2018).

[51] M. Pillai, J. Goglio and T. Walker, Matrix Numerov method for solving Schrödingers equation, Am. J. Phys. 80, 1017 (2012).

[52] http://www.physics.wisc.edu/ tgwalker/NumerovExamples/

[53] A. Messiah, Quantum Mechanics (Dover Publications New York, 2014).

[54] Kobi (2019). Wigner3j symbol (https://www.mathworks.com/matlabcentral/fileexchange/20619-wigner3j-symbol), MATLAB Central File Exchange. Retrieved March 02, 2019.

[55] I. Sobelman, Atomic Spectra and Radiative Transitions(Springer-Verlag Berlin Heidelberg, 1992).